Rail-Structure Interaction

Master Thesis

Gijs Hoppenbrouwers

Delft University of Technology

TU Delft

MASTER THESIS

CIEM0500

An investigation into the Rail-Structure Interaction in Railway Bridges in the Netherlands

Author:
Gijs Hoppenbrouwers
5060591
gijs.hoppenbrouwers@gmail.com

Submitted to:
dr. ir. Pierre Hoogenboom
ir. Cor Kasbergen
dr. Zhen Yang
dr. ir. Dennis Schoenmakers
ir. Jan Willem de Vos

June 26, 2024

Preface

This thesis marks the completion of my MSc in Civil Engineering, with a focus on Structural Engineering. The research investigates the interaction between railway bridges and the rails they support. This work was conducted at Wagemaker, an engineering and consultancy firm, where the need for this investigation was identified and where I received substantial support for its successful execution.

This report is intended for readers in the field of civil engineering, particularly those specialising in Structural Engineering and with a specific interest in the longitudinal stresses in rails caused by the presence of railway bridges.

I would like to express my appreciation to my supervisors at Wagemaker, Dennis Schoenmakers and Jan Willem de Vos, for their constant availability, quick responses to my inquiries, and the engaging weekly meetings that significantly contributed to the success of this thesis. I am also deeply thankful to my supervisors at TU Delft: Cor Kasbergen, for his guidance, feedback, and availability; Pierre Hoogenboom, for his structural insights and assessments; and Zhen Yang, for his valuable feedback on railway engineering aspects. Their support and advice have been indispensable throughout this process.

Gijs Hoppenbrouwers
Rosmalen, June 2024

Summary

In the Netherlands, there is a large and widely used railway system that includes numerous railway bridges. This master thesis investigates the problems caused by these railway bridges. Since World War II, continuous welded rails have been used extensively throughout the Netherlands. These rails offer several advantages on embankments, such as reduced maintenance due to less vibration, increased passenger comfort, and reduced noise. However, continuous welded rails can cause problems when they run continuously over a bridge, as is the case in the Dutch railway system. Bridges are not continuous structures and have joints between the decks or between the deck and the transition structure. These joints allow the bridge deck to expand and contract due to temperature changes, move due to longitudinal forces from train braking and acceleration, and deflect due to the vertical load of the train, causing rotations at the ends of the bridge decks. This relative displacement between the bridge deck and the continuously welded rails creates additional stresses in the rails. These additional stresses must not exceed the maximum allowable stress of the rail material, as this could cause the rails to buckle or fracture. Fixed points are often used in practice to limit the movement of the bridge deck and keep additional rail stresses within acceptable limits. This investigation, however, focuses on understanding the interaction between the rails and the structure without the use of fixed points. The study assumes a railway bridge in the Netherlands with a ballast bed and uses concrete precast bridge decks.

To gain initial knowledge of the problem and the various railway components and bridges, a literature review was conducted, and two existing railway bridge projects were analysed. It quickly became evident that there are two different bridge types relevant to the study of additional rail stresses: those without embankment influence and those with embankment influence. The study then identified parameters that could influence the magnitude of additional rail stresses to use them as variables in further investigations.

Two longitudinal force models were created in SCIA Engineer: one without embankment influence (Model 1) and one with embankment influence (Model 2). These models are spring models where the stiffness of connections and elements is schematised as springs. The models were validated with hand calculations and used to obtain results for the influence of various parameters such as bridge deck span length, elastomeric bearings, bridge pier length, and foundation stiffness. The results of the two models were compared to understand the influence of the embankment. Additionally, the spring elongations of the non-linear springs between the bridge deck and the rails, representing the ballast bed, were examined to determine if they were in the linear or non-linear part of the spring characteristic to see if the springs slipped enforcing stress redistribution. Finally, the models assessed the individual contributions of three load cases (thermal, longitudinal traffic load, and vertical traffic load) to the combined additional rail stress.

The results lead to the following conclusions:

- When a structure is not influenced by the embankment, the magnitude of additional rail stresses depends on the stiffness of the substructure. The stiffness of the weakest component, in this case, the elastomeric bearings, has a significant influence.
- When a structure is influenced by the embankment, the magnitude of additional rail stresses mainly depends on the dominant stiffness of the embankment, with the stiffness of the substructure having little to no influence.
- Structures with embankment influence experience lower additional rail stresses due to the additional stiffness provided by the embankment. Problems with exceeding maximum permissible rail stresses occur mainly in relatively long railway bridge structures without embankment influence.
- The vertical load has the largest contribution to the combined additional rail stresses for both structure types.
- The thermal load has a larger influence on structures with embankment influence because these structures are more constrained by the embankment and thus more vulnerable to thermal deformations.
- Linear summation of individual stress contributions from different load cases generally results in higher or equal stresses compared to non-linear combinations, making linear summation a conservative ap-

proach. The stress difference between linear summation and non-linear combination is usually only a few megapascals. If the springs between the bridge deck and the rails slip into the non-linear branch, this difference increases slightly but remains small.

Based on these conclusions, the following recommendations can be made to prevent additional rail stresses from exceeding maximum permissible stresses without the use of fixed points and to streamline the process of longitudinal force analysis for engineers:

- To prevent exceeding the maximum permissible stress in structures without embankment influence, consider using larger elastomeric bearings or less slender bridge decks that are less susceptible to deflection, thereby reducing additional rail stress, especially from vertical loads.
- Since linear summation of individual contributions to additional rail stresses results in conservative and faster calculations, it is recommended to use linear calculations in the initial phase. Then, perform a final design review with non-linear calculations to ensure accuracy. This approach will significantly speed up the design process, as models will not need to run for hours or days each time.

Nomenclature

Abbreviation	Meaning
CWR	Continuous Welded Rails
HSL	High Speed line
NP	Normal Profile
UIC	Union International des Chemins de Fer
RSI	Rail-Structure Interaction

Symbol	Definition
A	Area [m^2]
E	Youngs modulus [N/m^2]
F_L	Longitudinal force [kN]
I	Moment of inertia [m^4]
Δl	Change in length [m]
l	length of the element [m]
N	Normal force [N]
α	Thermal expansion coefficient [$^\circ C^{-1}$]
δ_p	Bending of the pier [mm]
δ_φ	Rotation of the foundation [mm]
δ_h	Horizontal movement of the foundation [mm]
ΔT	Temperature change compared to reference temperature [$^\circ C$]

Contents

List of Figures

List of Tables

1

Introduction

The railway system in the Netherlands is highly dense, featuring numerous switches, signals, rail-road crossings, tunnels, and bridges. Following World War II, significant technological advancements were made. One notable development was the replacement of conventional rail with continuous welded rail (CWR).
Conventional rail systems consist of individual rail segments bolted together longitudinally. These joints were the structural weak points, causing significant vibrations when trains passed over them. This resulted in extensive maintenance for both the rails and the wheels. The introduction of continuous welded rails greatly reduced these vibrations, subsequently lowering maintenance needs and decreasing noise levels, which improved comfort for passengers and residents near the tracks.(Enshaeian and Rizzo, 2020)
However, continuous welded rails also present a significant disadvantage, which is the focus of this master's thesis. The issue arises because CWR crosses the joints of railway bridges, spanning from one bridge deck to another, as well as from bridge decks to embankments. The rigidity of CWR prevents it from accommodating the movement of bridge decks, creating additional stress in the rails. This stress results from the discontinuity introduced by the railway bridge system in an otherwise continuous railway system.
These additional stresses can occur due to three main types of loading situations:

- Thermal expansion or contraction
- Longitudinal Traffic load
  - Braking of a train
  - Acceleration of a train
- Vertical Traffic load

This additional rail stress must remain below the maximum permissible stress limits for both tension and compression, determined by the material properties of the rails. If these stress limits are exceeded, it can lead to buckling or fracture of the rails, potentially causing train derailments. The buckling of the rails may also occurs on the embankment itself, as shown in Figure 1.1 but this rarely happens. However, due to the presence of a bridge structure, the probability of increasing stresses in the rails is higher, so this receives extra attention.

Figure 1.1: Deformed rail, (Globe Gazette, n.d.)

The interaction between railways and bridge structures can lead to significant problems, as seen recently. In January, trains on the high-speed line between Amsterdam and Rotterdam were restricted to a maximum speed of 120 km/h in some sections, despite being designed for 300 km/h. This reduction is due to starting cracks in nine railway bridges along the line. The investigation is ongoing, but it is clear that the interaction between the railway system and the bridge structure plays a crucial role in this issue. This highlights the importance of understanding rail-structure interaction in railway bridges.(ProRail, 2024)

In practice, when additional rail stresses become too high due to the presence of a railway bridge structure, a fixed point is applied. This fixed point limits the horizontal movement of the bridge deck, thereby reducing the additional rail stresses. However, in this investigation, it is important to determine if the additional rail stresses can remain below the permissible limit without the use of a fixed point. The goal of this master's thesis is to increase the knowledge about rail-structure interaction without the use of fixed points. This leads to the following main research question:

- How can the understanding of the longitudinal force transfer in railway bridges in the Netherlands be enhanced, so that rail stresses do not exceed safety limits without the use of fixed points?

Answering this main research question requires an understanding of several factors related to the rail-structure interaction. Specifically, the investigation must consider how different components of a railway bridge affect the magnitude of additional rail stresses. These components are thus included as variables in this investigation. Additionally, the influence of embankment stiffness varies between longer and shorter railway bridges, necessitating a deeper understanding of these differences.
From an engineering perspective, longitudinal force calculations typically involve linearly adding the individual stresses from various load cases. However, since the interaction between rails and the bridge deck is modeled using non-linear springs, it is crucial to verify if the linear summation method yields conservative estimates. This will help ensure the accuracy and safety of stress assessments.
Moreover, it is important to determine which of the three load cases (thermal expansion or contraction, longitudinal traffic load, and vertical traffic load) contributes most to the overall additional rail stress. This knowledge will aid in addressing the most significant factors affecting rail stress.
To address these aspects, the following sub-research questions are formulated:

- Which parameters affect the additional rail stresses and are therefore variable? Among these variable parameters, which has the most influence on the magnitude of the additional rail stress?
- What are the differences between railway bridge structures without embankment influence and with embankment influence, and how do variable parameters affect these different constructions?
- Can the additional rail stresses from individual loads be added together to determine the combined effect, and if not, is the summation a conservative estimate?
- Which individual load contributes the most to the combined additional rail stress?

In this thesis, the research questions will be addressed and presented. The investigation will focus on railway bridges in the Netherlands, particularly emphasising extreme scenarios. Furthermore, the scope of the longitudinal force analysis will be limited to ballast-supported rails on a single-track railway bridge using precast bridge decks. The aim is to enhance understanding of the factors influencing the magnitude of additional rail stress in rail-structure interaction.

In this thesis, the research questions will be systematically addressed, following a step-by-step approach. The first chapter provides a comprehensive introduction to the topic, outlining both the main and sub-questions. The second chapter focuses on a literature review to gain initial knowledge about the problem, elements of railway systems, loads, and design regulations.
Chapter 3 discusses the project analysis of two existing railway bridges: Theemswegtrace in Rotterdam and Eygelshoven in Limburg. Chapter 4 details the methodology used to construct the longitudinal force model, including hand calculations, model building, and data collection methods for analysis.
Chapter 5 presents the validation of the longitudinal force models developed in Chapter 4, where initial model results are verified. Chapter 6 presents the results of the longitudinal force analysis introduced in the preceding chapter, detailing the influence of variable parameters, differences between structures with and without embankment influence, and load contributions.
The thesis concludes with a final chapter that offers a comprehensive conclusion and recommendations. This section addresses the research questions and provides several practical recommendations.

2

Literature study

The movement of the bridge deck and the corresponding increases in additional rail stresses have several causes. These factors need to be investigated before modeling the interaction between them and drawing conclusions. Additional knowledge about these causes will be obtained through a literature review. The search for literature is described in the thesis proposal, and the literature found will be used for this study.
The movement of the bridge deck is attributed to three primary types of loads on the rails, which induce additional rail stresses. Firstly, thermal expansion and contraction of the bridge deck induce additional stresses in the rails. Secondly, longitudinal traffic loads, generated by the braking and acceleration of trains on the railway bridge, act directly on the top of the rails. Lastly, vertical traffic loads, imposed by trains traveling over the bridge system, also contribute to the additional rail stresses. These load situations are discussed in section 2.1.
The magnitude of the stresses in the rails depends on the interaction between the structure and the rails. This interaction determines how much force is resisted by the structure and how much is absorbed by the rails as rail stresses. This rail-structure interaction will be discussed in section 2.1. As indicated in chapter 1, the problem with additional rail stresses is caused by the use of continuous welded rails in Dutch railways. The reasons for using these rails, along with their advantages and disadvantages, are discussed in section 2.2.
All constructions in the European Union must comply with certain safety limits, which are listed in design code regulations. These regulations are stored in the Eurocode, with additional guidelines by ProRail and the NS. The models created for this thesis must meet these imposed safety limits, which are described in section 2.3.

2.1. Rail-Structure Interaction (RSI)

The interaction between rails and the bridge structure significantly influences the additional stress in continuous welded rails. This is primarily due to relative displacement between different components. Continuous welded rails are tightly constrained by sleepers, fasteners, ballast, and their own stiffness, whereas the bridge deck can move horizontally and deflect vertically. These relative displacements create additional stresses in the rails. (Midas, n.d.) Figure 2.1 illustrates the relative displacement, indicating that the variance in stiffness among different components in the railway system is a key factor contributing to this displacement. These differences in displacements depend on various parameters, including the material and cross-sectional properties of the components and their connections. The magnitude and direction of loads also play a crucial role in these displacements.
Therefore, this section is divided into two subsections. The first subsection discusses the components of the railway system to provide initial knowledge about the different elements and their properties. The second subsection covers the various loads that result in additional rail stresses, including thermal, longitudinal, and vertical loads.

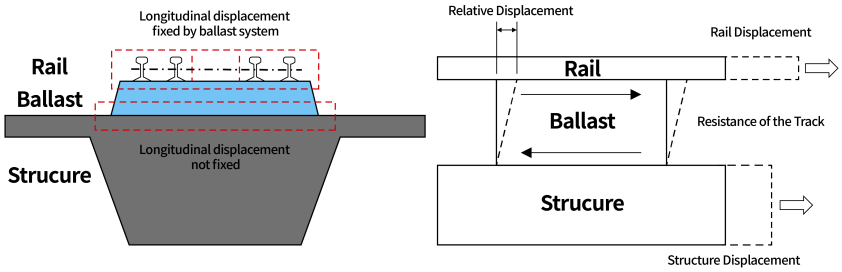

Figure 2.1: Different displacements of the rail and the structure and the relative displacement, (Midas, n.d.)

2.1.1. The components of the railway system

As depicted in Figure 2.1, the displacements of various components within the railway system's construction vary, contributing to relative displacements that influence the magnitude of additional stresses in the rails under different loading conditions. These variations primarily come from differences in material properties and fastening methods among the elements. The stiffness and thermal expansion coefficients of these elements play crucial roles in determining relative displacements and, consequently, in affecting the magnitude of additional stress in the continuous welded rails. These material properties and fastening methods are integral to the rail-structure interaction model developed in this thesis, where they are represented as elements and springs.

To gain deeper insights into this phenomenon, it is essential to consider all elements in the system: rails, sleepers, fasteners, ballast bed, bridge deck, and embankment. Each of these components interacts with one another, collectively contributing to the overall system properties. This subsection is subdivided into several parts to elucidate how these elements interact and contribute to the railway system's behavior. Understanding these different components, combined with the project analyses in chapter 3, will facilitate the identification of parameters affecting the magnitude of additional rail stresses. These parameters will be investigated as variables in this investigation.

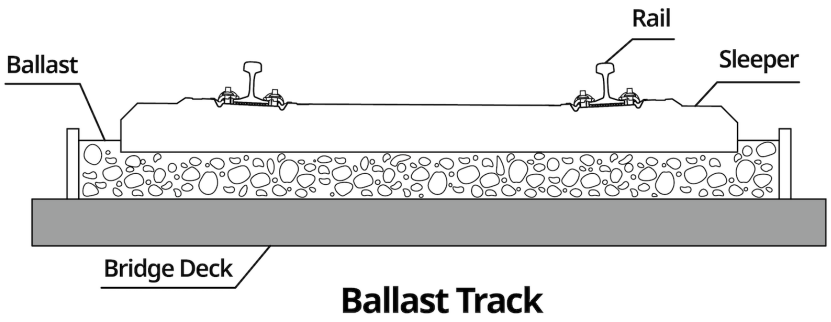

Figure 2.2: Cross section of a ballast railway bridge track, (Midas, n.d.)

2.1.1.1. Rails

The rail is the first element that will be discussed in this subsection. The rail is a very important part of the railway system. The rail is in direct contact with the wheels of the train ensures the guidance of the train over the system and, together with the shape of the wheels, ensures that the train does not derail.

The most common rail type used in the Netherlands and Europe is the vignoles rail, which includes various profiles as illustrated in Figure 2.3. In the Netherlands, railway tracks utilize three main rail profiles: NP46 (Normal Profile), UIC54 (Union Internationale des Chemins de Fer), and UIC60. NP46 is used on select regional lines, while UIC54 is widely applied on most core railway lines in the Netherlands. UIC60 is reserved for specific lines, such as high-speed and high-load routes like the HSL-Zuid and the Betuweroute. All rail profiles are constructed from steel, resulting in a uniform thermal expansion coefficient of $1.2 \cdot 10^{-5}$ $[°C^{-1}]$ (Verheijen, n.d.) (Esveld, 2005).

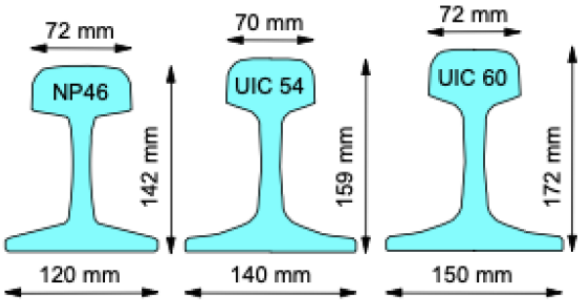

Figure 2.3: Vignoles rail profiles, (Esveld, 2005)

The rail profiles consist of three main parts: the rail head, rail web, and rail foot. The rail head ensures contact with the train wheels, guiding them along the track. The rail web is designed with a specific thickness to maintain rail stiffness. The rail foot plays a crucial role in the overall structure by distributing stress to the sleepers, influencing the moment of inertia, and serving as the attachment point to the sleepers (Esveld, 2005).
In Europe, including the Netherlands, the track width between the insides of two rail heads is standardised at 1435 mm. This uniform width facilitates seamless train traffic between different countries, enhancing operational efficiency and compatibility (Esveld, 2005).

Rail Profile	Weight [kg/m]	Thermal expansion coeficient (α) [10^{-5}]	Young's Modulus (E) [10^{11} N/m^2]	Cross sectional area (A) [cm^2]	Inertia I_y[cm^4]	Inertia I_z[cm^4]
NP46	46.66	1.2	2.1	59.44	1605.9	307.5
UIC54	54.77	1.2	2.1	69.77	2337.9	419.2
UIC60	60.21	1.2	2.1	76.70	3038.3	512.3

Table 2.1: Properties of the different vignoles rail profiles used in the Netherlands

For this investigation, the UIC54 rail type is selected as it is the most commonly used in the Netherlands. This profile is widely adopted, and its cross-sectional properties vary minimally among the three different profiles available. Therefore, the choice of rail profile is expected to have only a minimal influence on the magnitude of additional rail stresses.

2.1.1.2. Sleepers

In a ballasted railway system, sleepers play a crucial role in transferring loads from the rails to the ballast bed, forming the superstructure of the railway, as illustrated in Figure 2.2. Sleeper not only support the rails but also ensure a consistent spacing distance between the two rails.
In the Netherlands, three main materials are used for sleepers in railway systems: timber, concrete, and plastic. Timber sleepers have been phased out since 2005 due to their short lifespan and adverse effects on sustainability in adverse weather conditions. Currently, ProRail utilizes concrete sleepers, known for their durability and resistance to weather conditions. However, the use of concrete sleepers significantly increases CO2 emissions, posing a notable disadvantage. To address sustainability concerns, ProRail is exploring the potential of plastic sleepers for future implementation, although they have not yet been adopted in existing systems. The distance between sleepers is standardized at 60 centimeters (ProRail, n.d.).
According to ProRail guidelines (OVS00056-5.1), there are two main types of sleepers used in railway construction: sleeper type NS90 and 14-0XX. These sleeper types are visualised in 2.4a and 2.4b (ProRail, 2023b).

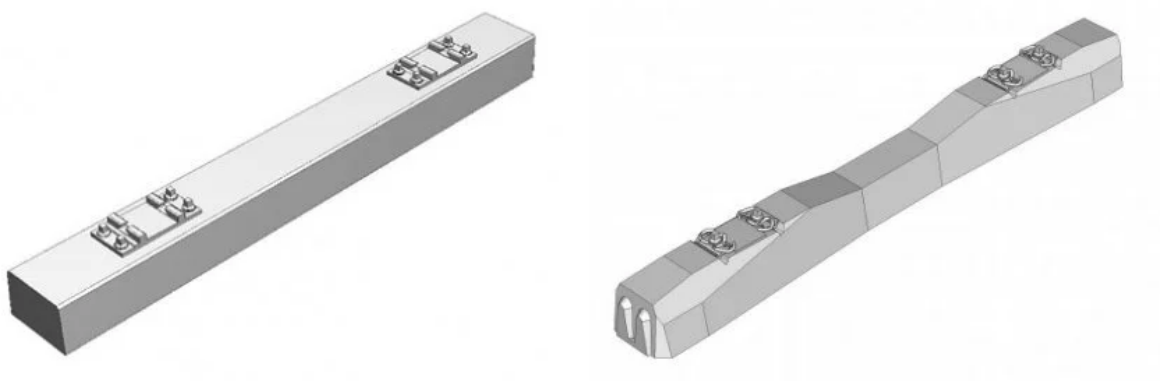

(a) Sleeper 14-002 (b) Sleeper NS90

Figure 2.4: The different sleepers used in the Netherlands (Meteoor, n.d.-b)(Meteoor, n.d.-a)

2.1.1.3. Fasteners

Fasteners are integral components used to connect rails to sleepers in railway systems. They play a crucial role in securing the rails to the sleepers, ensuring that forces in the rails are effectively transmitted to the overall structure while minimising vibrations between the rails and sleepers. Additionally, fasteners must provide sufficient sliding resistance to manage longitudinal forces and accommodate thermal expansion of the rails. (Esveld, 2005)

In the Netherlands, the railway infrastructure utilizes two main types of fasteners:

- Vossloh Fasteners: These include types W14 and W30, which are specifically designed for connecting rails to NS90 sleepers. W14 serves as the standard fastener for NS90, while W30 is used for heavier applications but is not compatible with rail type NP46. (ProRail, 2016a, ProRail, 2019)
- Spring Clamp Fasteners: These fasteners, such as skl3 and skl19, are employed with 14-0XX sleepers. Skl19 is suitable for all rail types, whereas skl3 cannot be used with rail type NP46. Both types are engineered to support railway speeds up to 200 km/h with an axle load of 22.5 tons and up to 120 km/h with an axle load of 25 tons. (ProRail, 2023a, ProRail, 2016b)

An overview of the four different fastener systems is presented in Table 2.2.

(a) Vossloh fastener (Esveld, 2005) (b) Spring clamp fasteners SKL (Voestalpine, n.d.)

Figure 2.5: The different fasteners used in the Netherlands

Fastener type	NP46	UIC54	UIC60	Sliding resistance (kN)	Clamping force (kN)
W14	x	x	x	7	6
W30		x	x	12	12
SKL3		x	x	7	6
SKL19	x	x	x	7	6

Table 2.2: Product specification of the different fasteners (ProRail, 2023a)(ProRail, 2016b)(ProRail, 2016a)(ProRail, 2019)

2.1.1.4. Ballast

As stated in the thesis topic scope in the introduction, the content of the thesis is focused on railway bridges with a ballast rail system. Ballast is a traditional method of constructing railway systems. The ballast bed consists of a layer of coarse, unbounded grains. The resistance of the ballast in vertical direction is high because they can take high compression stresses, however they can not take any tension stresses. In the transverse direction the resistance is limited. The ballast is made of cubic, sharp shaped grains and will help to equally spread the load over the ground surface. (Esveld, 2005)
When ballast is used on a new railway bridge the minimum thickness of the ballast bed must be at least 0.35 meters. With renovating of old rails on a railway bridge this requirement is 0.30 meter instead of 0.35 meter. On bridges ballast mats need to be used. (ProRail, 2023b)

2.1.1.5. Bridge deck

Railway bridges in the Netherlands are constructed using various materials, including different types of bridge decks. This thesis focuses specifically on concrete bridge decks, which are categorized into two primary types: prefabricated (prefab) and in situ concrete, as depicted in Figure 2.6.

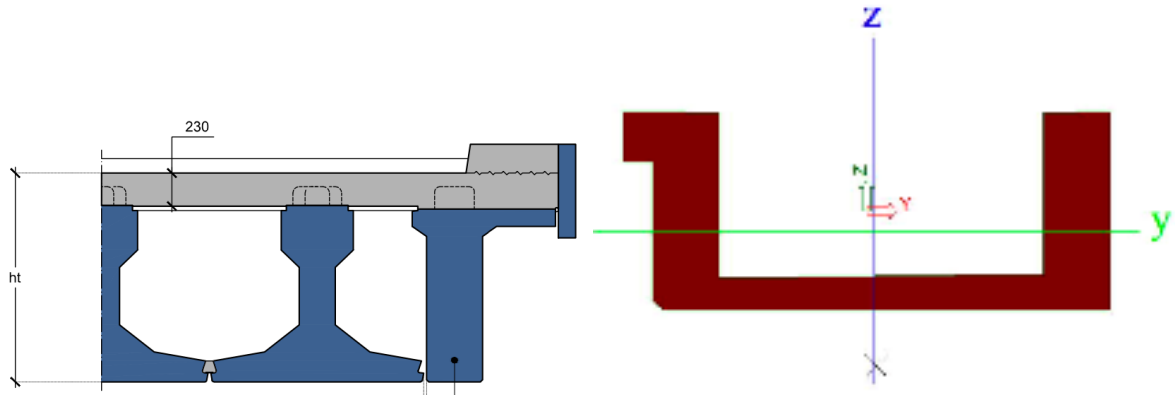

(a) Prefab bridge deck HIP beam Haitsma Beton, (Spanbeton, 2017) (b) Insitu bridge deck, (Wagemaker, 2018)

Figure 2.6: Different concrete bridge decks

In the longitudinal force analysis, the stiffness of the bridge deck is a critical parameter. It determines how much the bridge deck bend under vertical traffic load, subsequently inducing horizontal movement and additional stresses in the rails (ProRail, 2018).
For this investigation, prefabricated concrete bridge decks are considered. Specifically, ZIPXL precast bridge decks from Spanbeton, as shown in Figure 2.6a, are chosen. These bridge decks consist of a prefabricated part (visualized in blue) with a concrete class of C60/75, complemented by a cast-in situ slab (visualized in grey) with a concrete class of C35/45. The selection of profile height, main girders, and boundary girders for each bridge span will be detailed further in subsubsection 4.2.1.1, considering their cross-sectional properties (Spanbeton, 2017)(Wagemaker, 2018).
In the examination of in situ concrete bridge decks, an additional loading case arises, namely shrinkage and creep. However, with prefabricated concrete bridge decks, the effects of shrinkage and creep are largely damped out during the prefabrication period and can therefore be considered negligible and excluded from the analysis.

2.1.1.6. Embankment

As described in the introduction chapter 1, this investigation examines two types of railway bridges for the longitudinal force analysis. These are the railway bridges with and without embankment influence. This embankment will provide a lot of stiffness for the entire system and therefore affect the magnitude of the additional rail stresses. Notably, the continuous welded rails extend onto the embankment, underscoring its integral role as part of the overall system. This integrated configuration emphasises the importance of considering the embankment in the assessment of stress factors and structural dynamics surrounding the

bridge and rail system. The embankment, consisting of a sand bed, ensures the system's capacity, stability, and efficient drainage of melt and rainwater from the ballast. (Esveld, 2005)
In the transition zone from the bridge to the embankment, a longitudinal discontinuity arises due to differences in stiffness between the bridge structure and the embankment. This stiffness inequality and subsequent settlement lead to challenges in track comfort and stability, resulting in high maintenance costs. To address these issues and improve the transition, a transition structure is employed. This research primarily focuses on comprehending the resistance provided by the embankment against longitudinal forces, with less emphasis on its internal structure. The influence of the embankment on the longitudinal force model will be represented using springs.

In cases where additional stresses in the rails exceed permissible limits at the transition zone between the structure and the embankment, a compensation provision may be employed. An illustration of such a provision is presented in Figure 2.7. This approach involves discontinuing the continuous welding of rails at the transition, thereby reducing stresses to ensure they fall within acceptable safety limits.
While compensation provisions offer a potential solution, this investigation into longitudinal forces in rail-structure interaction assumes a scenario without their use. This decision is driven by associated disadvantages, such as complicating maintenance procedures and incurring additional costs. Moreover, not using this provision is mandatory in the Netherlands.
By excluding the compensation provision, the focus remains on gaining comprehensive knowledge about longitudinal forces in rail-structure interaction, aligned with the conditions that railway bridges in the Netherlands must adhere to.

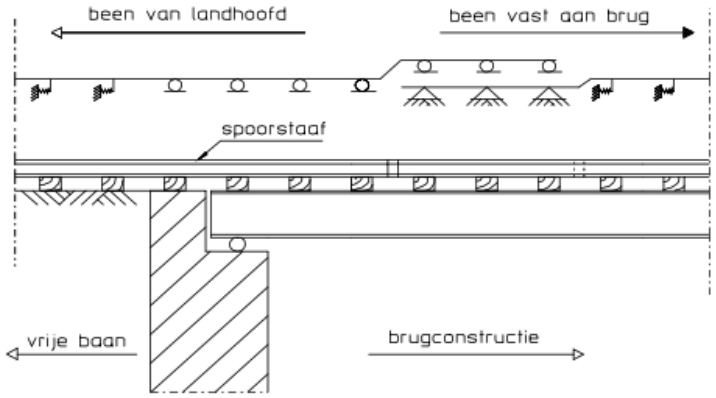

Figure 2.7: Compensation provision, (ProRail, 2018)

2.1.2. Loads on the railway system

There are three types of loads that are important to consider when the rail-structure interaction is investigated. These are the thermal load, the longitudinal traffic loads, and the vertical traffic loads. All these three different loads on the railway system will be discussed in this subsection in different sub-subsections.

2.1.2.1. Thermal Load

When the rails are not fastened, they are able to freely expand or contract as a consequence of temperature changes. The change in length is as follows:

$$\Delta l = \alpha \Delta T l \tag{2.1}$$

where:

- Δl : Change in length [m]
- α : Thermal expansion coefficient [$^\circ C^{-1}$]
- ΔT : Temperature change compared to reference temperature [$^\circ C$]
- l : Length of the element [m]

(Esveld, 2005)

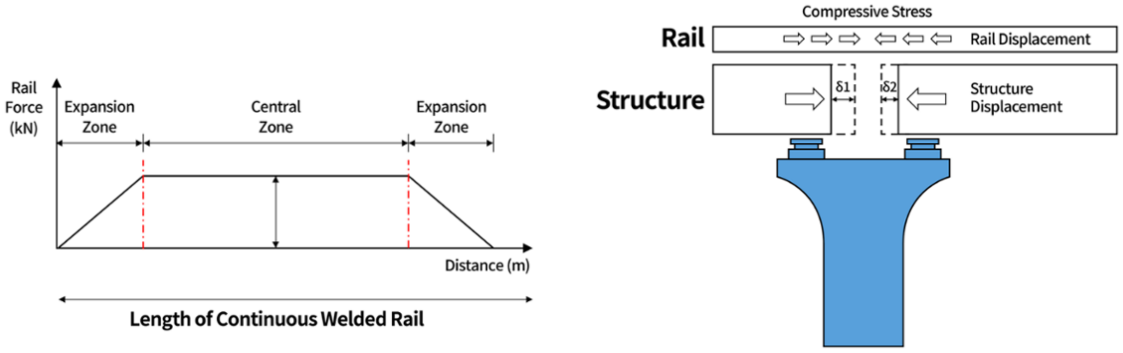

(a) Rail force distribution in CWR under temperature changes

(b) Rail-structure interaction due to thermal loads

Figure 2.8: Expansion and normal load distribution due to thermal load (Midas, n.d.)

However, as explained in the previous subsection, the expansion of rails is constrained by the combined shear resistance of the rails, sleepers, fasteners, and ballast. In continuous welded rails, the rail lengths are sufficiently long that longitudinal expansion is fully restricted in the 'central zone', as illustrated in Figure 2.8a. The normal force induced in the rails by temperature changes can then be calculated using the following formula: (Esveld, 2005)

$$N = -EA\alpha\Delta T \tag{2.2}$$

where:

- N : Normal force [N]
- E : Youngs modulus [N/m^2]
- A : Area [m^2]

The minus in Equation 2.2 indicates that an increase in temperature results in a compressive normal force. Figure 2.8b illustrates that the bridge structure can freely expand or contract due to temperature changes, whereas the rails, being fixed and continuous, cannot. Besides the temperature-induced stresses in the rails, additional stresses also arise from temperature changes in the bridge deck. The expansion and contraction of the bridge deck due to temperature cause relative displacements between the rails and the bridge structure. Since the rails are continuously welded and cannot expand or contract autonomously, additional stresses are generated.(Esveld, 2005)
The temperature changes that needs to be taken into account when the thermal loads are taken into account are presented in Table 2.3. (ProRail, 2018)

Construction element	**Minimum** [$^\circ C$]	**Reference** [$^\circ C$]	**Maximum** [$^\circ C$]	**Decrease in temperature** [$^\circ C$]	**Increase in temperature** [$^\circ C$]
Rail	-23	25	55	-48	30
Construction with ballast	-15	10	35	-25	25

Table 2.3: Temperature changes of different construction elements, values from (ProRail, 2018)

2.1.2.2. Longitudinal Traffic Loads

The interaction between the rail and the railway bridge is investigated in this thesis. In this system, a train runs over the railway bridge, exerting longitudinal loads that the system must resist. These longitudinal loads consist of braking and acceleration forces generated by the train. It is essential to consider these loads at various locations on the railway bridge to account for quasi-static behavior and identify the most critical locations.
Longitudinal traffic loads act on the top of the rails, with braking loads exerting force in the direction of the train's travel and acceleration loads exerting force in the opposite direction. This directional aspect is illustrated in Figure 2.9.

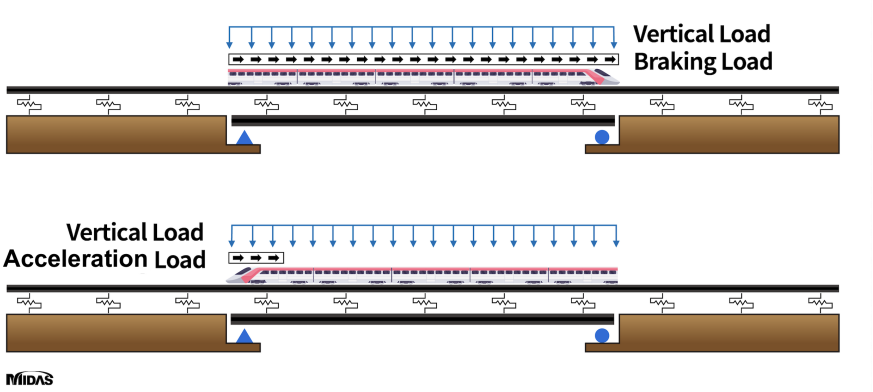

Figure 2.9: Braking and acceleration forces on a bridge structure, (Midas, n.d.)

2.1.2.3. Vertical Traffic Loads

As also stated in the previous sub-subsection a train travels over the investigated system and this needs to be taken into account. A train not only exert longitudinal traffic loads but also have vertical traffic loads, such as the weight of the train it selves and the weight of its passengers or cargo. In investigating rail-structure interaction, it is crucial to place the vertical traffic load in the most unfavorable position, subjecting it to various loading models according to the Eurocode. The loads will be placed on different possible unfavourable locations to find this critical location and to account for the quasi-static behaviour. Further, more in-depth information about these loading models will be presented in section 2.3.
When trains exert vertical loads at the most critical points on a railway bridge, the bridge deck bends, causing rotations at both ends of the deck. The rails are anchored to the bridge deck through sleepers embedded in the ballast bed. As the bridge deck bends, the fixed attachment of the rails to the deck tries to elongate the continuous welded rails (CWR). However, the inherent rigidity and fixed length of CWR prevent this elongation, leading to additional stresses, as illustrated in Figure 2.10. (Midas, n.d.)

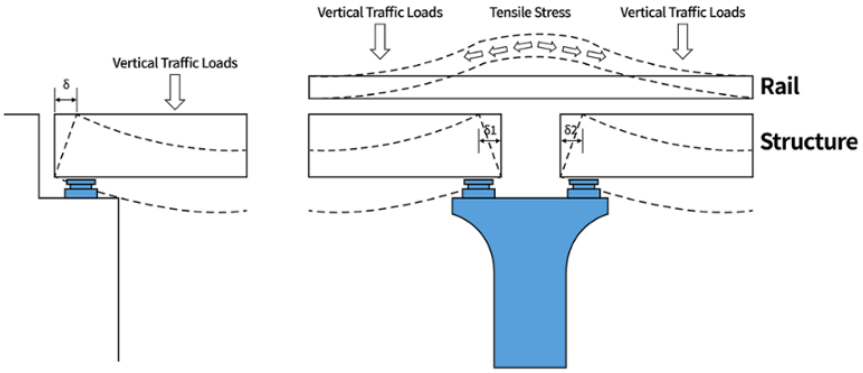

Figure 2.10: Increase in stress in the CWR due to deck bending, (Midas, n.d.)

2.2. Continuous Welded Rails (CWR)

As indicated in the problem statement of chapter 1, the transition from conventional rails to continuous welded rails (CWR) in the Netherlands brought significant changes to the railway system. While the introduction of CWR has several advantages, it also presents challenges, particularly in the context of railway bridge structures. (Enshaeian and Rizzo, 2020)
Conventional rail systems consist of individual rail segments bolted together with gaps between them, allowing for expansion and contraction due to temperature changes. However, these joints are structurally weak points, leading to noise, vibrations, and increased wear and tear on both the train wheels and the rails. This necessitates frequent maintenance. (Lim et al., 2003)(Enshaeian and Rizzo, 2020)
Continuous welded rails, on the other hand, are welded together, eliminating the joints and thus the associated problems of conventional rails. This results in smoother transitions for trains, reduced noise and

vibrations, and less wear and tear on the rail infrastructure, leading to lower maintenance costs and a longer life cycle for the track. Furthermore, the reduced vibrations enhance passenger comfort and allow for higher train speeds. (Lim et al., 2003)(Enshaeian and Rizzo, 2020)

(a) Conventional track

(b) Continuous Welded Rail track

Figure 2.11: Different track types(Midas, n.d.)

Despite these benefits, continuous welded rails have a notable disadvantage: they are highly susceptible to buckling and fractures under specific conditions. This susceptibility is particularly problematic at the joints of railway bridges, where the rigidity of CWR cannot accommodate the movement of bridge decks. Factors such as extreme temperature changes, braking, and acceleration of trains can cause significant longitudinal stresses in the CWR, leading to potential rail buckling or fractures. (Enshaeian and Rizzo, 2020)
This thesis focuses on understanding and mitigating the additional stresses that CWR experiences in the context of railway bridge systems. The interaction between the continuous welded rails and the bridge structure is crucial, as the discontinuity introduced by the bridge system imposes additional stresses on the otherwise continuous rails. (Enshaeian and Rizzo, 2020)

2.3. Design Code Regulations

To ensure structural safety across Europe, the European Union has established standardized design codes, applicable to all structures in EU member countries. These codes, with minor adjustments in the national annexes, must be adhered to by all structures, including railway systems.
This thesis investigates the rail-structure interaction of railway bridges in the Netherlands. As the Netherlands is an EU member, all calculations in this thesis must comply with the Eurocode regulations. Adjustments specific to the Dutch context are detailed in the Dutch annex and supplemented by ProRail's design regulations. ProRail, the rail network manager in the Netherlands, provides additional guidelines for railway infrastructure. The relevant Eurocodes for this topic include NEN-EN 1990: Basis of structural design, NEN-EN 1991-2: Traffic loads on bridges, both with their Dutch annexes, and ProRail's design requirements for bridges (Part 6).
This section is structured as follows: the first subsection discusses load models, examining how the Eurocode specifies the implementation of various loads on railway bridges. The second subsection addresses the combined response of the railway-bridge structure to different loads. The final subsection outlines the additional stress limits that the system must adhere to.

2.3.1. Loading situations

The three loading cases must comply with design code regulations. The Eurocode provides guidelines on vertical loads and longitudinal forces. The specific load values for these types of loads are detailed in the following sub-subsections. (European Commitee for Standardization, 2011)(European Commitee for Standardization, 2019)(ProRail, 2018)

2.3.1.1. Vertical Traffic Loads

The vertical traffic loading effects on the bridge are determined using various load models, each corresponding to specific types of rail traffic crossing the bridge under analysis. The longitudinal model developed in this thesis will incorporate the following load models: (European Commitee for Standardization, 2011)

- Load model 71
- Load model SW/0
- Load model SW/2

In the Netherlands, it is essential to consider these three load models, as they account for different types of rail traffic, such as passenger and cargo trains, and potential future changes in train types. This ensures that structures are designed to sustain loads over their entire lifetime. While there are additional loading models for HSL traffic and unloaded wagons, they are not considered in this thesis. (European Commitee for Standardization, 2011)(European Commitee for Standardization, 2019)(ProRail, 2018)

Load Model 71
The load model 71 gives the statics response of the railway structure due to normal rail traffic. The load model is visualised in Figure 2.12.

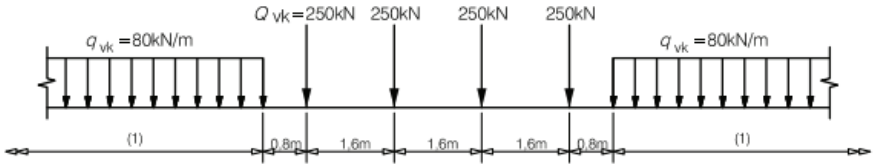

Figure 2.12: Load model 71, (European Commitee for Standardization, 2011)

The values in this model must be multiplied by a factor α. In the updated Dutch Annex, α is set at 1.0 for the combined reaction in longitudinal force analysis of rail-structure interactions under varying loads. Initially, α had a value of 1.21, as employed in the reference projects discussed in chapter 3. (European Commitee for Standardization, 2019)

Load Model SW/0 and SW/2
The second and third load models are the SW/0 and SW/2 models. SW/0 is the load model for the static response to a vertical traffic load due to normal rail traffic on continuous beams. SW/2 is the load model for the static response to a vertical traffic load due to heavy rail traffic. These models share the same geometry but have different load magnitudes and distance values. The model is visualised in Figure 2.13, and the corresponding values are provided in Table 2.4. (European Commitee for Standardization, 2011)

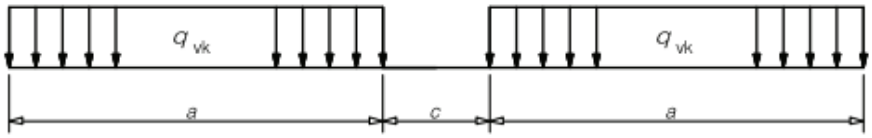

Figure 2.13: SW/0 and SW/2 load models, (European Commitee for Standardization, 2011)

Load models	$\mathbf{q}_{vk}$ **[kN/m]**	**a [m]**	**c [m]**
SW/0	133	15	5.3
SW/2	150	25	7

Table 2.4: Characteristic values for the SW/0 and SW/2 load models, (European Commitee for Standardization, 2011

For SW/0, the loads must be multiplied by the factor α, as discussed earlier in connection with load model 71. In contrast, SW/2 does not require multiplication by the factor α.(European Commitee for Standardization, 2011)

2.3.1.2. Longitudinal Traffic Loads

Longitudinal traffic loads significantly influence longitudinal force analysis in railway systems. These loads primarily consist of braking and acceleration forces exerted by trains on the rails, resulting in additional stresses that must remain within safety limits.

Longitudinal forces act on the system through the rails, with braking forces acting in the direction of the train's movement and acceleration forces acting in the opposite direction. (European Commitee for Standardization, 2011).

Acceleration forces: Q_{lak}= 33 [kN/m] $L_{a,b}$[m]≤ 1000 [kN]
For load models: 71, SW/0 and SW/2

Braking forces: Q_{lbk} = 20 [kN/m] $L_{a,b}$[m]≤ 6000 [kN]
For load models: 71 and SW/0
Q_{lbk} = 35 [kN/m] $L_{a,b}$[m]
For load model SW/2

(European Commitee for Standardization, 2011)
For longitudinal force models using Load Models 71 and SW/0, the characteristic values must be multiplied by the same α value specified for vertical traffic load models. It is crucial to account for the combination of longitudinal forces with the overall railway construction. When multiple tracks are present on the structure, their respective travel directions and the associated longitudinal and vertical traffic loads must be considered. However, this thesis focuses on the analysis of single-track railway bridges. (European Commitee for Standardization, 2011)(European Commitee for Standardization, 2019)

2.3.2. Combined rail-structure reaction on varying loads

When continuous welded rails are used, the combined resistance of the rail and bridge constructions becomes crucial, effectively countering various forces such as longitudinal movement, thermal expansion, and more. For a detailed discussion on the different construction components contributing to this resistance, refer to section 2.1, which covers aspects such as the stiffness of the bridge deck against bending, the thermal expansion coefficient of the bridge deck, and the rail's specific stiffness, including its resistance against longitudinal movement.
The Eurocode offers an example for calculating the spring stiffness of each bridge pier, although implementation may vary based on engineering input. The spring stiffness for the longitudinal spring model can be determined using the following formula:

$$K = \frac{F_l}{(\delta_p + \delta_\varphi + \delta_h)} \tag{2.3}$$

where:

F_L : Longitudinal force [kN]
δ_p : Bending of the bridge pier [mm]
δ_φ : Rotation of the foundation [mm]
δ_h : Horizontal movement of the foundation [mm]

(European Commitee for Standardization, 2011)
An illustration of the different deformations of the bridge pier is given in Figure 2.14.

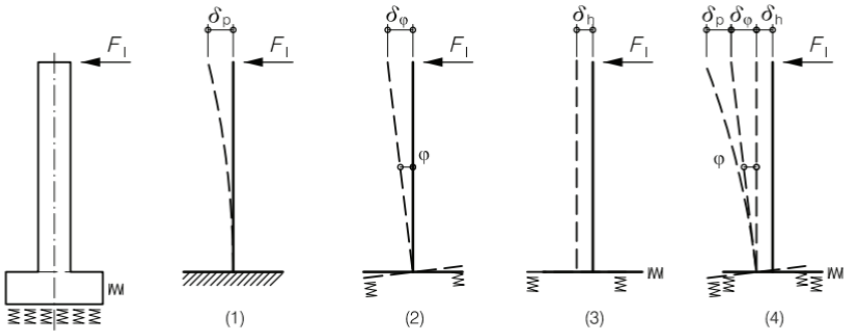

Figure 2.14: The different deformations of the bridge pier used in railway bridges, (European Commitee for Standardization, 2011)

The longitudinal force analysis can be modeled using a spring model, as suggested in Figure Figure 2.15. In this model, the connection between the rails and the bridge deck is shown as number 5. The ballast bed, consisting of ballast, sleepers, and fixings, is represented by a horizontal non-linear spring. This figure also clearly illustrates that the overall system experiences increased stiffness when influenced by the embankment (number 3). (European Commitee for Standardization, 2019)

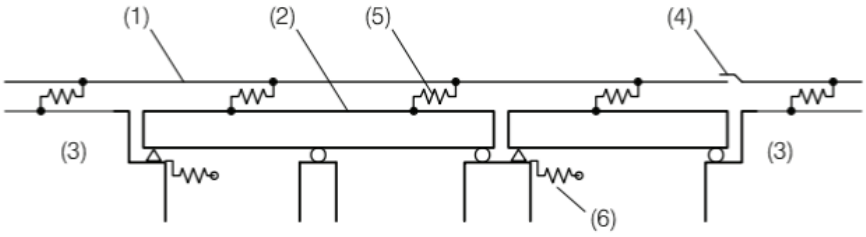

Figure 2.15: Loading responses of the interaction between railway bridge and rail, (European Commitee for Standardization, 2011)

Where:

(1) : Rail
(2) : Bridge deck
(3) : Embankment
(4) : Compensation provision (not used in this investigation)
(5) : Non linear springs in longitudinal direction, connection between rail and construction
(6) : Spring in longitudinal direction representing the resistance coming from the support or bridge pier

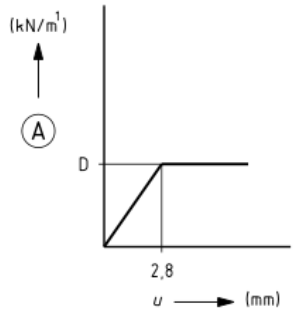

Figure 2.16: Force-displacement diagram for a rail in ballast, (European Commitee for Standardization, 2019)

The non-linear spring representing the connection between the rail and the bridge deck has the associated spring characteristic presented in Figure 2.16. There are two types of values given for this spring characteristic that represent this connection: one for the loaded spring (when the train is at the location of the spring) and one for the unloaded spring (when the train is not at the location of the spring). The limiting values for

these two situations are given below:

Rail in ballast, high value, loaded track $F_{L2} = 40kN/m \quad \rightarrow \quad k_H = \frac{40}{2.8} = 14.29kN/mm$
Rail in ballast, high value, unloaded track $F_{L2} = 20kN/m \quad \rightarrow \quad k_H = \frac{20}{2.8} = 7.14kN/mm$

This thesis focuses on longitudinal forces, therefore only the high values are shown above. Lower values are also available, but they are used for other mechanical purposes than longitudinal forces. (European Commitee for Standardization, 2019)

When engineers prefer not to include the complete influence length of the embankment in the longitudinal force model, possibly due to concerns about excessive model size and lengthy calculation times, the Eurocode provides an alternative. It suggests using a spring that can represent the embankment's stiffness over the influence length. This spring has a horizontal characteristic, which can be calculated using the following formula:

$$K_{track} = K\sqrt{\frac{EA}{K}} \tag{2.4}$$

Where for this case E and A are the Young's Modulus and area of the rails, and K can be calculated with K = $\frac{D}{2.8mm}$, where D = 20 kN/m for an unloaded track and D = 40 kN/m for a loaded track. (ProRail, 2018)

2.3.3. Additional stress limits

The main problem addressed in this thesis is the potential for rails to exceed permissible stress limits, leading to buckling or fractures that must be prevented. By conducting a longitudinal force analysis, it becomes possible to calculate the additional stresses in the rails due to the presence of the railway structure. According to the Eurocode specifications, the additional stress in the rails must not exceed the following limits:

Compressive stress ≤ 72 N/mm^2
Tensile stress ≤ 92 N/mm^2
(European Commitee for Standardization, 2011)

These limits are applicable for UIC54 and UIC60 rail types, for straight tracks or tracks with a minimum arc radius r ≥ 1500 m, and for ballast tracks. (European Commitee for Standardization, 2011)(European Commitee for Standardization, 2019)

3

Projects analysis

This chapter delves into the analysis of two projects conducted by Wagemaker, aiming to understand the differences, challenges, and implementation of longitudinal forces within a comprehensive model. The objective is to gain insight into how complex structures with various elements and connections could be represented in a longitudinal force model to calculate additional rail stresses due to the presence of the structure.
The first section of this chapter examines the Theemswegtracé in Rotterdam, providing a general description of the project and exploring how this complex structure could be represented in a longitudinal force model. Subsequently, the second section explores another project by Wagemaker involving a rail crossing the new vehicle road at Eygelshoven in Limburg. Here, the focus of the project is on analysing how the complex structure, with its diverse elements and connections, can be accurately represented in a model. This model aims to simplify real-world complexities while ensuring safety and using correct material and cross-sectional properties.
Upon completing this chapter, a clearer understanding emerges regarding the translation of railway bridges into longitudinal force models. This newfound knowledge serves as a crucial foundation for subsequent sections of the thesis, where it will be applied to implement various aspects of longitudinal force modeling. Additionally, it will contribute to gaining insights into the significance of including certain parameters as variables to investigate their influence on the magnitude of additional rail stresses.

3.1. Theemswegtracé

The Port of Rotterdam, one of Europe's largest ports, serves as a critical hub for various transportation modes. The railway connection from the west side of the port to the hinterland utilises the Betuweroute, with a notable bottleneck being the Calandbrug. Increased shipping traffic to the Brittanniëhaven has necessitated more frequent openings of the Calandbrug, impacting railway operations. Additionally, the growing volume of incoming shipping has led to increased rail traffic. Compounding these challenges is the fact that the Calandbrug reached the end of its technical lifespan in 2020. To alleviate these issues, the first segment of the Betuweroute was relocated through the construction of the Theemswegtracé, a 4-kilometer railway track completed between 2018 and 2021. The track runs from Merseyweg to Moezelweg, where it connects to the existing Havenspoorlijn.(Mobilis, n.d.)(Wagemaker, 2018)

The configuration of the Theemswegtracé is depicted in 3.1a, clearly delineating the various components of the railway track. The track consists of several distinct parts, such as in situ concrete bridges, prefab concrete bridges, steel bridges, and embankments. The corresponding part numbers for each segment of the track are illustrated in 3.1b. This visual representation provides insight into the diverse structures and elements comprising the track (Wagemaker, 2018).

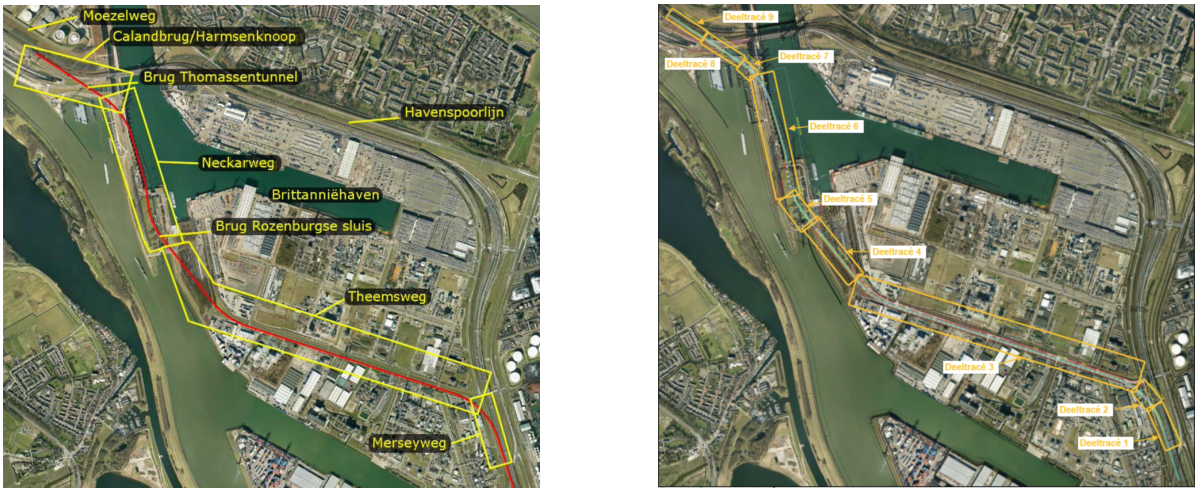

(a) Theemswegtracé with the corresponding names

(b) Theemswegtracé with the corresponding part numbers

Figure 3.1: Theemswegtracé(Wagemaker, 2018)

During the project, Wagemaker shared responsibility for conducting the longitudinal force analysis. This thesis section primarily focuses on the second and third part of the track. The second part comprises an in situ concrete railway bridge, while the third part features a prefab railway bridge. The structure of the third part will be described later to explore how it could potentially be translated into a longitudinal force model. This focus on the third part comes from its initial relevance for this thesis, as it involves prefab bridges where considerations like shrinkage and creep are initially not necessary. However, this analysis can later be extend to include in situ railway bridges, incorporating a translation of the construction of the second part into a potential model. (Wagemaker, 2018)
To achieve a thorough understanding of how this structure can be modeled, it is essential to initially acquire information about its construction and delineate all the elements that require modeling. Therefore, the following parts will provide an explanation of the two parts, outlining the constituent elements of each.

Part 2: In situ railway bridge

Figure 3.2: A segment of part two of the Theemswegtracé

Part two of the Theemswegtracé comprises two individual in situ railway bridges, each dedicated to a specific direction of travel. The north bridge have a total length 128.6 meters, while the south bridge extends over

150.1 meters. Both bridges are constructed with four spans, resulting in the total bridge lengths mentioned. A cross-sectional view of these railway bridges in the second part of the track is illustrated in Figure 3.3. These rails are supported by sleepers laid on the bridge deck, with ballast placed around them. Fasteners secure the rails to the sleepers.(Wagemaker, 2018)

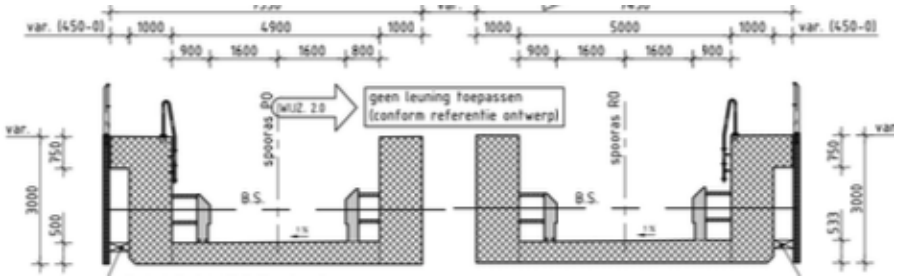

Figure 3.3: Cross section Trace 2 Theemswegtracé, (Wagemaker, 2018)

The substructure of the railway bridge in part 2 of the Theemswegtracé is depicted in Figure 3.4. This illustration demonstrates that the bridge deck rests on elastomeric bearings, which are connected to the bridge pier located beneath them. These piers, in turn, are founded on piles, ensuring robust support for the entire structure.

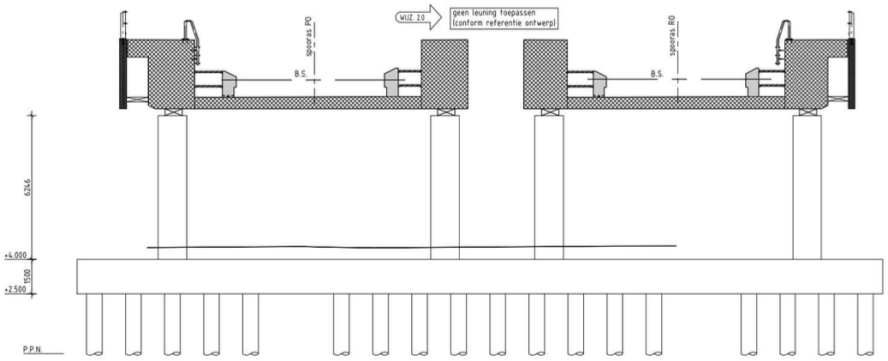

Figure 3.4: Cross section of including the substructure of part 2 of the Theemswegtracé, (Wagemaker, 2018)

Part 3: Prefab railway bridge

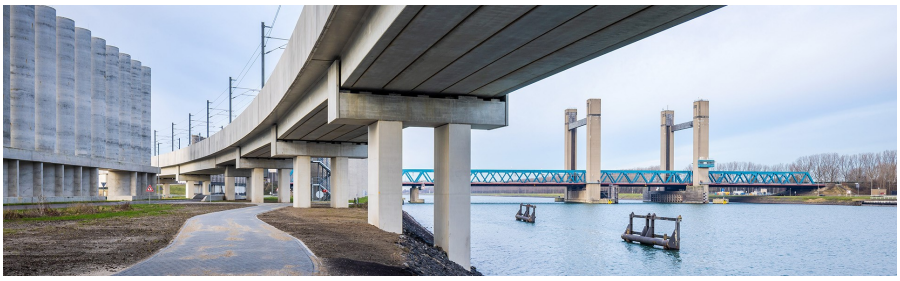

Figure 3.5: A segment of part three of the Theemswegtracé

The third part of the Theemswegtracé showcases a prefab railway bridge accommodating travel in both directions on a shared bridge deck with consistent cross-sections. Spanning approximately 1780 meters, part 3 of the TWT encompasses various span lengths. Notably, this section's structure integrates only three different span lengths—30, 33, and 39 meters—allowing for the utilisation of different bridge deck cross-sections during construction. These three distinct span lengths and their corresponding cross-sections are visualized in Figure 3.6.
On the prefab bridge deck, a ballast structure is placed. This ballast structure consists of ballast with sleepers embedded within it, onto which the rails are connected using fasteners.

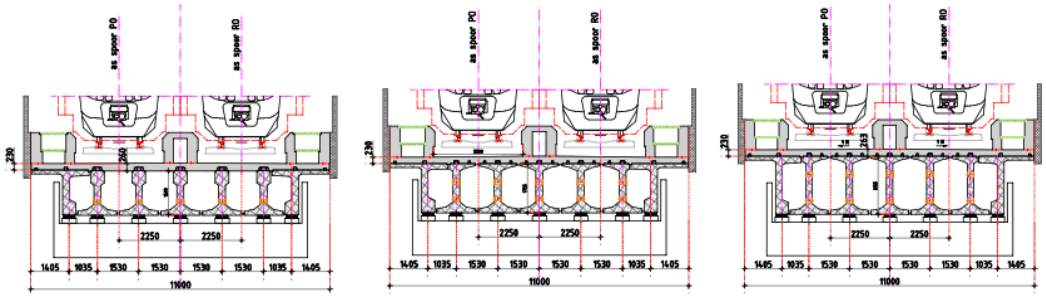

Figure 3.6: The three different cross sections of Trace 3 Theemswegtracé, (Wagemaker, 2018)

The substructure of part 3 of the Theemswegtrace is depicted in Figure 3.7. This illustration provides a clear view of the various elements involved. The bridge deck is supported by elastomeric bearings, with a thin concrete layer ensuring a constant distance between the bridge deck and the bridge pier, regardless of the height of the elastomeric bearings. These bearings rest on a beam that distributes the resulting forces over two piers, which are connected to the foundation. The foundation, in turn, is built on piles, ensuring stability and support for the entire structure.

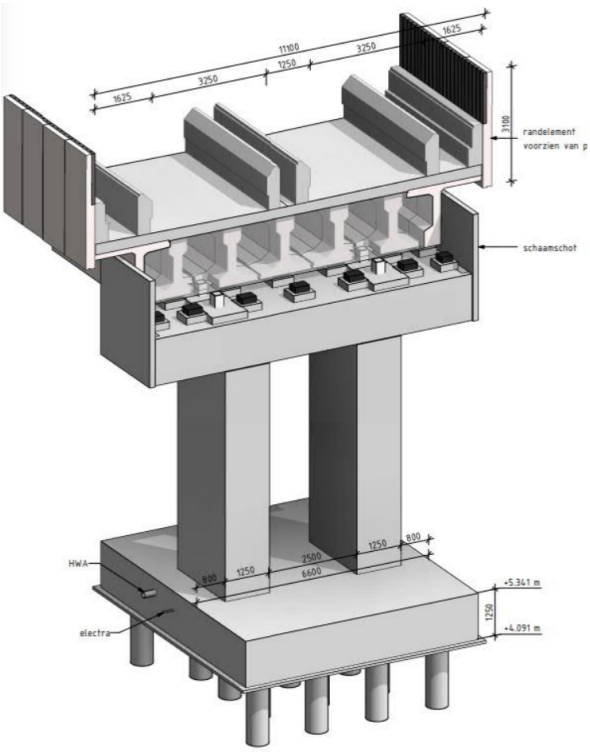

Figure 3.7: Visualisation of the substructure of part 3 of the Theemswegtracé, (Wagemaker, 2018)

3.1.1. Longitudinal force analysis

Now that all the various elements of the structure are known, it is possible to think about how a possible longitudinal force model for part 3 of the Theemswegtracé could be represented. This will be presented in this subsection.

According to the literature, one approach to calculate longitudinal force distribution in railway systems could involve employing a spring model. In this model, the different elements and the interconnections between them could be represented by horizontal and vertical springs. Based on the information about part 3 of the Theemswegtrace obtained in section 3.1, a possible representation of a segment of part 3 of the Theemswegtracé in a longitudinal force model is illustrated in Figure 3.8.

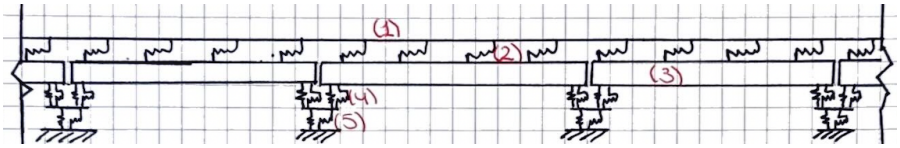

Figure 3.8: Overview drawing of a potential modeling of a segment of part 3 of the Theemswegtracé

When analysing longitudinal forces, angular forces on the railway bridge are not considered. Therefore, using a two-dimensional model is suitable for capturing the longitudinal behaviour of the system.
In Figure 3.8, the rail is denoted as number 1 and can be represented as a 1D-beam element in the model. Since the railway system consists of two rails on which the train runs, the cross-sectional properties of the modeled beam should reflect the values of both rails. This implies that the area and moment of inertia of the modeled beam are twice the values of a single rail.
Number 3 in Figure 3.8 corresponds to the prefab bridge deck of trace 3 in the Theemswegtracé project. For the longitudinal force model, this element is represented as a beam with cross-sectional and material properties matching those of the prefab slab depicted in Figure 3.6. The longitudinal force model focuses on one travel direction. Since trains travel in both directions across the entire cross-section of the prefab bridge deck, the cross-sectional properties of the entire prefab bridge deck are considered in the model. The span length determines the appropriate cross-section of the bridge deck used in this analysis.
As described in the general description of the structure of part 3 of the Theemswegtracé, it becomes evident that a ballast structure is placed on the prefab bridge deck. This ballast structure connects the rail with the bridge deck and possesses a certain horizontal and vertical stiffness. This connection could be represented as a spring, designated as number 2 in Figure 3.8. The ballast structure is relatively stiff in the vertical direction, with minimal vertical movement between the rail and the prefab bridge deck. Therefore, the vertical stiffness of this spring can be considered almost infinite. On the other hand, the horizontal spring stiffness could be represented by the spring characteristic as given by the Eurocode in Figure 2.16. However the horizontal spring stiffness could vary based on engineering input and other factors.
As visualised in Figure 3.7, the bridge deck is placed on elastomeric bearings, which rest on a beam distributing the resulting forces over two piers. These piers are supported on a pile foundation. The elastomeric bearing could be represented as a spring, denoting their resistance against horizontal and vertical motion, illustrated with number 4 in the Figure 3.8. The vertical movement between the bridge deck and the beam atop the pier is relatively low, thus the vertical stiffness can be considered almost infinitely high. In the horizontal direction, the spring characteristic depends on the number of elastomeric bearings used and the resistance against horizontal movement of a single elastomeric bearing.
The distribution beams, piers, and pile foundation could indeed be modeled as separate elements in the longitudinal force model, each with their own cross-sectional and material properties. However, considering that the focus of the longitudinal force model is primarily on the stresses in the rails, the individual stresses, forces, and displacements of these elements may not be of interest in this case. Therefore, it is also feasible to represent these three elements collectively as one horizontal and vertical spring. This spring would effectively represent the combined resistance of the system of elements against horizontal and vertical deformations, as visualised in Figure 3.8 as number 5.
Determining the values of these springs can be achieved by modeling these elements together in a separate model and analysing their displacement when a certain load is applied to the system, as illustrated in Figure 2.14. Alternatively, these values could be calculated based on engineering input and analysis.
As demonstrated, there are different approaches to incorporating these elements into the longitudinal force model, and the choice depends on the specific requirements and considerations of the analysis at hand.

Based on the results of the analysis conducted by Wagemaker, it was found that the rail stresses exceeded the limits. Consequently, it was determined that the horizontal movement of the bridge deck should be more restricted. This was achieved by implementing a stiffer connection between the bridge deck and the substructure. Specifically, the bridge deck needed to be more stiffly restricted on one side of each bridge deck, and this was accomplished using fixations.
Wagemaker opted to use braking bridge piers and non-braking bridge piers for this purpose. Braking piers provide more stiffness to the side of the bridge deck supported by these piers. However, the placement of longitudinal fixed points could also be adjusted to achieve the desired effect, depending on engineering input and considerations.

Overall, the decision regarding the placement and type of fixations is based on engineering judgment and analysis of the specific requirements and constraints of the project.

This is one method for analysing longitudinal forces for the Theemswegtracé. Other methods may also be employed, depending on the engineer's findings.

3.2. Eygelshoven Rail-Road crossing

The vehicle infrastructure in the former mining area in Limburg required improvement to enhance accessibility to the region and stimulate economic and tourism activities. To address this, the province of Limburg introduced the plan to realise the 'Buitenring Parkstad Limburg' on March 31, 2011. This project aimed to upgrade the vehicle highway system in the area, facilitating better connections between cities and villages, and enhancing links with the national and international highway systems. The plan involved constructing a new regional road connection comprising 2x2 lanes, utilising existing roads in part. Construction activities commenced in 2014 and were completed by the summer of 2019. (Wagemaker, 2015)(Besix, n.d.)
The new road intersects the existing railway system at two points, requiring non-level crossings to prevent interference between the two systems. These rail-road crossings are depicted in the project overview in Figure 3.9 and include:

- The railway system crossing with the road from Heerlen to Kerkrade (KW170)
- The railway system crossing with the road from Sittard to Heerlen (KW04)

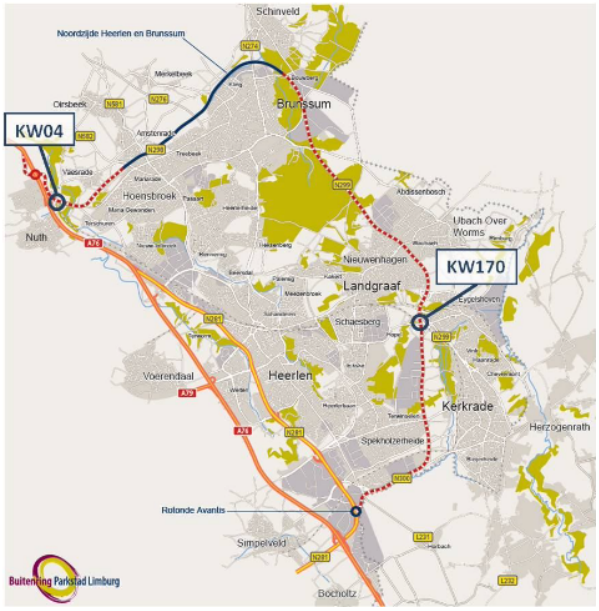

Figure 3.9: Improvement of the vehicle traffic system with the 'Buitenring Parkstad Limbrug", (Wagemaker, 2015)

Wagemaker had responsibility for the engineering of both intersections. This analysis focuses on the Eygelshoven intersection, specifically rail intersection KW170, with a focus on rail stresses arising from the rail-structure intersection.
To devise a longitudinal force model that accurately captures the additional rail stresses induced by the structure's presence, it is imperative to comprehensively analyse the general construction. This involves identifying the constituent elements of the construction and understanding how these elements are interconnected. Once the general construction has been thoroughly analysed, it will be possible to translate this information into a possible longitudinal force model. This model will clarify how the rail-road crossing can be represented to assess the impact on rail stresses.

Structure
A visual depiction of the rail-road crossing at Eygelshoven is provided in Figure 3.10. Here, the various components of the construction are illustrated, offering clear insight into the placement of elements and their

interactions. This visualisation will be examined in detail to analyse the structure's features.

Figure 3.10: Visual design of Eygelshoven, (Wagemaker, 2015)

In the visualisation, the road is positioned beneath the railway, supported by a bridge pier serving as an intermediate support, along with two soil-retaining walls at both ends of the railway bridge. The project utilises two in-situ concrete bridge decks, each with a length of 25.1 meters. Additionally, transition structures are employed before and after the bridge to ensure a smoother transition between the bridge and the embankment. Elastomeric bearings are placed between the bridge pier and the bridge deck. (Wagemaker, 2015)
A cross-section of the bridge, depicted in Figure 3.11, provides further insight into the structure's details. Notably, only the right side of the cross-section is relevant, as the left side serves as a passing place. The bridge deck measures 1400 by 7400 millimeters, while the floor supporting the vehicle road has dimensions of 1250 by 7400 millimeters, founded on a shallow foundation. Additionally, a ballast bed is situated on the bridge deck, consisting of ballast, sleepers, and fasteners securing the rails to the sleepers. (Wagemaker, 2015)
It is worth mentioning that the railway crosses the vehicle road at a 45-degree angle, adding to the complexity of the intersection. (Wagemaker, 2015)

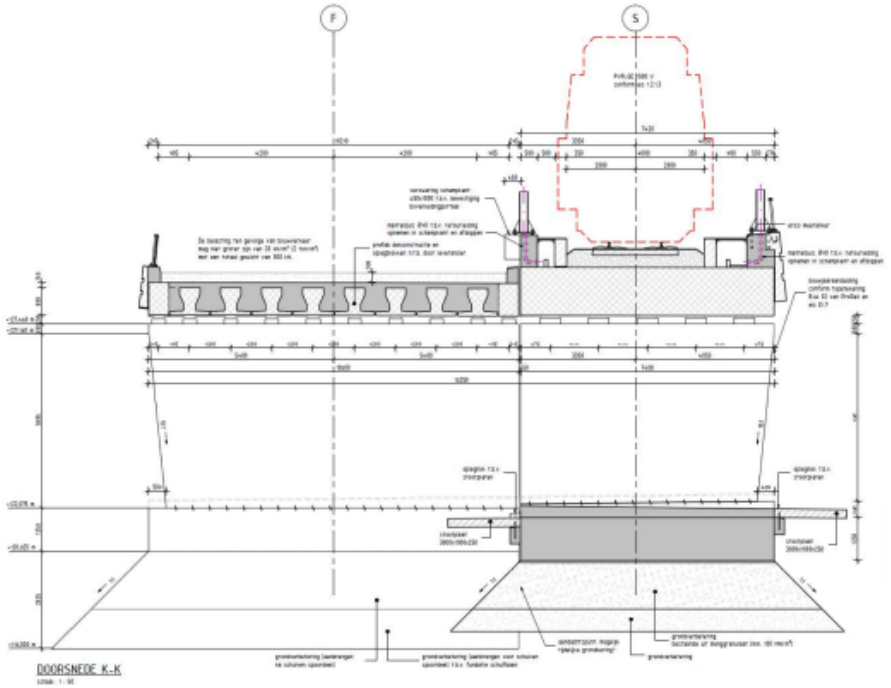

Figure 3.11: Cross section of Eygelshoven, (Wagemaker, 2015)

3.2.1. Longitudinal force analysis

Now that the structure details have been outlined, it is time to explore how these structural elements could be translated into a longitudinal force model. Longitudinal forces in a railway system intersecting with a structure can be effectively modeled using springs. These springs symbolise the stiffness of the connections between various elements. A cross-sectional depiction illustrating how the Eygelshoven project could be represented in a longitudinal spring model is presented in Figure 3.12.

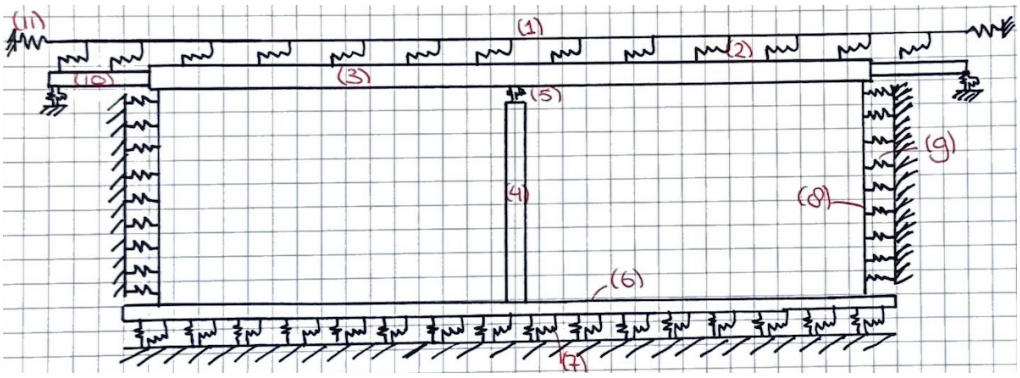

Figure 3.12: Cross section of model of project Eygelshoven

Once again, similar to the approach adopted for the Theemswegtracé, the model employed for Eygelshoven is two-dimensional, capturing responses and forces in both vertical and horizontal directions. The rail is represented using a beam element in the spring model, with cross-sectional properties such as area and moment of inertia doubled to account for the two rails.

As described in the structure details, two in-situ bridge decks are employed, each supported by two soil-retaining wall and an intermediate pier. Both bridge decks have a length of 25.1 meters, as depicted by number 3 in the model cross-section. These bridge decks could be represented in the model as two beam elements, with cross-sectional and material properties matching those used in the project, as shown in Figure 3.11, and with a length of 25.1 meters.

Furthermore, transition structures are utilised at both ends of the bridge to ensure a smoother transition between the bridge structure and the embankment, depicted by number 10 in the cross-section.

Number 2 in the Figure 3.12 represents the connection of the rail to the bridge deck and the transition structure. In the vertical direction, this spring will have an almost infinitely high value because the vertical movement between the bridge deck and the rail is limited. In the horizontal longitudinal direction, the spring value is determined by the loaded and unloaded cases, as outlined in section 2.3.
Number 4 in the cross-section of the project represents the intermediate support of the bridge deck, which is supported by a pier. In this model, the pier is represented as a 1D beam element with the cross-sectional properties of the pier.
Similarly, the side walls in this project (illustrated with number 8 in the figure) are also modeled as a 1D beam with the respective cross-sectional properties.
Number 5 represents the elastomeric bearings situated between the bridge pier and the bridge deck. In the system model, these elastomeric bearings are represented by horizontal and vertical springs. Due to minimal vertical movement of the bridge deck relative to the pier, the spring characteristic in the vertical direction is almost infinite. The horizontal spring characteristic varies depending on the number of elastomeric bearings used and the resistance of each elastomeric bearing against horizontal movement.
Beneath the railway bridge, the vehicle road is constructed at depth, supported by a floor. This floor could be modeled as a beam element with cross-sectional properties matching Figure 3.11 (represented by number 6 in Figure 3.12). The shallow foundation of the floor means that the soil beneath it provides resistance against movement for the structure and generates resulting forces. This resistance of the soil against horizontal and vertical movement could be modeled as springs, represented by number 7 in the figure, and depends on the soil strength.
Number 8 in Figure 3.12 represents the soil resistance against the side walls of the vehicle road tunnel beneath the railway bridge. The soil provides substantial longitudinal resistance to the system, especially when a train brakes or accelerates, as it can be compressed, generating significant resistance against longitudinal movement. It is crucial to note that the soil can only resist compression forces and not tension forces. This resistance against movement can be modeled using springs.
The final spring in the figure, represented by number 11, serves as the spring that represents the ending of the model. Alternatively, it can be chosen to include the influence zone of the embankment instead of using a model ending spring, allowing for different modeling approaches. The value of this ending spring can be calculated using Equation 2.4.

4

Methodology

This chapter explains the methodology for constructing the longitudinal model. The goal is to describe all the steps taken to build the models used in this investigation and how the results are stored and analysed to answer the research questions and achieve the purpose of gaining more knowledge about rail-structure interaction. The chapter is subdivided into three sections: Hand Calculations, Model, and Collection of Results and Method of Analysis.
In the first section, hand calculations are performed for a simplified structure with three different loading types: thermal, longitudinal, and vertical. These calculations provide insight into the influence of different parameters and validate the results of the final models if they align with expected magnitudes.
In the second section, the models used in this investigation are described. The different models have various parameters, which can be either fixed or variable. This section describes these parameters, including their cross-sectional and material properties, and their investigation bandwidth if they are variable. Furthermore, this section details the loads applied to the models, including their magnitudes, the different locations of the loads on the models, and how these loads are combined to capture the combined response. Finally, this section outlines the assessment criteria, specifying the criteria that the rail stresses in the models must meet. This includes the safety ranges for the additional rail stresses indicated in the literature study plus the initial rail stresses in the absence of a structure, such as a rail on the embankment.
In the third and final section of this chapter, the collection of results and the method of analysis are explained. This section describes how the results will be obtained for the various sets of parameters of the different variables, how these results will be stored, and how these results can be analysed to understand the influence of the different parameters on the resulting additional rail stresses.

4.1. Hand calculations

In this section, hand calculations for each loading situation are performed and cross-referenced with SCIA Engineer software to validate their accuracy. Ensuring that the internal forces from hand calculations align with the software results confirms the reliability of both methods.
Subsection 4.1.1 introduces the thermal load as a temperature increase and its structural impact, subsection 4.1.2 examines the longitudinal traffic load from train braking forces, and subsection 4.1.3 addresses the vertical traffic load from load model 71 and its influence on structural behavior.
The same cross-sectional and material properties are used for all three loading types. For the bridge deck, a beam with a height of 1000 mm and a width of 3143 mm, made of concrete class C30/37, is used, based on the Theemswegtracé bridge deck. The rail uses the UIC54 type, and since the model is two-dimensional and involves two rails, the area and moment of inertia are doubled. The properties for the deck and rail are as follows:

- EA_{deck} : 1.03×10^{11} N
- EA_{rail} : 5.86×10^{9} N
- EI_{deck} : 8.57×10^{15} Nmm^2
- EI_{rail} : 1.97×10^{13} Nmm^2

4.1.1. Thermal load

The hand calculations progress from a simplified structure to an increasingly refined one. For the thermal load hand calculations, a temperature rise of 25 degrees Celsius is chosen for the bridge deck, in line with Eurocode recommendations (see Table 2.3). This temperature increase is significant as it reflects real-world conditions for a concrete bridge deck with ballast. Additionally, performing hand calculations for a temperature increase allows for comprehensive analysis, with the option to later explore temperature decreases if needed, just by changing the sign of the temperature change. Therefore, the decision is made to focus on a temperature increase of 25 degrees Celsius for the hand calculations.

The most refined model that will be considered for the hand calculations is visualised in Figure 4.1

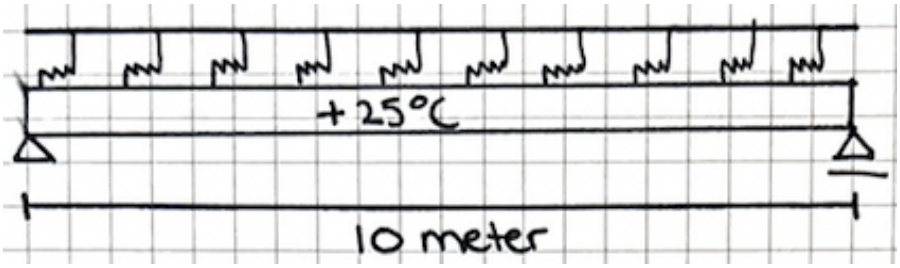

Figure 4.1: The most refined model for thermal load for the hand calculation

To simplify the structure, the springs are initially replaced with connecting bars. In this first consideration, the 10 springs, spaced 1 meter apart, are substituted by two connecting bars at the ends of the bridge deck, linking it with the rail. This allows for an examination of the bridge deck-rail interaction. For this simplified model, it is assumed that the stiffness parameters EA and EI of the connecting bars are infinite. This simplified structure is illustrated in Figure 4.2.

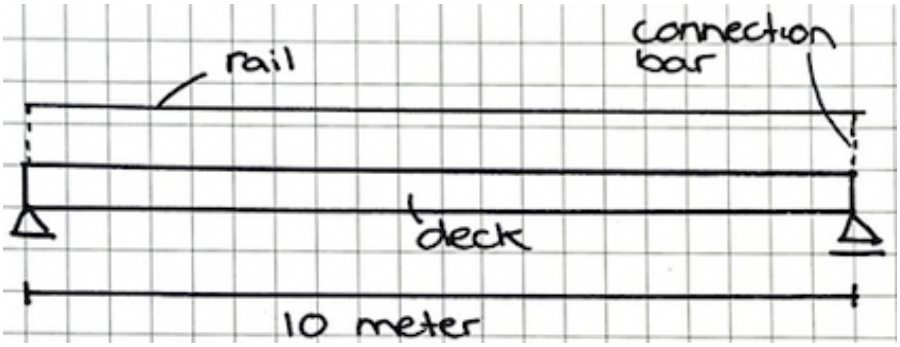

Figure 4.2: Simplified structure for thermal load for hand calculations

The bridge deck experiences a temperature change of +25°C, leading to thermal expansion. The thermal expansion coefficient, denoted by α, is 10^{-5}, indicating the degree of expansion for every unit change in temperature.

The rail and the bridge deck are connected. When the bridge deck experiences a temperature rise of 25 degrees, it undergoes extension. Since the rail and the bridge deck are connected, the rail will also extend, with a different magnitude due to differences in stiffness (EA). The rails are rigidly connected to the bridge deck with infinitely stiff connection bars. This difference in stiffness can lead to a phenomenon known as a "kwispel-effect," resulting in vertical bending of the structure due to the temperature change. Two critical conditions must be met: the strain of the rail and the bridge deck must be equal, and the normal force in the rail and the bridge deck must have equal magnitudes but opposite signs. Ensuring these conditions are met is crucial for maintaining structural integrity.
The strain of the bridge deck and the rail are given in Equation 4.1 and Equation 4.2:

$$\varepsilon_{deck} = \alpha \cdot \Delta T + \frac{N_{deck}}{EA_{deck}} \tag{4.1}$$

$$\varepsilon_{rail} = \frac{N_{rail}}{EA_{rail}} + \varepsilon_{kwispel} \tag{4.2}$$

The effect due to the "kwispeleffect" is illustrated in Figure 4.3:

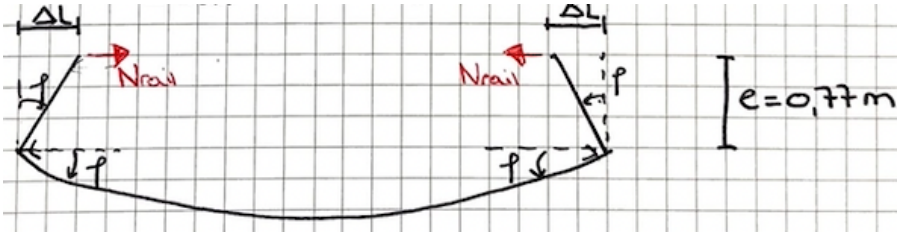

Figure 4.3: "Kwispeleffect"

The differences in length due to the "kwispeleffect" is:

$$\Delta L = \varphi \cdot e \tag{4.3}$$

The rotation φ due to the "kwispeleffect" also results in a rotation of the rail, as visualised in Figure 4.4:

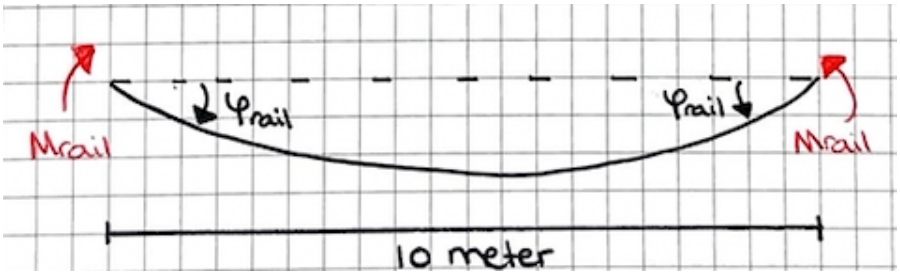

Figure 4.4: Rotation due to the "kwispeleffect"

The relationship between φ_{rail} and M_{rail} can be determined from the "vergeet me nietjes", as follows:

$$\varphi_{rail} = \frac{M_{rail} \cdot L}{2EI_{rail}} \tag{4.4}$$

The rotation phenomenon also occurs in the bridge deck, resulting in:

$$\varphi_{deck} = \frac{M_{deck} \cdot L}{2EI_{deck}} \tag{4.5}$$

The connection bars between the rail and the bridge deck results in a rigid connection between the two elements. This means that $\varphi_{deck} = \varphi_{rail} = \varphi$. Implementing this relationship and rewriting, results in:

$$M_{rail} = \frac{2EI_{rail} \cdot \varphi}{L} \tag{4.6}$$

$$M_{deck} = \frac{2EI_{deck} \cdot \varphi}{L} \tag{4.7}$$

The moment in the bridge deck must balance with the moment in the rail and the normal force in the rail. This results in the following equation:

$$M_{deck} = N_{rail} \cdot e - M_{rail} \tag{4.8}$$

Substituting Equation 4.6 and Equation 4.7 into Equation 4.8, results in:

$$\frac{2EI_{deck} \cdot \varphi}{L} = N_{rail} \cdot e - \frac{2EI_{rail} \cdot \varphi}{L} \tag{4.9}$$

$$\varphi(\frac{2EI_{deck}}{L} + \frac{2EI_{rail}}{L}) = N_{rail} \cdot e \tag{4.10}$$

$$\varphi = \frac{N_{rail} \cdot e \cdot L}{2EI_{deck} + 2EI_{rail}} \tag{4.11}$$

The difference in length due to the "kwispeleffect" occurs on both sides, resulting in:

$$\varepsilon_{kwispel} = 2 \cdot \frac{\Delta L}{L} \tag{4.12}$$

Using the relationship stated in Equation 4.3 and substituting it into Equation 4.12 results in:

$$\varepsilon_{kwispel} = 2 \cdot \frac{\varphi \cdot e}{L} \tag{4.13}$$

Substituting Equation 4.11 into Equation 4.13 gives:

$$\varepsilon_{kwispel} = \frac{N_{rail} \cdot e^2}{EI_{deck} + EI_{rail}} \tag{4.14}$$

Now that $\varepsilon_{kwispel}$ is known, it can be substituted into Equation 4.2, and also again stated Equation 4.1, gives:

$$\varepsilon_{deck} = \alpha \cdot \Delta T + \frac{N_{deck}}{EA_{deck}} \tag{4.15}$$

$$\varepsilon_{rail} = \frac{N_{rail}}{EA_{rail}} + \frac{N_{rail} \cdot e^2}{EI_{deck} + EI_{rail}} \tag{4.16}$$

Consistent with the previously stated critical conditions, this calculation must ensure that the strain in both the bridge deck and the rail are equal. Additionally, the normal force in the bridge deck and the rail must have equal magnitudes but opposite signs. Substituting Equation 4.15 and Equation 4.16, and noting that N_{deck} = -N_{rail}, results in:

$$\alpha \cdot \Delta T + \frac{N_{deck}}{EA_{deck}} = -\frac{N_{deck}}{EA_{rail}} - \frac{N_{deck} \cdot e^2}{EI_{deck} + EI_{rail}} \tag{4.17}$$

$$N_{deck} \cdot \left(\frac{1}{EA_{deck}} + \frac{1}{EA_{rail}} + \frac{e^2}{EI_{deck} + EI_{rail}}\right) = -\alpha \cdot \Delta T \tag{4.18}$$

Rewriting gives:

$$N_{deck} \cdot \left(\frac{1}{EA_{deck}} + \frac{1}{EA_{rail}} + \frac{e^2}{EI_{deck} + EI_{rail}}\right) = -\alpha \cdot \Delta T \tag{4.19}$$

$$N_{deck} = -\frac{\alpha \cdot \Delta T}{\frac{1}{EA_{deck}} + \frac{1}{EA_{rail}} + \frac{e^2}{EI_{deck}+EI_{rail}}} \tag{4.20}$$

Now everything is known this gives the following results:

- N_{deck} : -595.40 kN
- N_{rail} : 595.40 kN
- φ : 2.665 $\cdot 10^{-4}$ rad
- M_{deck} : 457.94 kNm
- M_{rail} : 0.52 kNm

The resulting internal force diagrams from the hand calculations are shown in Figure 4.5:

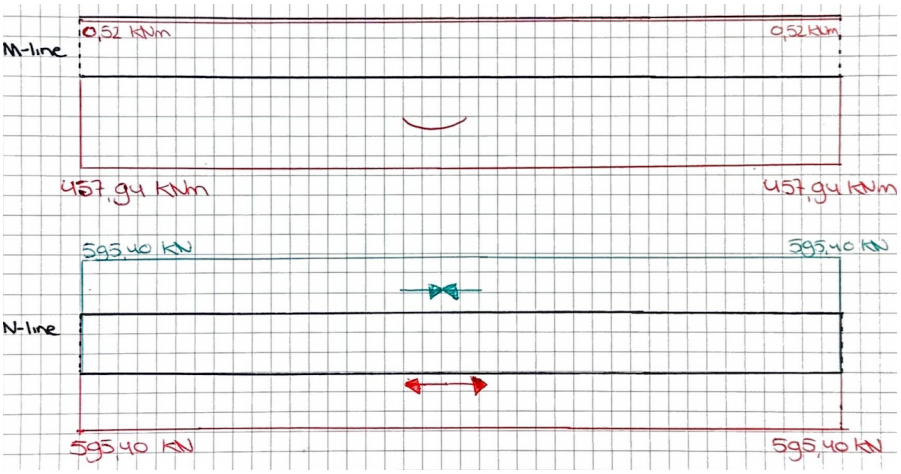

Figure 4.5: Internal force diagrams obtained from hand calculations for Thermal Load for the simplified structure

To verify these internal force diagrams, the same structure is modeled in SCIA Engineer, and the internal forces are calculated when the bridge deck is subjected to a temperature rise of 25°C. This results in the following bending moment and normal force lines:

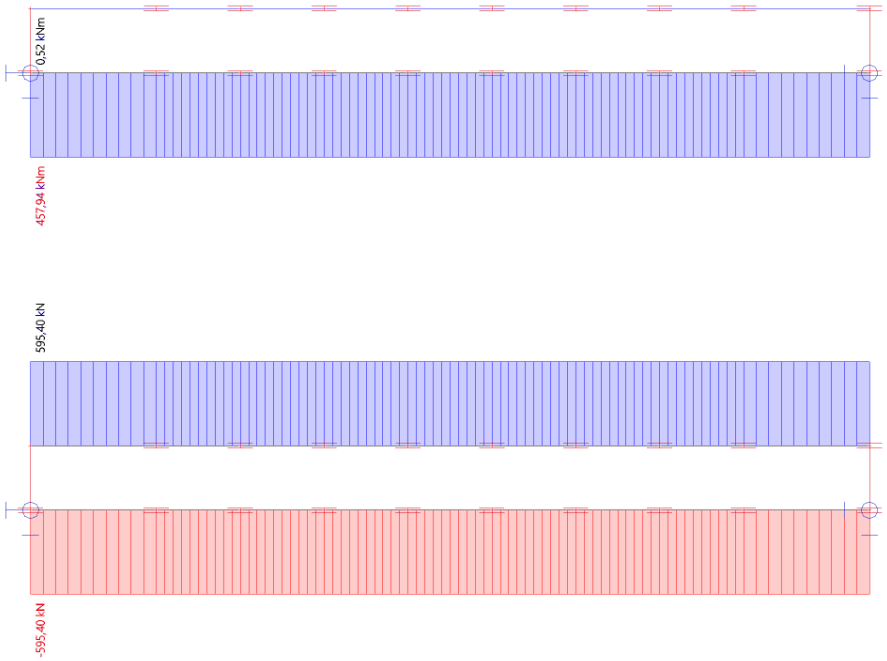

Figure 4.6: Internal force diagrams obtained from SCIA for Thermal Load for the simplified structure

It can be observed that the internal forces agree, confirming the correctness of the hand calculations.

This indicates that the structure can be further refined. This will be achieved by increasing the number of infinitely stiff connection beams in the structure, as shown in Figure 4.7.

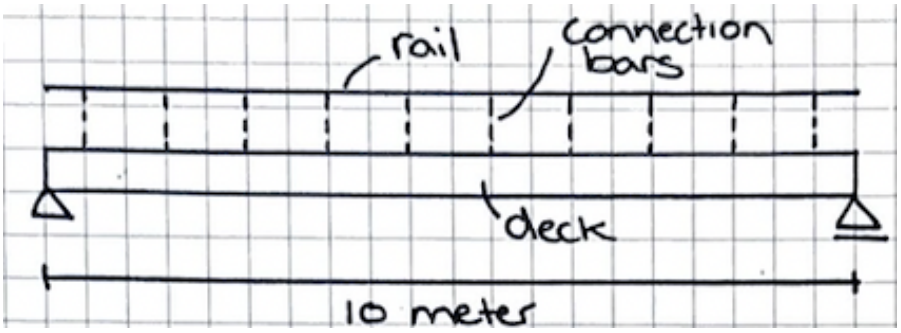

Figure 4.7: More refined structure for thermal load for hand calculations

Similar to the simplified version, the "kwispeleffect" occurs in this refined structure, as illustrated in Figure 4.8. Notably, the φ values are not the same for different bars.

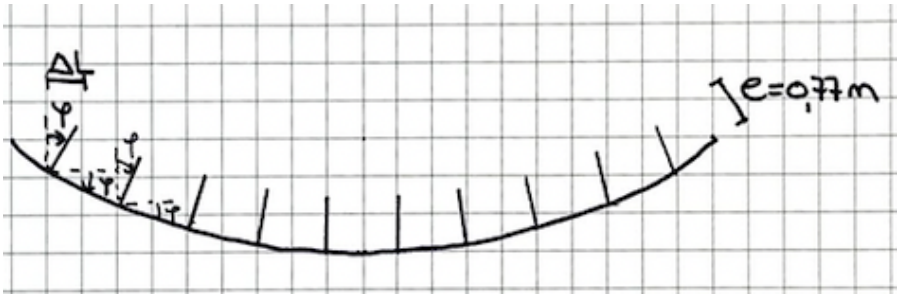

Figure 4.8: "Kwispeleffect" with more connection bars

Furthermore, it is observed that the strain due to temperature change of the deck remains consistent, and the condition that the strain equals the normal force divided by the EA stiffness of the rail and deck also remains unchanged.
As a result, the internal forces remain constant for this refined version. However, it is noted that the forces begin from 0.5 meters from the support points, as this is where the first connection between the materials occurs due to the rigid connection between the two materials.
The internal force diagrams obtained from the hand calculations, along with the validation internal force diagrams from SCIA Engineer are visualised in Figure 4.9 and Figure 4.10.

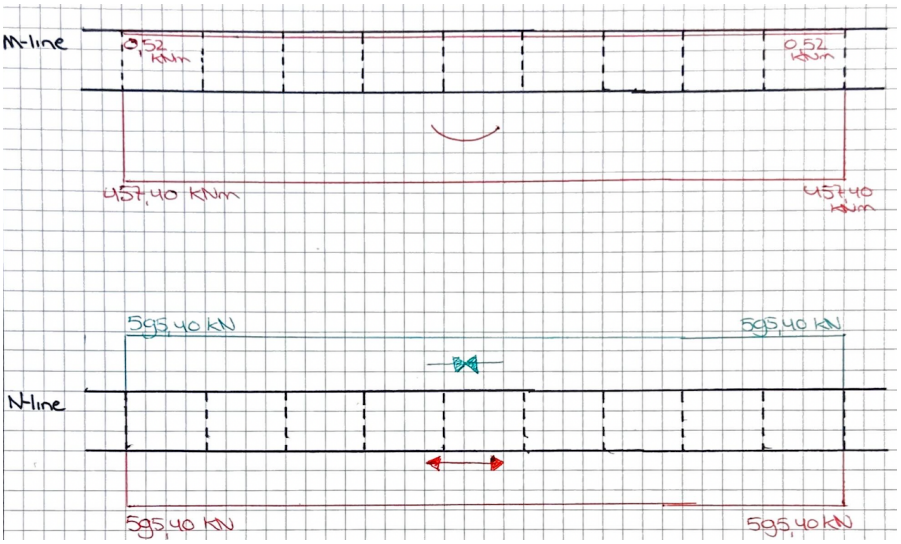

Figure 4.9: Internal force diagrams obtained from hand calculations for Thermal Load for the more refined structure

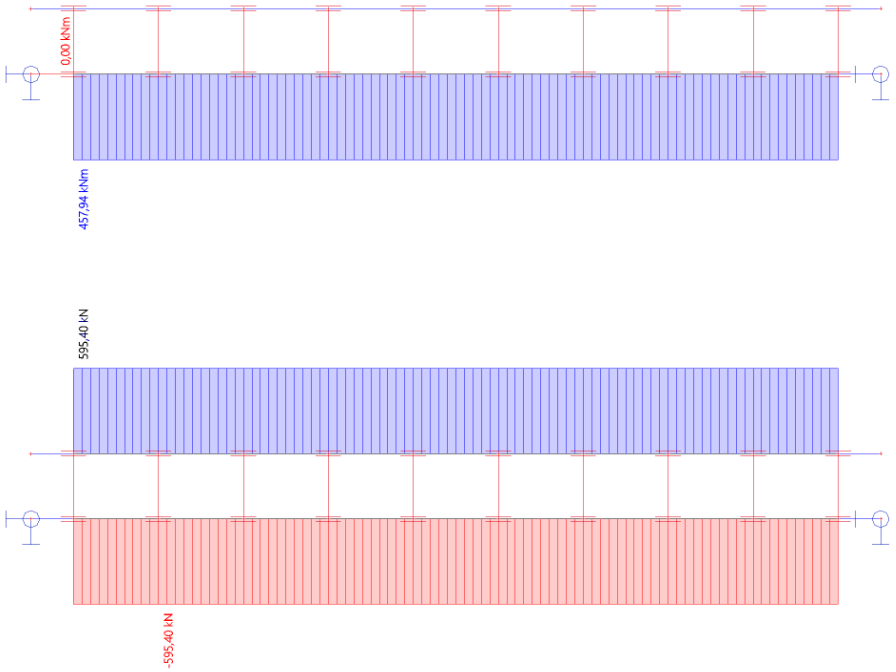

Figure 4.10: Internal force diagrams obtained from SCIA for Thermal Load for the more refined structure

Confirming that the hand calculations align with the values obtained from SCIA Engineer, it is evident that they are consistent with each other. This provides confidence to proceed with the final refinement for the hand calculations, which involves replacing the rigid connecting bars with horizontal springs.

The introduction of springs in the structure adds an additional term to the calculation, as the connection between the rail and the bridge deck is no longer rigid but replaced with springs of a certain stiffness. This additional term is given in Equation 4.22.

$$\varepsilon_{spring} = \frac{N_{deck}}{EA_{spring}} \tag{4.21}$$

Knowing that EA = k_H·L, results in:

$$\varepsilon_{spring} = \frac{N_{deck}}{k_H \cdot L} \tag{4.22}$$

There are ten springs in the structure, with the first spring positioned 0.5 meters from the beginning and the last spring positioned 9.5 meters from the same point. The intermediate distance between the springs is 1 meter each, ensuring symmetry in the structure. This symmetry simplifies the hand calculations, as calculations need to be performed for only one half of the structure, with the results reflecting symmetrically in the other half.

The differences in horizontal locations of the springs introduce variations in their effects on the internal forces within the structure. This influence is determined by the horizontal distance of each spring from the center of the structure, as illustrated in Figure 4.11.

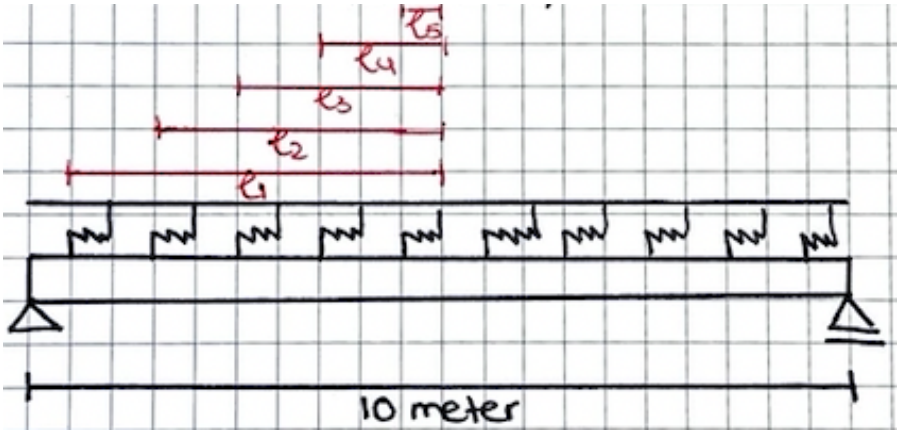

Figure 4.11: The horizontal location of the springs

To calculate the internal forces using the springs, the different influence lengths must be determined:

- $L_1 = \frac{10000-1000}{2} = 4500$ mm
- $L_2 = \frac{10000-3000}{2} = 3500$ mm
- $L_3 = \frac{10000-5000}{2} = 2500$ mm
- $L_4 = \frac{10000-7000}{2} = 1500$ mm
- $L_5 = \frac{10000-9000}{2} = 500$ mm

The spring characteristic used in these calculations is $k_H = 14.29$ MN/m.

With all parameters known, the strain of the spring can now be incorporated into the formula to calculate the internal forces in the structure.

$$N_{deck,i} \cdot (\frac{1}{k_H \sum L_i} + \frac{1}{EA_{deck}} + \frac{1}{EA_{rail}} + \frac{e^2}{EI_{deck} + EI_{rail}}) = -\alpha \cdot \Delta T \tag{4.23}$$

$$N_{deck,i} = -\frac{\alpha \cdot \Delta T}{\frac{1}{k_H \sum L_i} \frac{1}{EA_{deck}} + \frac{1}{EA_{rail}} + \frac{e^2}{EI_{deck}+EI_{rail}}} \tag{4.24}$$

Here, i indicates the location where the internal forces are calculated. Therefore, $N_{deck,1}$ represents the normal force after spring 1, and similarly for springs 2 through 5. The results are presented inTable 4.1.

	N_{deck} [kN]	N_{rail} [kN]	φ [rad]	M_{deck} [kNm]	M_{rail} [kNm]
Location 1	-15.65	15.65	7.006E-06	12.04	0.01
Location 2	-27.27	27.27	1.221E-05	20.97	0.02
Location 3	-35.29	35.29	1.579E-05	27.14	0.03
Location 4	-39.99	39.99	1.790E-05	30.76	0.04
Location 5	-41.54	41.54	1.859E-05	31.95	0.04

Table 4.1: Internal forces thermal load hand calculations

This results in the following internal force diagrams of both the hand calculations and SCIA Engineer, and are presented in Figure 4.12 and Figure 4.13.

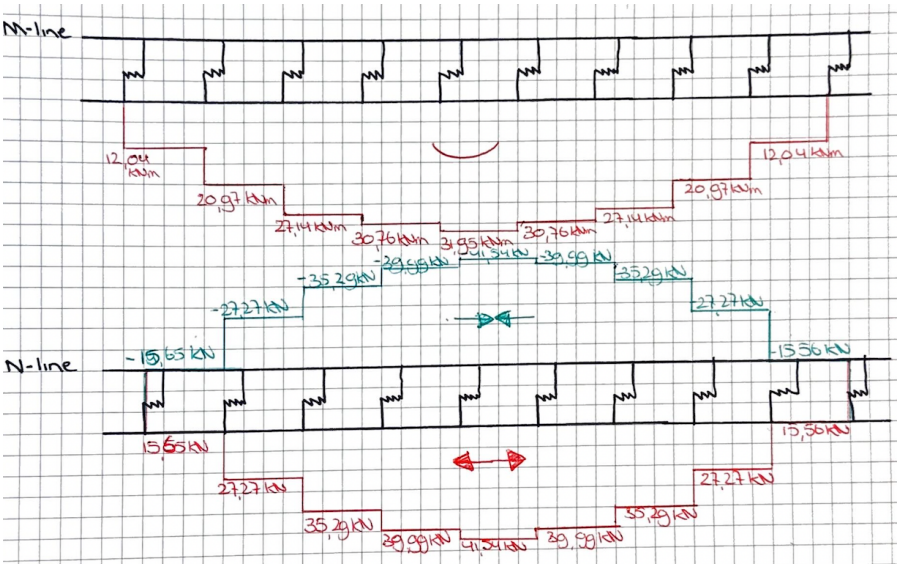

Figure 4.12: Internal force diagrams obtained from hand calculations for Thermal Load for the most refined structure

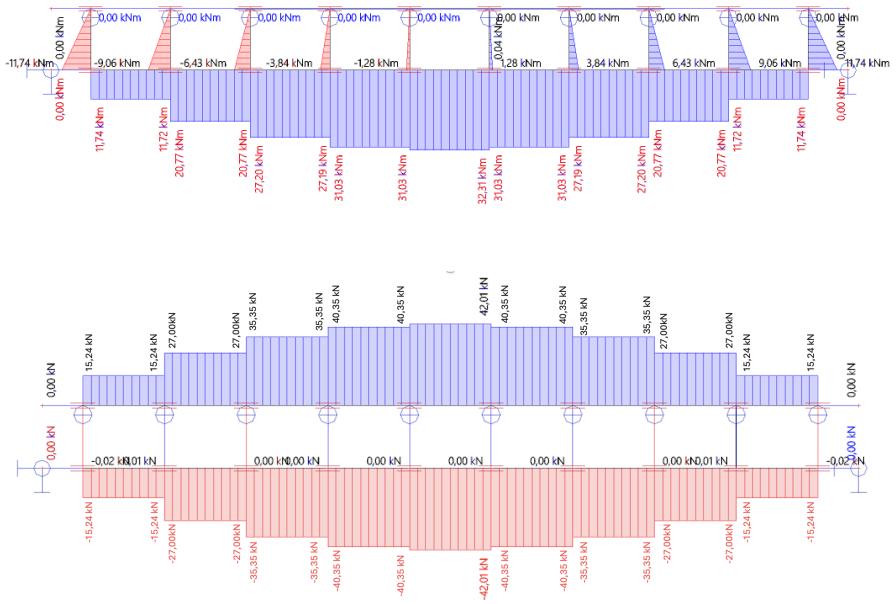

Figure 4.13: Internal force diagrams obtained from SCIA for Thermal Load for the most refined structure

The hand calculation values align with those from SCIA Engineer, confirming the accuracy of the thermal load calculations.

4.1.2. Longitudinal traffic load

The second loading situation that also needs to be covered with hand calculations is the longitudinal traffic load. In this hand calculation a few assumptions will be made to make it possible to perform the calculations by hand. The results from the hand calculations will be compared and checked with SCIA Engineer, and it becomes clear whether the assumptions were correct and whether they only make a relatively small difference in the final answers.

Longitudinal traffic loads consist of both braking and acceleration of a train. In these hand calculations, the focus is primarily on the braking forces. However, it is worth noting that the calculations for braking loads can also be translated into acceleration forces, with differences only in magnitude and direction.

For this calculation, the force corresponding to load model 71 will be utilised. The magnitude of this force can be calculated with Equation 4.25, assuming a bridge length of 10 meters. More detailed explanations of the load models and the longitudinal forces themselves are included in section 2.3.

$$Q_{lbk} = 20[kN/m] \cdot L_{a,b}[m] \tag{4.25}$$

The total braking load amounts to 200 kN, evenly distributed over the 10-meter length of the bridge, resulting in a distributed load of 20 kN/m to the right, applied at the top of the rail.

The model that needs to be calculated for the hand calculations is visualised in Figure 4.14:

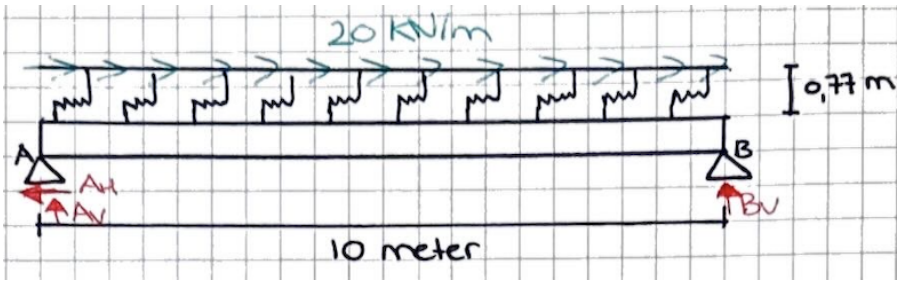

Figure 4.14: The most refined model for longitudinal traffic load for the hand calculation

The first step of the hand calculations involves determining the support reactions. In the Figure 4.14, highlighted in red, there are three unknowns: A_H, A_V, and B_V. These represent the horizontal and vertical reactions, respectively. To solve for these unknowns, three equilibrium conditions are utilised: horizontal force equilibrium, vertical force equilibrium, and bending moment equilibrium. With three unknowns and three equations, it is possible to calculate the support reactions by hand.

$$\sum F_H = 0 \quad \rightarrow \quad 20 \cdot 10 - A_H = 0 \quad \rightarrow \quad A_H = 200\,kN \leftarrow \tag{4.26}$$

$$T|_A = 0 \quad \rightarrow \quad -20 \cdot 10 \cdot 0.77 + B_V \cdot 10 = 0 \quad \rightarrow \quad B_V = 15.4\,kN \uparrow \tag{4.27}$$

$$\sum F_V = 0 \quad \rightarrow \quad A_V + B_V = 0 \quad \rightarrow \quad A_V = -15.4\,kN \downarrow \tag{4.28}$$

The springs positioned between the rail and the bridge deck are situated atop the 'infinitely stiff' connection bars. These springs possess horizontal spring values but cannot withstand any bending moment. Consequently, the bending moment beneath the rail at the connection between the rail and the connection bar is zero, resembling a hinge.
This setup allows for the rail to be analysed separately from the rest of the structure. It facilitates the determination of the shear forces that the connection bars must bear to transfer the horizontal forces to the supports. Additionally, it enables the determination of normal force lines in the rail.
Since the longitudinal braking force acts directly on the rail itself, there is no eccentricity, and no vertical load is acting on the rail in this situation. Therefore, there are no bending moment and shear forces in the rail, and these lines will not be drawn.

Rail
The distributed horizontal longitudinal traffic load acting on the rail is transferred from the rail to the spring and the connection bars, and then further to the bridge deck supports. To determine the internal force lines for both the rail and the rest of the structure, it is crucial to know the shear forces in the connection bars. This information is used for the interaction between the two separately analysed parts of the structure, namely the rail and the bridge deck with connection bars. As illustrated in Figure 4.15, there are ten connection bars, each with its own shear force.

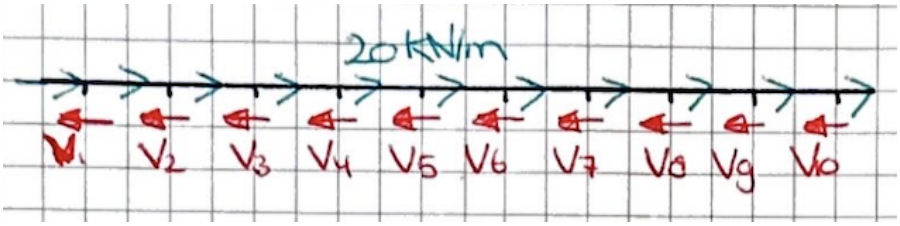

Figure 4.15: The reaction forces for the connection bars

The braking force is evenly distributed along the rail, and similarly, the connection bars are evenly distributed over the length of the rail. Consequently, the shear force acting on the connection bars is also evenly distributed. With a total braking load of 200 kN spread over ten connection bars, it follows that each connection bar will bear 20 kN of load. This results in the following normal force line for the rail:

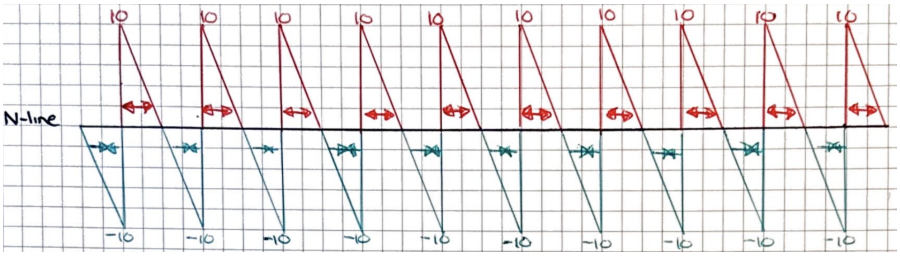

Figure 4.16: The normal force in the rails obtained from hand calculations for Longitudinal Traffic Loads

These normal force line of the rail needs to be checked with SCIA Engineer to validate if the assumptions are correct.

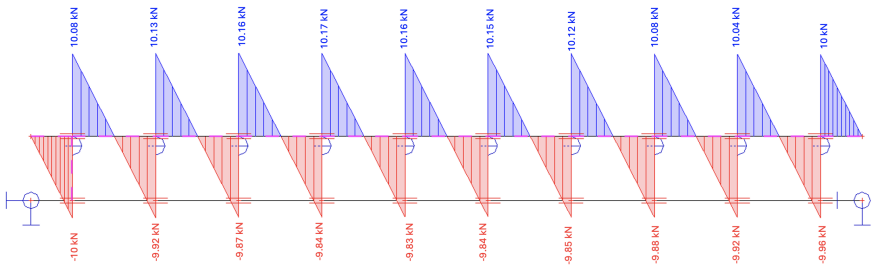

Figure 4.17: The normal force in the rails obtained from SCIA for Longitudinal Traffic Loads

Upon cross-checking these two normal force lines, it becomes apparent that the values are nearly identical and the shapes are indistinguishable. The discontinuities observed in the normal force lines correspond to the shear force in the connection bars. Notably, this shear force is approximately 20 kN, as assumed, although not precisely 20 kN but with minor variations in the decimal places. These variations are minor and fall within the acceptable range of accuracy for hand calculations.

Bridge deck and connection bars

Now that the shear forces in the connection bars are known and it is known that the bending moment beneath the rail is zero. The internal forces in the rest of the structure can be determined. The structure is a kind of Vierendeel beam where the forces can be determined by the knowledge that the sum of the moments in every joint needs to be equal to zero. To determine the forces the structure needs to be cut into different segments and then the forces can be determined. The first segment is illustrated in Figure 4.18.

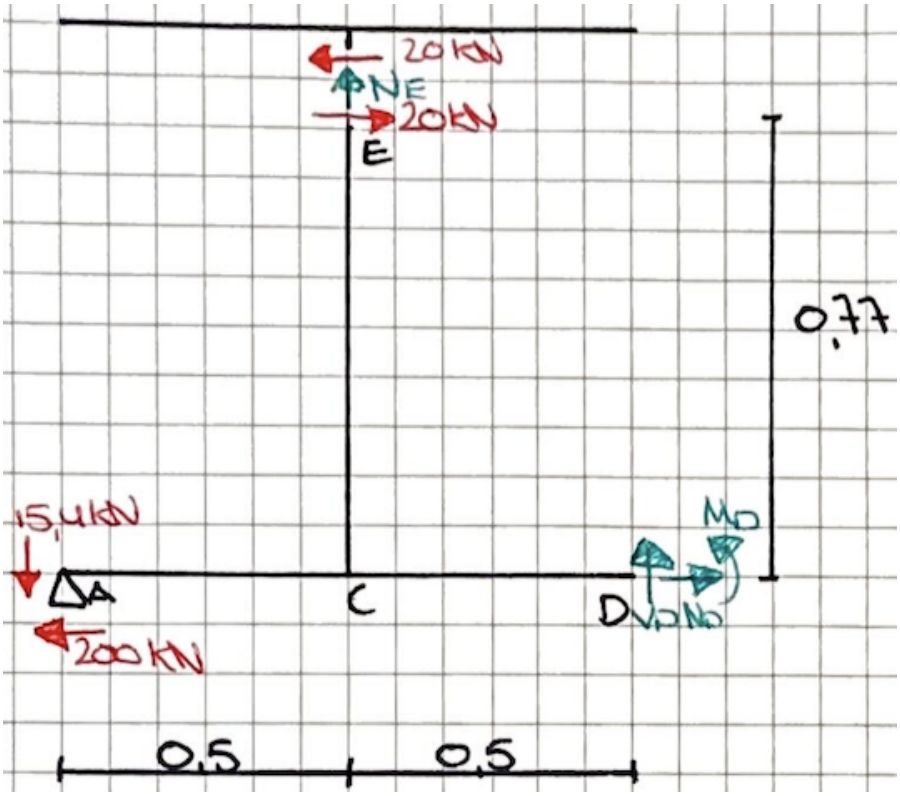

Figure 4.18: The first segment with the forces for longitudinal load

As observed in Figure 4.18, there are four unknowns, depicted in green, while there are only three equilibrium conditions. Consequently, this structure is statically indefinite. To facilitate the calculation of this structure by hand, certain assumptions must be made.
The first assumption is that since only an external horizontal braking force acts on the system, and there is no vertical force acting on it, the normal force in the connection bars is assumed to be negligible and can be disregarded. Another assumption is that the bending moment halfway along each connection bar is equal to zero. Therefore, in the illustrated case, M_D would be equal to zero.
With these two assumptions, the drawing can be simplified into the following system, as presented in Figure 4.19.

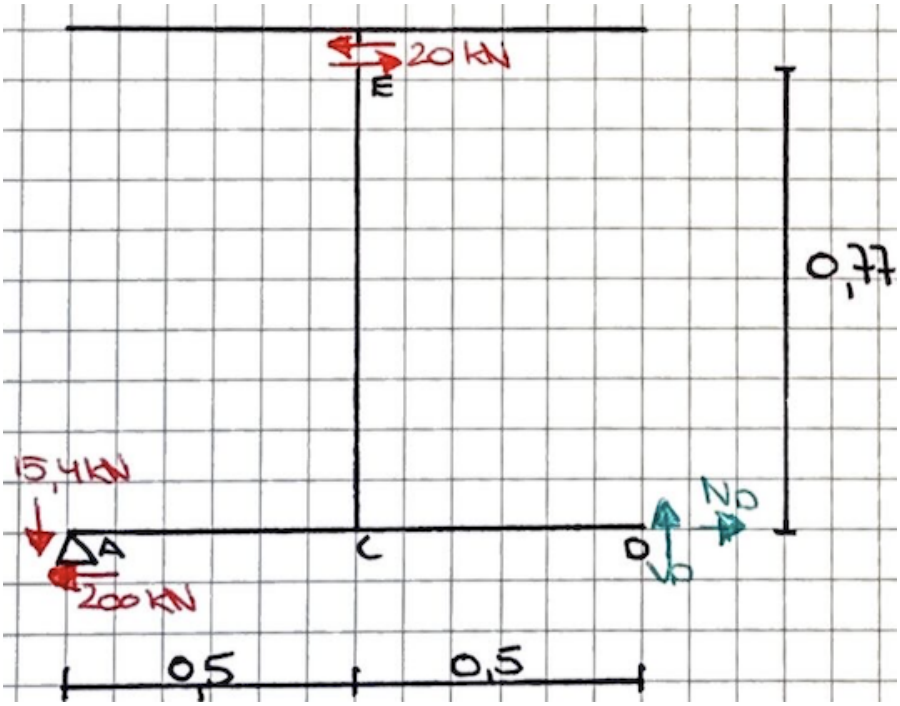

Figure 4.19: The first segment with the forces for longitudinal load 2

This results in a statically determinate system where the internal forces can be calculated by hand. As described earlier, for a Vierendeel beam, the bending moments at the joints must be zero. In this case, there are three moments corresponding to the moment equilibrium at joint C: M_{CA}, M_{CE} and M_{CD}.

$$M_{CA} = 15.4 \cdot 0.5 = 7.7 kNm \curvearrowright \tag{4.29}$$

$$M_{CE} = 20 \cdot 0.77 = 15.4 kNm \curvearrowleft \tag{4.30}$$

This leads to the following moments at joint C as depicted in Figure 4.20, where moment equilibrium must be maintained. The known values are indicated in red, while the unknown values are shown in green, with all values expressed in kNm.

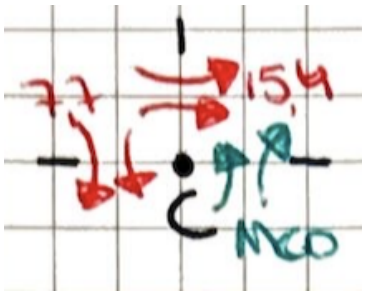

Figure 4.20: Joint C

This leads to the following formula to establish the sum of moments at joint C equal to zero:

$$\sum M_C = M_{CA} - M_{CE} + M_{CD} = 0 \tag{4.31}$$

$$7.7 - 15.4 + M_{CD} = 0 \tag{4.32}$$

$$M_{CD} = 7.7 kNm \curvearrowright \tag{4.33}$$

The bending moment is determined by the shear force at point D. With a distance of 0.5 meters to point D, the shear force at D is calculated as follows:

$$M_{CD} = V_D \cdot 0.5 \tag{4.34}$$

$$7.7 = V_D \cdot 0.5 \tag{4.35}$$

$$V_D = 15.4kN \uparrow \tag{4.36}$$

This yields the following results around the first connection bar:

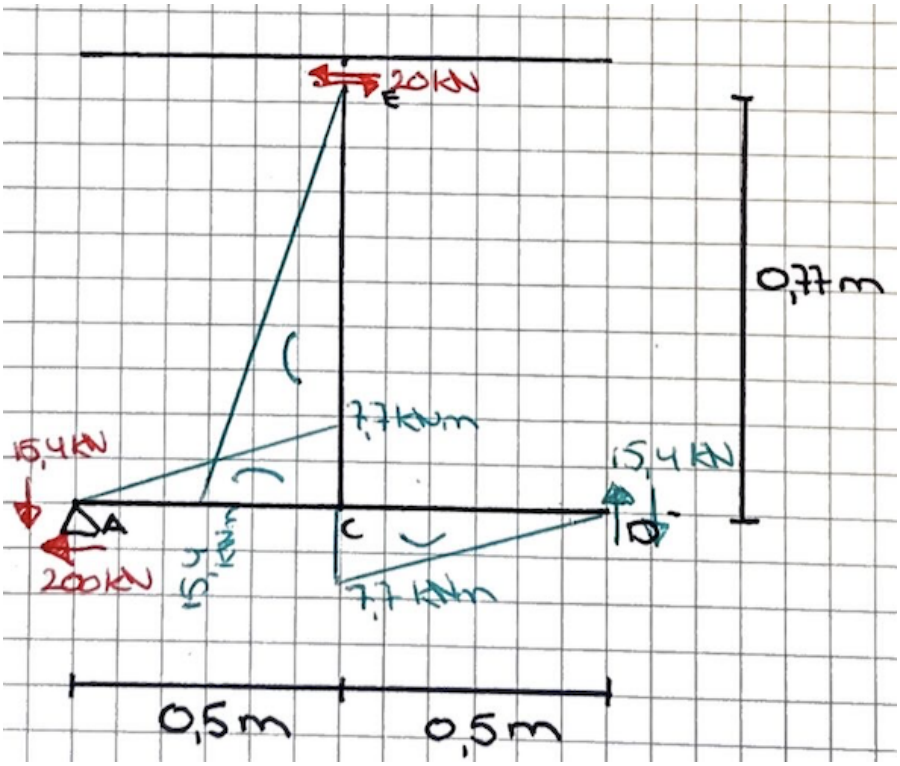

Figure 4.21: Internal forces first segment

The normal force in the bridge deck can also be calculated by applying horizontal force equilibrium. This is expressed in Equation 4.37.

$$\sum F_H = 0 \quad \rightarrow \quad -200 + 20 + N_D = 0 \quad \rightarrow \quad N_D = 180\,kN \quad Tension \tag{4.37}$$

Given that the shear forces at the connections of the connection bars and the rail are all equal to 20 kN, they generate a consistent bending moment of 15.4 kNm at the joints. Since the distances between the connection bars are all 1 meter and identical, the distribution of internal forces remains uniform across all sections for both shear and bending moments, mirroring that of the first part.
To determine the normal forces, the process from the first segment can be repeated, allowing the normal forces line to be drawn for the entire structure. This yields the following internal force lines, with positive values depicted in red and negative values in green, presented in Figure 4.22.

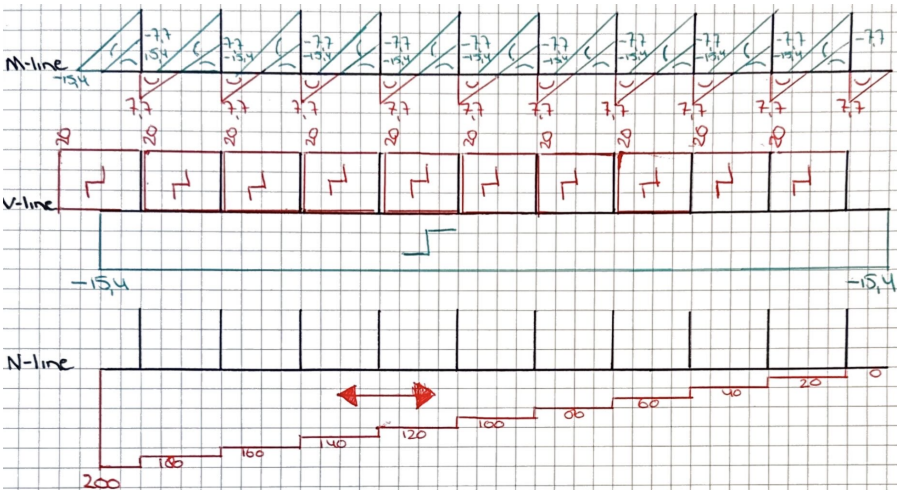

Figure 4.22: Internal force diagrams for the rest of the structure obtained from hand calculations for Longitudinal Traffic Loads

These lines also need to be checked with SCIA Engineer to validate the correctness of the hand calculations. The SCIA diagrams are visualised in Figure 4.23.

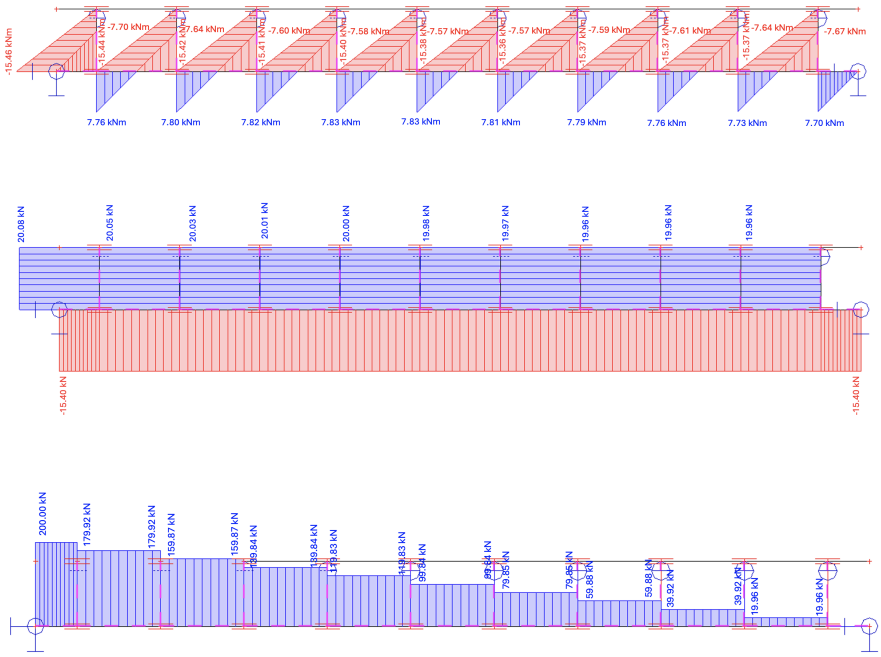

Figure 4.23: Internal force diagrams for the rest of the structure obtained from SCIA for Longitudinal Traffic Loads

Upon comparing the hand calculations with the results from SCIA Engineer, it is evident that they are nearly identical, with minor differences observed only in decimal places. The shapes of the internal force lines remain consistent, and the values are within the same order of magnitude. Therefore, it can be concluded that the hand calculations for the longitudinal forces were accurate, and the assumptions made were acceptable.

4.1.3. Vertical traffic load

The final loading consideration involves the vertical traffic load exerted by trains traveling over the system. Similar to previous loading scenarios, hand calculations will be conducted with certain assumptions and simplifications, which will be refined as necessary.
For the hand calculations of the vertical traffic load, the 71 load model described in section 2.3 is selected. This load model comprises four point loads of 250 kN each, positioned in the middle and equally distributed

over the 6.4 meters, resulting in a distributed load of 156.25 kN/m. Placing the load model in the middle of the structure ensures symmetry in forces, given the symmetric geometry of the structure, thereby simplifying the hand calculations. Although variations in loading models and load positions may introduce slight deformations in the calculations, for the sake of simplicity and clarity, we will adhere to the described situation.
The final model for the hand calculations of the vertical traffic load is illustrated in Figure 4.24.

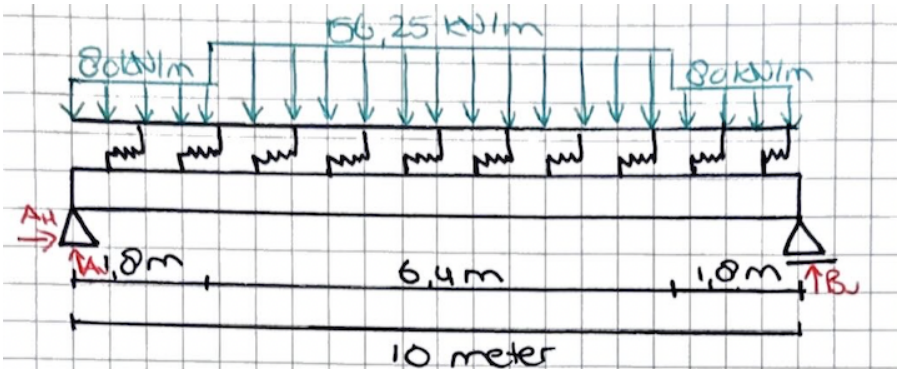

Figure 4.24: The most refined model for vertical traffic load for the hand calculation

The first step involves calculating the support reactions. In red, the three unknown support reactions are depicted. Three equilibrium conditions must be satisfied: horizontal equilibrium, vertical equilibrium, and bending moment equilibrium. With three unknowns and three equilibrium conditions, all support reactions can be determined.

$$\sum F_H = 0 \quad \rightarrow \quad A_H = 0\,kN \tag{4.38}$$

$$T|_A = 0 \quad \rightarrow \quad -80\cdot 1.8\cdot 0.9 - 156.25\cdot 6.4\cdot 5 - 80\cdot 1.8\cdot 9.1 + B_V\cdot 10 = 0 \quad \rightarrow \quad B_V = 644\,kN\uparrow \tag{4.39}$$

$$\sum F_V = 0 \quad \rightarrow \quad 2\cdot 80\cdot 1.8 + 156.25\cdot 6.4 - A_V - B_V = 0 \quad \rightarrow \quad A_V = 644\,kN\uparrow \tag{4.40}$$

Similar to other loading scenarios, the springs between the rail and the bridge deck are positioned atop the 'infinitely stiff' connection bars. These springs possess horizontal spring values but cannot withstand any bending moment. Consequently, the bending moment beneath the rail at the connection between the rail and the connection bar is zero, similar to a hinge.
This allows for the rail to be analysed separately from the rest of the structure to determine the normal forces that the connection bars must bear to transfer the vertical forces to the supports. Additionally, the shear force and bending moment lines in the rail can be determined.
Therefore, the rail will be considered first, followed by the analysis of internal forces in the bridge deck and the connection bars.

Rail
The vertical traffic forces exerted on the structure transfer through normal forces in the connecting bars to the bridge deck and further to the supports. Beginning with the analysis, the first step is to determine the normal forces in the connection bars. Subsequently, the shear force line and bending moment line in the rail are delineated. The system under consideration is depicted in Figure 4.25.

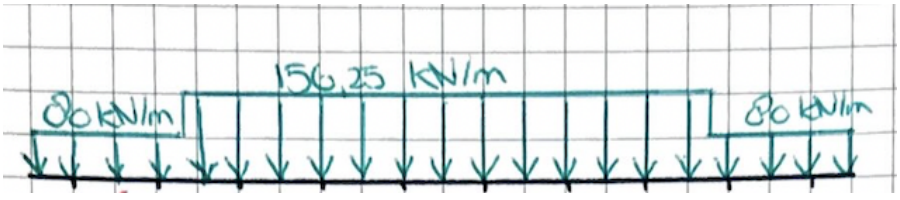

Figure 4.25: The vertical traffic load on the rails

These normal forces can be calculated by cutting the rail into pieces and assuming that the connection bar take the load from half the distance from the right and from the left.
For each segment, vertical force equilibrium must be maintained, allowing for the calculation of the normal forces in the connection bars. Due to symmetry, only half of the normal forces need to be calculated, as the other half will be identical. Each individual segment is illustrated in Figure 4.26.

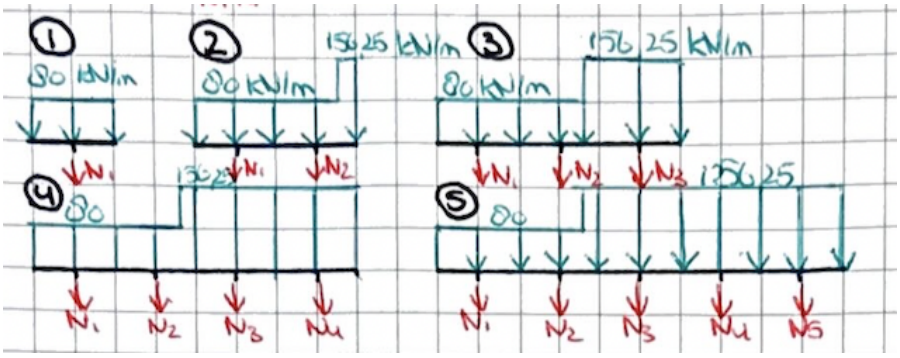

Figure 4.26: The rail cut into pieces to calculate the forces in the connection bars

$$\sum F_{V_1} = 0 \quad \rightarrow \quad 80 \cdot 1.0 + N_1 = 0 \quad \rightarrow \quad N_1 = -80\,kN\,compression \tag{4.41}$$

$$\sum F_{V_2} = 0 \quad \rightarrow \quad 80 \cdot 1.8 + 156.25 \cdot 0.2 + N_1 + N_2 = 0 \quad \rightarrow \quad N_2 = -95.25\,kN\,compression \tag{4.42}$$

$$\sum F_{V_3} = 0 \quad \rightarrow \quad 80 \cdot 1.8 + 156.25 \cdot 1.2 + N_1 + N_2 + N_3 = 0 \quad \rightarrow \quad N_3 = -156.25\,kN\,compression \tag{4.43}$$

$$\sum F_{V_4} = 0 \quad \rightarrow \quad 80 \cdot 1.8 + 156.25 \cdot 2.2 + N_1 + N_2 + N_3 + N_4 = 0 \quad \rightarrow \quad N_4 = -156.25\,kN\,compression \tag{4.44}$$

$$\sum F_{V_5} = 0 \quad \rightarrow 80 \cdot 1.8 + 156.25 \cdot 3.2 + N_1 + N_2 + N_3 + N_4 + N_5 = 0 \quad \rightarrow N_5 = -156.25\,kN\,compression \tag{4.45}$$

This gives the following total result, illustrated in Figure 4.27. This result can be checked by performing the global vertical forces equilibrium, as is performed in Equation 4.46.

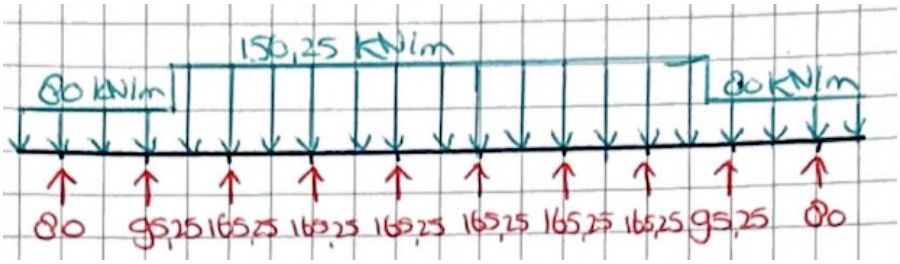

Figure 4.27: Resulting normal forces in the connection bars

$$\sum F_V = 0 \quad \rightarrow 2 \cdot 80 \cdot 1.8 + 156.25 \cdot 6.4 + 2 \cdot (-80 - 95.25 - 156.25 - 156.25 - 156.25) = 0 \quad \rightarrow 0 = 0\,correct \tag{4.46}$$

Now, the internal force lines for the rails can be determined. The shear force line is derived by summing all the forces depicted in the figure above. The moment line is established by calculating the moments above

each connection bar and applying $\frac{1}{8} \cdot q \cdot l^2$ at the midpoint between two connection bars to determine the bending moment in each span. These shear force and bending moment lines are illustrated in Figure 4.28.

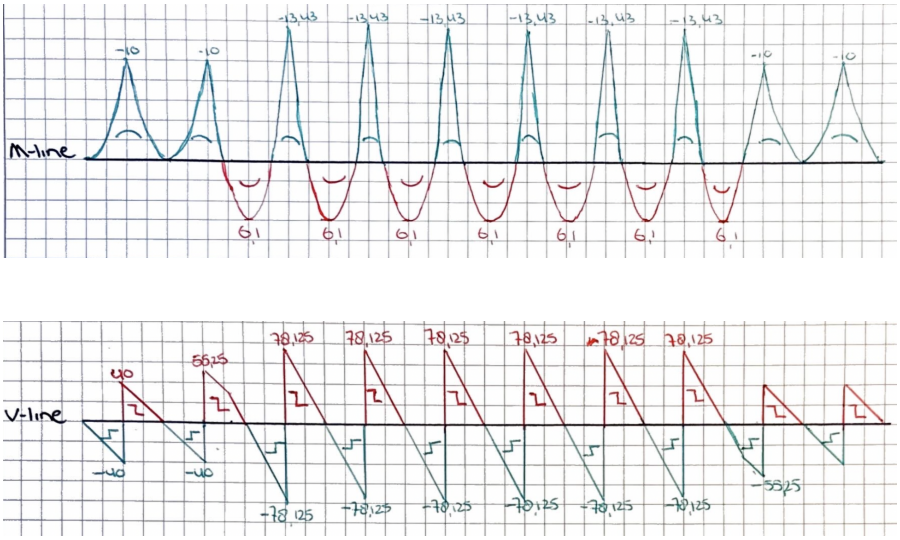

Figure 4.28: Internal force lines for the rails under vertical load, based on hand calculations

The results will be cross-checked with the SCIA Engineer internal force lines to ensure that the hand calculations are within the correct order of magnitude and that the shapes of the internal force lines are similar. The results obtained from SCIA Engineer are visualised in Figure 4.29.

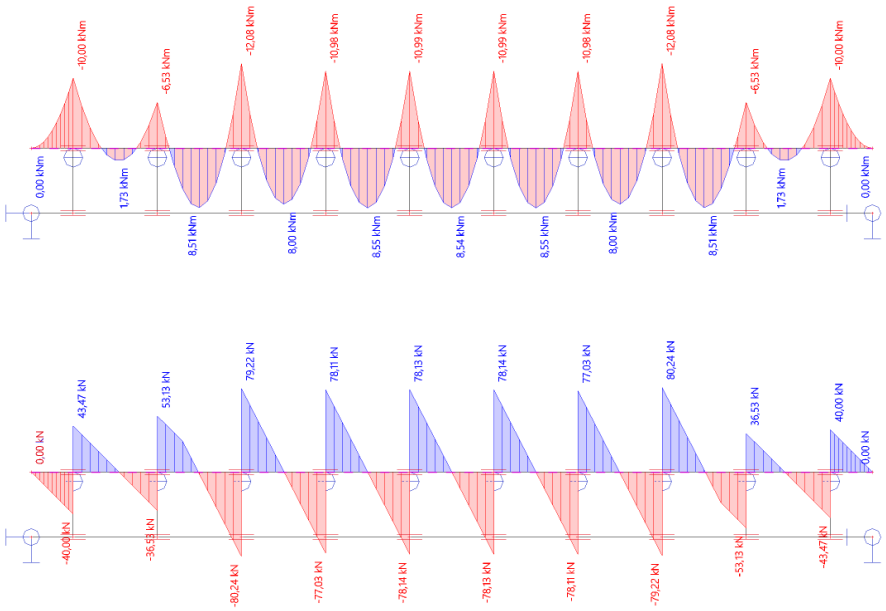

Figure 4.29: Internal force lines for the rails under vertical load, based on SCIA Engineer

It can be observed that the results are nearly identical, with both being within the same order of magnitude and exhibiting similar line shapes. Consequently, the hand calculations for the rail are acceptable.

Bridge deck and connection bars

Now that the internal forces in the rail and the normal forces acting in the connection bars due to the interaction with the rail are known, the internal forces of the rest of the structure can be determined. This will be performed with different segments, with cuts for the segments made at the same horizontal locations in the structure as those made for the rail.

The forces in the first segment are illustrated in Figure 4.30, where the red forces represent the known forces and the green forces represent the unknown forces.

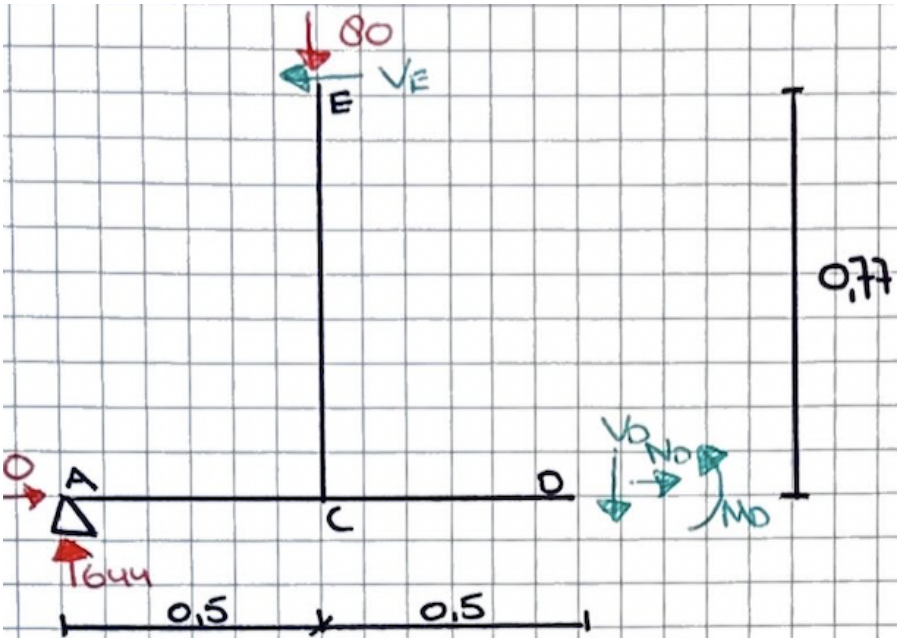

Figure 4.30: The first segment with the forces for vertical load

In this scenario, there are four unknowns and three equilibrium conditions, rendering the structure statically indeterminate and unworkable for hand calculation. Therefore, an assumption must be made. Given that the structure is subjected only to vertical external forces and that the horizontal reaction force is zero (as indicated in Equation 4.38), the assumption made is that the shear forces in the connection bars are also zero. Consequently, there is no shear force distribution in the connection bars, and since there is no horizontal support reaction, the normal forces in the bridge deck are also zero. Thus, in the Figure 4.30, the unknowns V_E and N_D can be disregarded. This simplifies the system to a statically determinate one, allowing for computation.

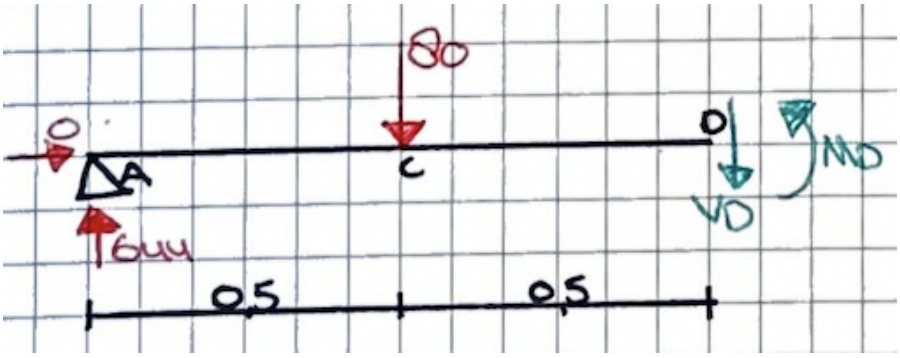

Figure 4.31: The first segment with the forces for vertical load 2

Now, the two unknowns can be computed using vertical and bending moment equilibrium. Initially, the shear force at D is calculated by applying vertical force equilibrium, as described in Equation 4.47.

$$\sum F_V = 0 \quad \rightarrow \quad -644 + 80 + V_D = 0 \quad \rightarrow \quad V_D = 564\,kN \downarrow \tag{4.47}$$

The second unknown in this situation is the bending moment at location D. This can be computed by applying the bending moment equilibrium around location D, as described in Equation 4.48.

$$T|_D = 0 \quad \rightarrow \quad M_D + 80 \cdot 0.5 - 644 \cdot 1.0 = 0 \quad \rightarrow \quad M_D = 604\,kNm\,\curvearrowleft \tag{4.48}$$

This process will be repeated for the rest of the sections, yielding the following results for the internal force lines for the bridge deck, as illustrated in Figure 4.32.

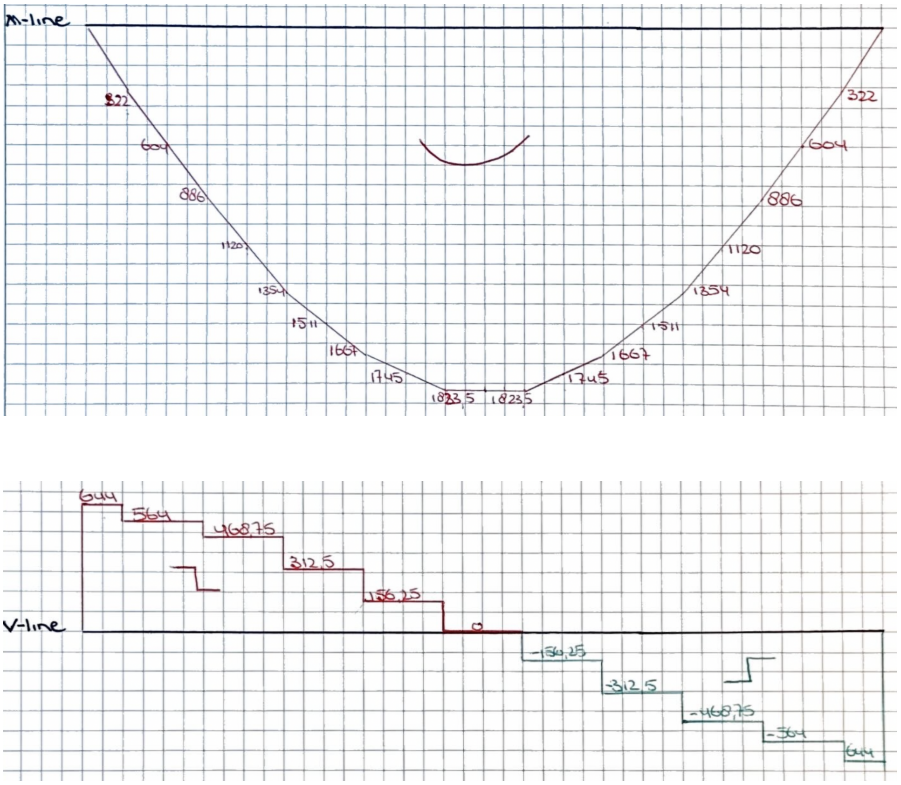

Figure 4.32: Internal force diagrams for the rest of the structure obtained from hand calculations for Vertical Traffic Loads

The internal force lines will once again be compared with the SCIA Engineer internal force lines in the bridge deck to ensure that the hand calculations are within the correct order of magnitude and that the shapes of the internal force lines are similar. The illustrations of these lines are visualised in Figure 4.33:

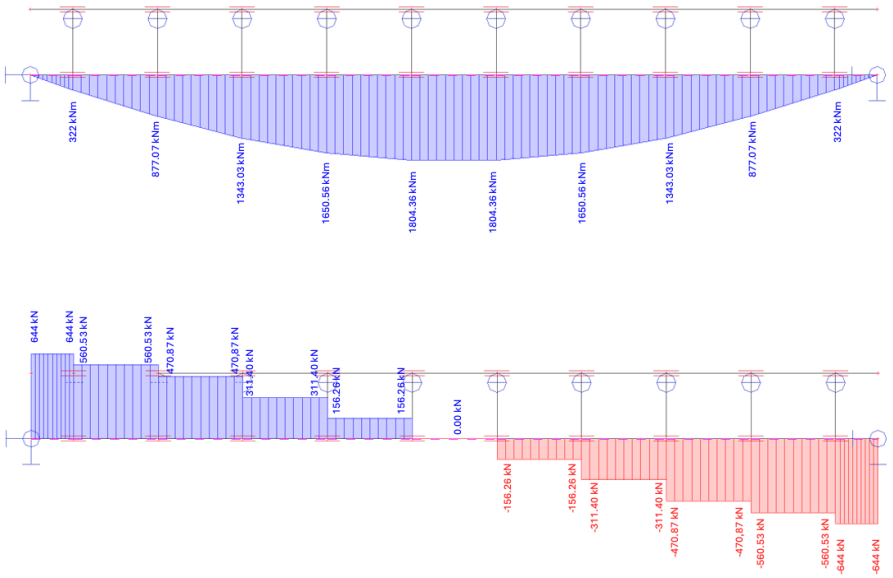

Figure 4.33: Internal force diagrams for the rest of the structure obtained from SCIA ns for Longitudinal Traffic Loads

When comparing the internal force lines, only minor differences are observed in the results. This indicates that the hand calculations provide a reliable indication, and the assumptions made were appropriate.
The magnitude of the shear force that was neglected in the hand calculations was also considered. According to SCIA, this has a varying value between 1.1 and 7.1 kN. Comparing this with forces in the deck of around 600 kN, this represents approximately 1 percent. It is logical that this only causes minor variations in the final answers.

4.2. Model

This section provides a detailed explanation of the model utilised in the thesis investigation, focusing on understanding rail-structure interaction. To achieve this, two longitudinal force models are developed: Model 1, which excludes the embankment influence, and Model 2, which includes the embankment influence. By comparing these models, insights into the impact of the embankment on additional stresses in the rails are gained. Both models feature variable parameters, adjusted throughout the investigation to understand their effects on the magnitude of the additional rail stress. The section is divided into three parts: model parameters, model loads, and assessment criteria.
In subsection 4.2.1, the parameters within the models are explained, including those subject to variation during the investigation, along with their respective investigation bandwidths and investigation steps.
Detailed in subsection 4.2.2, the model loads outline the applied loads for calculations. These loads are strategically positioned to analyse quasi-static behavior, a process elaborated upon in this section.
The final subsection addresses the assessment criteria, where the additional stresses that the rails must withstand are determined. This includes evaluating the initial stresses on a rail without the presence of a structure. By combining these factors with the permitted additional stresses, the maximum stress level for the rails in the investigation are established.

4.2.1. Model Parameters

This subsection provides a detailed overview of the parameters used in the longitudinal force models, each explained in separate sub-subsections.
In each sub-subsection, specific model parameters such as elements and springs are assigned numerical identifiers and sequentially detailed. Parameters are categorized as fixed, including cross-sectional properties, material specifications, and spring constants, or variable, with defined investigation bandwidths and default settings when other variables are modified.
The subsection begins with an in-depth exploration of Model 1 (subsubsection 4.2.1.1), followed by Model 2 (subsubsection 4.2.1.2). It further elaborates on parameter step determination in subsubsection 4.2.1.3, focusing on variables other than bridge length. Here, the cumulative impact of these variables on overall stiffness is evaluated, informing the calculation of parameter steps within specified investigation bandwidth. Finally, a summary table of variable parameters (subsubsection 4.2.1.4) is provided, detailing their investigation bandwidths, default settings, and relevance to each model.

4.2.1.1. Model 1: Model without embankment influence

This sub-subsection presents the first longitudinal force model utilised in the investigation, which excludes the influence of the embankment. The model is depicted in Figure 4.34.
In this railway bridge model, the embankment does not exert influence due to its considerable distance from the segment. As part of a longer railway bridge, this segment is bordered by other spans, making the embankment's impact negligible on the model's response. This exclusion of embankment influence is consistent with the treatment of a segment of part 3 of the Theemswegtracé, as discussed in section 3.1.

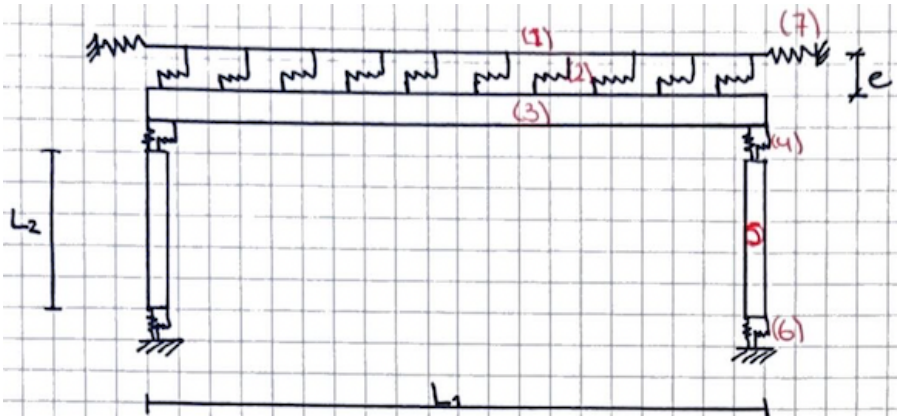

Figure 4.34: Model 1 without the influence of the embankment

This model will be described based on the numbered components in the figure.

Number 1:
The first parameter represents the rail, modeled as a beam element with a graphical cross-section that represent both rails. It encompasses both rails upon which the train traverses. Given the 2-dimensional context of the longitudinal force analysis, the rail accounts for properties of both rails. For this investigation, the rail is a fixed parameter, adopting the widely-used UIC54 rail standard in Europe (as described in section 2.1).

The cross-sectional and material properties assigned to this fixed parameter include a surface area of 13954 mm^2, a moment of inertia around the y-axis of 46758000 mm^4, a moment of inertia around the z-axis of 7857509000 mm^4, and an elasticity modulus of 210 GPa.

Number 2:
The second component in Figure 4.34 represents the connection of the rail with the bridge deck, established through a ballast structure comprising the ballast bed, sleeper, and the fastener system securing the rail to the sleepers. This connection is modeled by a non-linear spring and is considered as a fixed parameter in this investigation, with variations only in the spring values between loaded and unloaded conditions. Springs are positioned at intervals of 1 meters.

In the vertical direction, the spring is effectively infinitely stiff due to the negligible vertical motion relative to the bridge deck. Therefore, only a horizontal spring is depicted in Figure 4.34. However, in the horizontal direction, the spring demonstrates nonlinear characteristics, as detailed in Figure 2.16 and section 2.3. This nonlinear spring has different cut-off limits for loaded and unloaded cases, requiring careful consideration during model implementation.

Number 3:
The third component in Model 1 is the bridge deck, modeled as a beam element with specific cross-sectional and material properties tailored to the type of bridge deck used. In this investigation, the focus is on prefabricated bridge decks, specifically the ZIPXL prefabricated bridge decks from Spanbeton.
The bridge deck is characterised by its dilating length, denoted as L_1 in Figure 4.34. This length represents the span from the beginning of the deck to the point where it can no longer expand or contract due to temperature changes. Notably, the bridge deck's length is a variable parameter in this investigation.

The variation in deck length affects the cross-sectional properties of the deck. Therefore, adjusting the deck length also requires adjusting its cross-section. The investigation utilises precast bridge decks of the ZIPXL type from Spanbeton, suitable for lengths ranging from 15 to 60 meters. Investigation steps are set at 5-meter increments, with a default setting of 35 meters for the bridge length.
To determine the appropriate ZIPXL profile for each bridge length, the slenderness ratio of 16 is applied. For instance, a bridge length of 3500 mm would require a minimum profile height of 2187.5 mm, corresponding to the ZIPXL2000 profile. This principle of slenderness is applied uniformly across all bridge lengths, resulting in a standardised set of profiles detailed in Table 4.2.

Bridge length	Required height [m]	Used profile
15	0.9375	ZIPXL 700
20	1.25	ZIPXL 1000
25	1.5625	ZIPXL 1400
30	1.875	ZIPXL 1700
35	2.1875	ZIPXL 2000
40	2.5	ZIPXL 2300
45	2.8125	ZIPXL 2600
50	3.125	ZIPXL 2900
55	3.4375	ZIPXL 3200
60	3.75	ZIPXL 3500

Table 4.2: Used ZIPXL profile for every bridge length

In this investigation, the focus is on a single rail configuration for the bridge deck. The deck maintains a fixed width of 6500 mm, as depicted in Figure 4.35, referencing the single rail configuration of the Theemswegtracé. The figure illustrates three main girders flanked by two boundary girders on each side. A compression layer of 230 mm is applied to bridge decks ranging from ZIPXL700 to ZIPXL1700. For ZIPXL1800 and larger profiles, the compression layer is reduced to 200 mm.

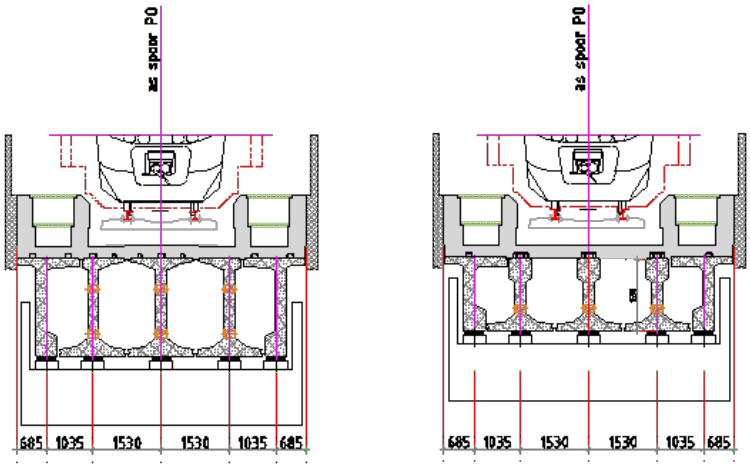

Figure 4.35: General bridge deck cross section for this investigation

For every bridge deck the distance to the centroid, the inertia around y and z needs to be calculated, and the total area needs to be calculated. This calculation will be performed for the bridge deck used for 35 meter, which is the ZIPXL2000.

Cross sectional properties ZIPXL2000

Main girders

Referring to Figure 4.35, the bridge deck features three main girders. The initial step in computing the total cross-sectional properties involves calculating the properties of the main girder. The main girders, divided into various squares and triangles, are illustrated in Figure 4.36.

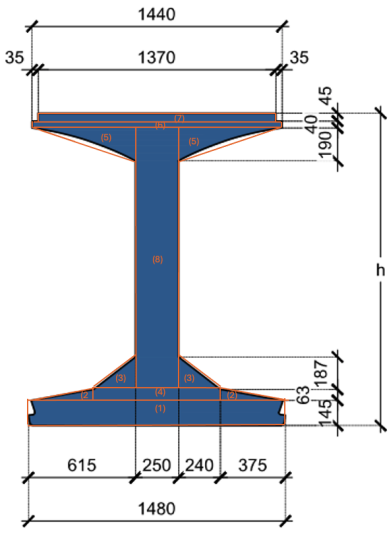

Figure 4.36: Main girder ZIPXL2000 divided into 7 shapes

For the squares, the area can be calculated by multiplying the width by the height, and for the inertia, the formula $\frac{1}{12} \cdot b \cdot h^3$ is used. Similarly, for the triangles, the area is calculated by multiplying the width by the height and dividing by two, while the inertia is calculated using the formula $\frac{1}{36} \cdot b \cdot h^3$.
To determine the centroid for the main girder of ZIPXL2000, the distance for every shape with respect to a reference point needs to be calculated. The reference points for the z-axis are the top of the compression layer, and for the y-axis, it is on the left boundary of the profile. The resulting area, inertia, and distances from the reference points are presented in Table 4.3.

Shapes	Area [mm^2]	Distance z [mm]	Distance y [mm]	Inertia around y I_y [mm^4]	Inertia around z I_z [mm^4]
Shape 1	214600	2127.5	740	3.76E+08	3.92E+10
Shape 2	11812.5	2034	250	2.60E+06	9.23E+07
Shape 3	22440	1929.67	535	3.00E+07	2.34E+07
Shape 4	45990	2023.5	740	1.52E+07	2.04E+09
Shape 5	56525	348.33	416.67	1.13E+08	1.11E+09
Shape 6	57600	265	740	7.68E+06	9.95E+09
Shape 7	61650	222.5	740	1.04E+07	9.64E+09
Shape 8	448000	1156	740	1.20E+11	2.33E+09

Table 4.3: Cross-sectional properties main girder for the various shapes

Summing up all the separate area's give the total area of the main girder for ZIPXL2000, which is 1009395 mm^2. Now the centroid can be calculated and is:

$$z_{centroid} = \frac{\sum_{i=1}^{n=8} A_i \cdot z_i}{A_{total}} = 1258.70mm \tag{4.49}$$

$$y_{centroid} = \frac{\sum_{i=1}^{n=8} A_i \cdot y_i}{A_{total}} = 740mm \tag{4.50}$$

The inertia around y and z can now be calculated. This can be done by adding all the individual inertia's and incorporating the Steiner term. The Steiner term is the area of each shape multiplied by the square of the distance from its own centroid to the total centroid of ZIPXL2000:

$$I_y = \sum_{i=1}^{n=8} I_{y_i} + \sum_{i=1}^{n=8} (A_i \cdot (z_i - z_{centroid})^2) = 5.48 \cdot 10^{11} mm^4 \tag{4.51}$$

$$I_z = \sum_{i=1}^{n=8} I_{z_i} + \sum_{i=1}^{n=8} (A_i \cdot (y_i - y_{centroid})^2) = 8.37 \cdot 10^{10} mm^4 \tag{4.52}$$

Boundary girders

As previously mentioned, the bridge deck consists of three main girders, two boundary girders, and an in-situ compression layer. The cross-sectional properties of the boundary girder can now be calculated following the same method used for the main girder.

An illustration of the boundary girder, divided into various shapes for calculation purposes, is depicted in Figure 4.37. The height of the boundary girder is dependent on the main girder used, which in this case is ZIPXL2000 with a height (h) of 2000 mm. Therefore, the profile-dependent height is calculated as 2000 - 150 - 120 - 450 = 1280 mm.

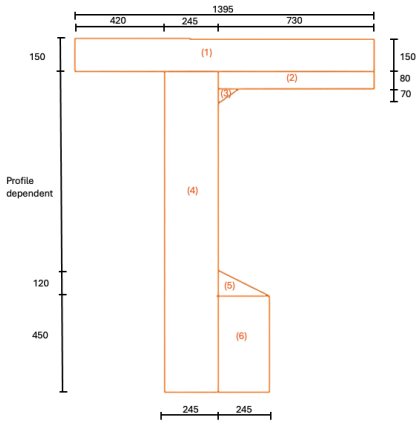

Figure 4.37: Boundary girder ZIPXL2000 divided into 6 shapes

The calculations yield the cross-sectional properties for each shape, as summarized in Table 4.4. The total area of the boundary girder is found to be 799125 mm^2.

Shapes	Area [mm^2]	Distance z [mm]	Distance y [mm]	Inertia around y I_y [mm^4]	Inertia around z I_z [mm^4]
Shape 1	209250	275	697.5	3.92E+08	3.39E+10
Shape 2	58400	390	1030	3.11E+07	2.59E+09
Shape 3	3500	453.33	731.67	9.53E+05	1.94E+06
Shape 4	453250	1275	542.5	1.29E+11	2.27E+09
Shape 5	14700	1710	828.33	1.18E+07	4.90E+07
Shape 6	60025	1975	787.5	1.86E+09	5.51E+08

Table 4.4: Cross-sectional properties boundary girder for the various shapes

The total area of the boundary girder is found to be 799125 mm^2. Now, the centroid with respect to the reference point can be determined:

$$z_{centroid} = \frac{\sum_{i=1}^{n=6} A_i \cdot z_i}{A_{total}} = 1005.46mm \tag{4.53}$$

$$y_{centroid} = \frac{\sum_{i=1}^{n=6} A_i \cdot y_i}{A_{total}} = 643.20mm \tag{4.54}$$

With the centroid known, the inertia around y and z can be calculated:

$$I_y = \sum_{i=1}^{n=6} I_{y_i} + \sum_{i=1}^{n=8} (A_i \cdot (z_i - z_{centroid})^2) = 3.63 \cdot 10^{11} mm^4 \tag{4.55}$$

$$I_z = \sum_{i=1}^{n=6} I_{z_i} + \sum_{i=1}^{n=8} (A_i \cdot (y_i - y_{centroid})^2) = 5.51 \cdot 10^{10} mm^4 \tag{4.56}$$

Compression layer

The final component of the total bridge deck is the compression layer. This layer comprises a single square with a width of 6500 mm and a height of 230 mm for profiles ZIPXL700 to ZIPXL1700, and a height of 200 mm for ZIPXL1800 and above. Since ZIPXL2000 is being considered, the compression layer has a height of 200 mm.

The area of the compression layer is calculated as $6500 \cdot 200 = 1300000$ mm^2. The centroid of the compression layer lies in the middle, with coordinates z = 100 mm and y = 3250 mm.

The inertia around y and z for the compression layer can be calculated using the formulas:

$$I_y = \frac{1}{12} \cdot 6500 \cdot 200^3 = 2.17 \cdot 10^7 mm^4 \tag{4.57}$$

$$I_z = \frac{1}{12} \cdot 200 \cdot 6500^3 = 7.04 \cdot 10^8 mm^4 \tag{4.58}$$

Total Bridge Deck Properties

The total bridge deck and the horizontal distances between its various components are illustrated in Figure 4.35. Initially, the centroid for the entire bridge deck needs to be computed to facilitate the calculation of the inertia's Steiner term.

Since the cross section is symmetric along the y-axis, the y-coordinate of the centroid will be exactly in the middle, at a distance of 3250 mm from the reference point.

The z-coordinate of the centroid can be calculated using the following formula:

$$z_{centroid} = \frac{E_{comp} \cdot A_{comp} \cdot z_{comp} + E_{prefab} \cdot (3 \cdot A_{main} \cdot z_{main} + 2 \cdot A_{bound} \cdot z_{bound})}{E_{comp} \cdot A_{comp} + E_{prefab} \cdot (3 \cdot A_{main} + 2 \cdot A_{bound})} = 960.37 mm \tag{4.59}$$

Where E_{comp} is the elasticity modulus of the compression layer (C35/45 concrete) and E_{prefab} is the elasticity modulus of the prefabricated part (C60/75 concrete).

The area of the total bridge deck is:

$$A_{total} = A_{comp} + 3 \cdot A_{main} + 2 \cdot A_{bound} = 5493210 mm^2 \tag{4.60}$$

With the total area known, the inertia around y and z for the total bridge deck can be calculated:

$$\begin{aligned} I_y = (I_{y.comp} + 3 \cdot I_{y.main} + 2 \cdot I_{y.bound}) + (A_{comp} \cdot (z_{comp} - z_{centroid})^2 + 3 \cdot A_{main} \cdot (z_{main} - z_{centroid})^2 \\ + 2 \cdot A_{bound} \cdot (z_{bound} - z_{centroid})^2) = 2.34 \cdot 10^{12} mm^4 \end{aligned} \tag{4.61}$$

$$\begin{aligned} I_z = (I_{z.comp} + 3 \cdot I_{z.main} + 2 \cdot I_{z.bound}) + (A_{comp} \cdot (y_{comp} - y_{centroid})^2 + A_{main} \cdot (3250 - y_{centroid})^2 \\ + 2 \cdot A_{main} \cdot (1720 - y_{centroid})^2 + 2 \cdot A_{bound} \cdot (685 - y_{centroid})^2) = 1.38 \cdot 10^{13} mm^4 \end{aligned} \tag{4.62}$$

This calculation is performed for all ten different bridge deck profiles, resulting in the cross-sectional properties listed in Table 4.5.

Bridge length [m]	Profile	Area bridge deck A [mm^2]	Moment of inertia Y I_y *10^{12} [mm^4]	Moment of inertia Z I_z *10^{12} [mm^4]
15	ZIPXL700	3990650	0.369	9.019
20	ZIPXL 1000	4306460	0.762	10.180
25	ZIPXL 1400	4896210	1.566	12.093
30	ZIPXL 1700	5493210	2.338	13.775
35	ZIPXL 2000	5926435	3.605	15.603
40	ZIPXL 2300	6298435	4.998	16.925
45	ZIPXL 2600	6670435	6.666	18.246
50	ZIPXL 2900	7042435	8.627	19.567
55	ZIPXL 3200	7414435	10.898	20.888
60	ZIPXL 3500	7786435	13.496	22.209

Table 4.5: Cross sectional properties for the different bridge lengths

Number 4:
The fourth component in Figure 4.34 represents the elastomeric bearings used to support the bridge deck on the bridge pier. In this investigation, elastomeric bearings are utilised, primarily composed of rubber with steel plates for increased tensile resistance. These elastomeric bearings are crucial for transferring forces from the superstructure to the substructure. They are modeled as springs with both horizontal and vertical spring stiffness. The choice of the elastomeric bearings has a significant impact on the horizontal and vertical spring stiffness. Therefore, the elastomeric bearings are a variable parameter in this investigation.

There are various options for elastomeric bearing elastomeric bearings, including different dimensions, thicknesses, and configurations with one or more steel plates. In the reference projects, such as Theemswegtracé and Eygelshoven, elastomeric bearings with horizontal stiffness values per bearing of 3.00 and 5.63 MN/m were used (Wagemaker, 2018) (Wagemaker, 2015). Therefore, for this investigation, the investigation ranges for the elastomeric bearings are between a horizontal stiffness of 1.5 and 8 MN/m per bearing. The vertical stiffness is coupled with the horizontal stiffness due to the dimensions used to achieve the horizontal stiffness. In Figure 4.35 can be seen that over the width of the bridge deck there are 5 elastomeric bearings used. So for the total stiffness the horizontal and vertical stiffness per bearing needs to be multiplied with five.
For the default setting, a 400 x 400 mm bearing with 4 rubber layers with a thickness of 9 mm and steel plates of 33 mm, along with bottom and top casings of 2.5 mm, will be used. This configuration yields a horizontal stiffness of 4 MN/m with a corresponding vertical stiffness of 1932 MN/m.(European Commitee for Standardization, 2018)

Number 5:
The fifth component, depicted as number 5 in Figure 4.34, represents the bridge piers of the railway bridge. These piers will be modeled as beam elements with cross-sectional and material properties specific to the type of piers, with cross sections of 2500 x 1250 mm and a concrete class of C30/37.
The length of the piers, denoted as L_2 in Figure 4.34, is typically determined by the clearance height required for traffic to pass underneath the bridge. As this clearance height can vary, it significantly impacts the stiffness of the substructure, consequently affecting the additional rail stresses. Therefore, the bridge piers length is considered a variable parameter in this investigation.

The length of the pier is a variable in this investigation, and it is assumed that the pier type will remain the same, so there is no adjustment for the cross-sectional properties, such as area and moment of inertia. The investigation range of the length L_2 is between 5 and 10 meters, with a default length of 7.5 meters.

Number 6:
The sixth parameter in Figure 4.34 represents the foundation of the railway bridge, symbolised by a horizontal spring. The stiffness of this spring is influenced by several factors, including the stiffness of the surrounding soil, the type of foundation (e.g., pile foundation or shallow foundation), the length and dimensions of the piles, and the properties of the slab used.
For this investigation, a pile foundation similar to that used in part 3 of the Theemswegtracé is assumed as a reference point. The stiffness of the foundation is crucial as it determines the distribution of stresses between

the rail and the supports. Hence, the stiffness of the foundation is identified as a variable parameter in this investigation.

The stiffness of the reference pile foundation in part 3 of the Theemswegtracé is determined by applying a 1000 kN horizontal load, resulting in a horizontal movement of 14.7 mm. (Wagemaker, 2018) This yields a horizontal stiffness of:

$$k_H = \frac{1000}{14.7} = 68\text{kN/mm} \tag{4.63}$$

The stiffness of the reference pile foundation is thus 68 MN/m, which is chosen as the default setting. The investigation range for the variable foundation stiffness spans from -50% to +50%, resulting in a range between 34 and 102 MN/m.

Number 7:
The final element, represented by number 7 in the figure, pertains to the model ending spring. This spring symbolises the stiffness of the continuous welded rail, derived from the combined stiffness of the neighboring bridge structures.

The spring represents the stiffness of neighboring bridge spans necessary to nullify embankment influence. To determine this stiffness, we need to ascertain how many unloaded bridge spans are required to attenuate the force exerted by a loaded span. For verification, one loaded span is modeled with a 20 kN/m braking load, flanked by 10 and 15 unloaded spans on either side. The displacement of the last node and the reaction force at that node are then examined, as visualised in Figure 4.38. The results are summarised in Table 4.6.

10 unloaded spans before and after one loaded span		
Displacement last node	0.144	mm
Reaction force in last node	-6.11	kN
15 unloaded spans before and after one loaded span		
Displacement last node	0.017	mm
Displacement last node	-0.72	kN

Table 4.6: Displacement and reaction forces for one loaded span and 10/15 unloaded spans

From these results, it can be concluded that after 10 unloaded spans, the loads of the loaded span are almost damped out, and after 15 unloaded spans, the load is even more damped out. For validation, it is also checked if this is also the case if 10 loaded spans are placed in between the unloaded spans instead of just one. This result is presented in Table 4.7.

15 unloaded spans before and after ten loaded span		
Displacement last node	0.028	mm
Displacement last node	-2.04	kN

Table 4.7: Displacement and reaction forces for ten loaded spans and 15 unloaded spans

From Table 4.7, it can be concluded that also with 10 loaded spans in between, the load is still damped out after 15 unloaded spans.

Now that the number of unloaded spans necessary to attenuate the load has been determined, the stiffness of these unloaded spans, and thus the ending spring for Model 1, can be derived. This analysis was performed for both configurations with 10 and 15 unloaded spans, resulting in the displacements of the first and last nodes as depicted in Figure 4.38. The difference between these displacements yields the delta displacement. Dividing a horizontal unity load of 1000 kN applied to the system by the delta displacement gives the stiffness of the two configurations, summarized in Table 4.8.

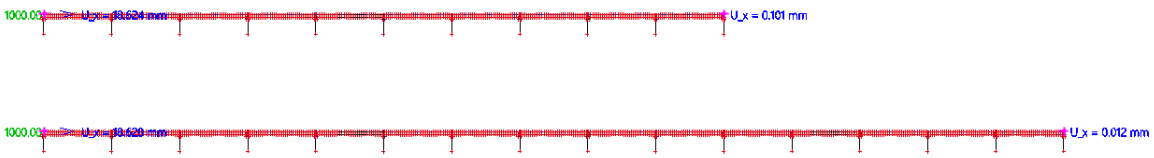

Figure 4.38: Displacement of first and last node to determine stiffness model ending spring

	Displacement first node [mm]	Displacement last node [mm]	Delta displacement [mm]	Stiffness of the unloaded parts [MN/m]
10 meter unloaded	18.624	0.101	18.523	53.99
15 meter unloaded	18.628	0.012	18.616	53.72

Table 4.8: Calculation of the stiffness of the unloaded parts

In Table 4.8, it is evident that the stiffness of the unloaded parts ranges from 53.5 to 54 MN/m. A stiffness value of 53.5 MN/m was selected for further analysis. This stiffness was then verified to ensure the accuracy of calculations and assumptions. To do this, a loaded span was modeled with a spring stiffness of 53.5 MN/m on both sides, and another loaded span was modeled without a spring but with 15 unloaded spans on both sides. This comparison resulted in the following displacements of the outer nodes and normal forces in the rails, as shown in Figure 4.39.

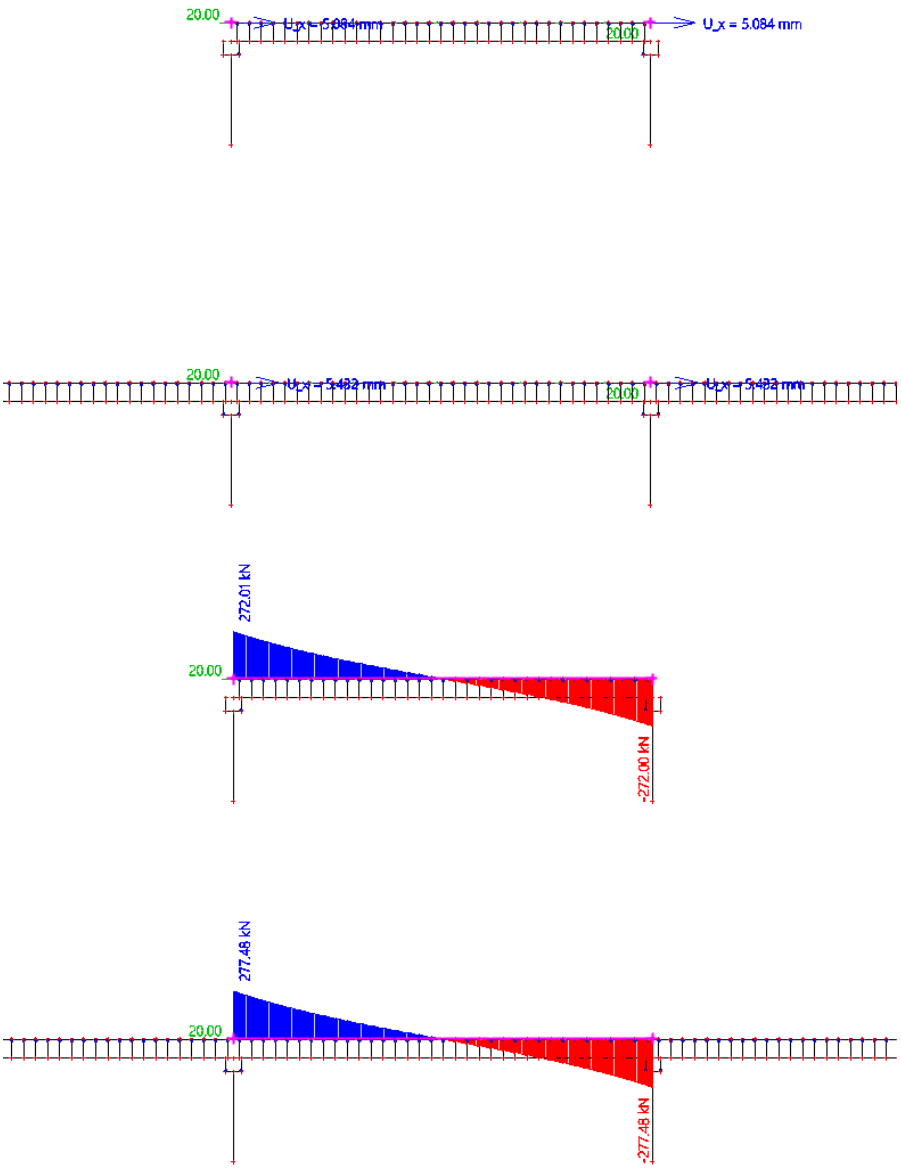

Figure 4.39: Checking of the model ending spring for Model 1

Out of Figure 4.39, it can be observed that the displacement and the normal forces of the different ways of modeling are almost similar. Therefore, it can be concluded that the model ending spring with a stiffness of 53.5 MN/m can be used for Model 1.

Eccentricity (e)

In Figure 4.34, the eccentricity between the rail and the bridge deck is denoted by e. This eccentricity is a fixed value of 730 mm between the top of the bridge deck and the top of the rail, as specified in the ProRail regulations (ProRail, 2023b).

As the dilating length changes, the bridge deck cross-section also changes. Although the distance between the top of the bridge deck and the top of the rail remains constant, in SCIA, the eccentricity is modeled as the distance from the center of gravity of the deck to the center of gravity of the rail, as in the real world. Therefore, this eccentricity will slightly vary in the SCIA models due to differences in the bridge deck profiles used.

4.2.1.2. Model 2: Model with embankment influence

The second model utilised for analysis in this thesis incorporates the influence of the embankment. This model is the most commonly encountered in real-life scenarios because the majority of railway bridges are not long enough for the influence of the embankment to be neglected. When a railway bridge is connected with the embankment, a transition structure is employed to facilitate the transition between the bridge deck and the embankment. Model 2, with the influence of the embankment, is depicted in Figure 4.40.

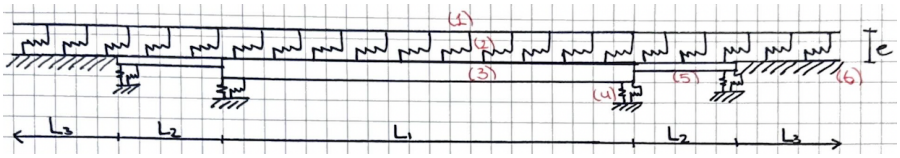

Figure 4.40: Model 2 with the influence of the embankment

Similar to Model 1, Model 2 will also be described based on the numbered components in the figure. Here, only the numbers that represent different elements from Model 1 will be explained to avoid duplication of information.

In the second model, the rail, bridge deck, connection from the rail to the bridge deck with a ballast structure, the elastomeric bearings, and the eccentricity are the same as for Model 1. Therefore, numbers 1, 2, 3 and e are identical for both structures. The varying parameters include the dilating length with the type of bridge deck, the stiffness of the elastomeric bearings and the foundation. Therefore the same investigation ranges and default settings are used as described in subsubsection 4.2.1.1.

Number 4:

Number 4 in Model 2 represents the stiffness of the foundation at the abutment of the railway bridge, symbolised by a horizontal spring. This foundation stiffness at the abutment serves a similar function to the bridge pier and foundation in Model 1, transferring loads into the bridge. The stiffness of the abutment depends on factors such as the type of piles used, their length, and the surrounding soil conditions. There are fewer piles under the abutment compared to the foundation of Model 1. Due to the significant impact of substructure stiffness on additional rail stresses, the abutment will be a variable parameter in this investigation for Model 2.

To ensure a pure comparison between Model 1 and Model 2, it was decided to maintain consistent parameters such as soil stiffness, type, and length of piles, identical to those used for the Theemswegtrace. However, under the abutment, there are half as many piles as under the foundation in Model 1. These abutment piles are placed at an angle to enhance horizontal stiffness, resulting in the foundation stiffness at the abutment being twice that of Model 1's default setting, totaling 136 MN/m. This value is varied within a range of -50% to +50%, yielding an investigation range from 70 to 205 MN/m.

Number 5:

Number 5 in Figure 4.40 represents the transition structure between the railway bridge and the embankment. This structure will be modeled as a beam element with the cross-sectional and material properties specific to the transition structure used. In the Netherlands, a standard transition structure is used. Therefore, the transition structure is a fixed parameter in this investigation.

The length of this transition structure is 4 meters, and the cross-sectional properties are a width of 4000 mm and a height of 350 mm. This gives a cross-sectional area of $1.2 \cdot 10^6$ mm^2 and a moment of inertia around y of $1.43 \cdot 10^{10}$ mm^4, and with a concrete class of C30/37.

Number 6:

The sixth number in Figure 4.40 represents the embankments on both sides of the railway bridge. These embankments influence the additional railway stresses. At the embankment, the rail is connected using the springs described in number 2 of subsubsection 4.2.1.1, and the embankment itself is rigidly supported, as shown in the figure.
The length of the embankment (L_3) is a fixed parameter to ensure that the complete influence length of the forces applied to the system is considered, allowing the model to terminate without a model-ending spring.

This fixed length was determined through a series of adjustments and checks:

- Initially, a very long embankment length of 300 meters was applied on both sides of the transition structure.
- The embankment length was then reduced to 200 meters, and the results were compared to those from the 300-meter embankment. The results were found to be the same.
- Subsequently, a length of 150 meters was considered. At this distance, all forces fell within the model, and the results matched those obtained with 300 meters of embankment.

Additionally, using 150 meters of embankment allowed the model to calculate three times faster than with 300 meters of embankment. Therefore, it was decided to fix the embankment length at 150 meters on both sides.

4.2.1.3. Investigation steps

The variables under investigation include elastomeric bearings, bridge piers, and foundations. These elements are arranged sequentially and directly linked, forming a series system where the spring stiffnesses interact cumulatively. In this serial system, the combined stiffness of the substructure is calculated through reciprocal summation. This subsection delves into the significance of these variables by varying their values across investigation ranges — specifically, the lower limit, upper limit, and default setting. This analysis is conducted for Model 1 to ascertain which substructure parameters exert the most influence.
Model 2 does not undergo this investigation because its inclusion of embankment stiffness suggests the substructure's stiffness is likely less dominant. Therefore, Model 1 is assumed to be dominant in this regard.
For elastomeric bearings, the stiffness investigation spans from 1.5 to 8 MN/m. Foundation stiffness ranges from 35 to 105 MN/m. The variable for bridge piers is their length, which, along with their cross-sectional properties, can be converted to stiffness using the formula:

$$k_H = \frac{3 \cdot EI}{l^3} \text{MN/m} \tag{4.64}$$

Here, E is the elasticity modulus of C30/37 concrete, which is 32837 MPa, and I is the moment of inertia, calculated as $\frac{1}{12} \cdot 1250 \cdot 2500^3 = 1.63 \cdot 10^{12}$ mm^4. The length of the pier, l, varies with a lower limit of 5 meters, an upper limit of 10 meters, and a default length of 7.5 meters. This results in the following investigation ranges for the pier stiffness: between 160 and 1251 MN/m, with a default stiffness of 380 MN/m.

By examining the combined stiffness values resulting from these variations, this investigation identifies which variable most closely aligns with the overall system stiffness. The results are presented in Table 4.9, Table 4.10, Table 4.11, and Table 4.12.

Layers	Lower limit stiffness	Upper limit stiffness	Default stiffness
Stiffness elastomeric bearings	6	40	20
Stiffness bridge pier	160	1281	380
Stiffness foundation	35	105	68
Combined stiffness	**4.96**	**28.33**	**14.85**

Table 4.9: Calculation of the combined stiffness with varying all variables

Layers	Lower limit stiffness elastomeric bearings	Upper limit stiffness elastomeric bearings	Default stiffness elastomeric bearings
Stiffness elastomeric bearings	6	40	20
Stiffness bridge pier	380	380	380
Stiffness foundation	68	68	68
Combined stiffness	**5.43**	**23.62**	**14.85**

Table 4.10: Calculation of the combined stiffness with varying support block stiffness

Layers	Lower limit stiffness bridge pier	Upper limit stiffness bridge pier	Default stiffness bridge pier
Stiffness elastomeric bearings	20	20	20
Stiffness bridge pier	160	1281	380
Stiffness foundation	68	68	68
Combined stiffness	**14.09**	**15.27**	**14.85**

Table 4.11: Calculation of the combined stiffness with varying bridge pier

Layers	Lower limit stiffness Foundation	Upper limit stiffness Foundation	Default stiffness Foundation
Stiffness elastomeric bearings	20	20	20
Stiffness bridge pier	380	380	380
Stiffness foundation	35	105	68
Combined stiffness	**12.31**	**16.09**	**14.85**

Table 4.12: Calculation of the combined stiffness with varying foundation

In these tables, it becomes clear that the stiffness of the elastomeric bearings is the most dominant variable among the three. In all considerations, the stiffness of the elastomeric bearing is the closest to the combined stiffness.

Therefore, investigations will focus on the lower limit, upper limit, and default setting for the foundation and bridge pier stiffnesses. Due to the importance of the elastomeric bearings, two additional points will be added in between, resulting in five investigation steps for the elastomeric bearings. This will be summarised in the following sub-subsection.
When this investigation is extended to Model 2, which uses an abutment instead of the pier and the same foundation, a similar conclusion can be drawn. Thus, for the foundation stiffness at the abutment, only the lower limit, upper limit, and default stiffness will be used.

4.2.1.4. Variable parameter overview

In the previous sub-subsections, all the parameters were discussed, including the number of investigation steps for each variable. This leads to the following overview sub-subsection, where all the discussed elements are summarised, and the specific values are provided.

The overview table in Table 4.13 lists each variable, indicating for which model they are valid, the investigation bandwidths, and the default settings. The default settings are used as a constant when a variable is not being varied.

Variables	Valid for model	Investigation bandwith	Default setting
Bridge deck	Both	Dilating lengths: Between 15-60 meters with steps of 5 meters Bridge types: ZIPXL profiles	Dilating length: 35 meters Bridge type: ZIPXL2000
elastomeric bearings	Both	Horizontal spring stiffness: between 1.5 and 8 MN/m with 3 investigation steps in between Vertical spring stiffness: coupled with the horizontal variation Number of bearings: 5	Horizontal spring stiffness: 4 MN/m Corresponding vertical spring stiffness: 1932 MN/m Corresponds to bearing: 400x400 mm with 4 rubber layers with a thickness of 9 mm and a steel plate of 3 mm and bottom and top casing of 2.5 mm Number of bearings: 5
Bridge pier	Model 1	Pier lengths: between the 5 and 10 meters Pier cross section: 2500 x 1250 mm with concrete class C30/37	Pier length: 7.5 meters Pier cross section: 2500 x 1250 mm with concrete class C30/37
Foundation	Model 1	Horizontal stiffness: between 35 and 105 MN/m	Horizontal stiffness: 68 MN/m
Abutment	Model 2	Horizontal stiffness: between 70 and 205 MN/m	Horizontal stiffness: 136 MN/m

Table 4.13: Variable parameter overview

As described in the previous sub-subsection, for the bridge pier, foundation, and abutment, the lower limit, upper limit, and default setting will be the investigation points. For the bridge deck, the investigation steps are given for every 5 meters, and the corresponding cross-sectional properties are provided in Table 4.5. For the elastomeric bearings, the lower limit, upper limit, default setting, and two intermediate points will be used as investigation points. These points, along with their vertical stiffness and dimensions, are presented in Table 4.14.

	Lower limit	Intermediate point 1	Default setting	Intermediate point 2	Upper limit
Horizontal stiffness per block [MN/m]	1.5	3.0	4.0	6.0	8.0
Corresponding vertical stiffness [MN/m]	303	1126	1932	3810	5877
Dimensions of the bearings	200 x 300 mm thickness of rubber of 9.0 mm	350 x 350 mm thickness of rubber of 9.2 mm	400 x 400 mm thickness of rubber of 9.0 mm	400 x 600 mm thickness of rubber of 9.0 mm	400 x 800 mm thickness of rubber of 9.0

Table 4.14: Investigation points of the elastomeric bearings

4.2.2. Model loads

To understand how the structure responds to applied loads, it is crucial to identify the forces acting on the system, their magnitudes, and locations of application. Considering the varying nature of train movement, load positions are adjusted to capture quasi-static behavior. Additionally, load combinations are formed to account for simultaneous load situations. This subsection elaborates on these aspects.

4.2.2.1. Loads on the system

As previously discussed, three main types of loads affect the system: thermal load, longitudinal traffic load, and vertical traffic load. Each load's magnitude and different models will be individually addressed.

Thermal load

Thermal loads arise from temperature differences between the neutral temperature and the lowest and highest temperatures. Decrease in temperature causes contraction and increase in temperature causes extension. As a result, thermal loads are imposed deformations, and depend on the amount of stiffness given by other materials coupled to them and their own material properties. A more detailed explanation can be found in section 2.1.

In this investigation, additional rail stresses due to the presence of the bridge structure are investigated. As a result, this investigation only takes into account temperature increases and decreases on the bridge deck and not on the rails themselves. This is because the temperature change of the rail also occurs on the embankment, and therefore does not cause additional rail stress due to presence of the bridge structure. The temperature increase and decrease of the deck can be found in Table 2.3.

Longitudinal traffic loads
The longitudinal traffic loads include the braking and acceleration loads of a train on the rail. These loads act on the top of the rail and give a load in the travel direction for braking and a load in the opposite direction for acceleration. The magnitude of the loads is prescribed by the Eurocode and described in section 2.3. And the magnitudes of these longitudinal forces given there are repeated below.

Acceleration forces: Q_{lak}= 33 [kN/m] $L_{a,b}$[m]≤ 1000 [kN]
For load models: 71, SW/0 and SW/2

Braking forces: Q_{lbk} = 20 [kN/m] $L_{a,b}$[m]≤ 6000 [kN]
For load models: 71 and SW/0
Q_{lbk} = 35 [kN/m] $L_{a,b}$[m]
For load model SW/2

(European Commitee for Standardization, 2011)
Where the load models 71, SW/0 and SW/2 are illustrated in Figure 2.12, Figure 2.13 and Table 2.4. These load models indicate where the loads act on if the load model is placed on the system.
This results in the following maximum acceleration and braking lengths for the different load models, as given in Table 4.15.

	Model	$L_{a,b}$	**Total force**
Acceleration	71	$\frac{1000}{33}$ = 30.3 m	33 · 30.3 = 1000 kN
	SW/0	$\frac{1000}{33}$ = 30.3 m ≤ 30 m = 30 m	33 · 30 = 990 kN
	SW/2	$\frac{1000}{33}$ = 30.3 ≤ 50 m = 30.3 m	33 · 30.3 = 1000 kN
Braking	71	$\frac{6000}{20}$ = 300 m	20 · 300 = 6000 kN
	SW/0	2 · 15 = 30 m	20 · 30 = 600 kN
	SW/3	2 · 25 =50 m	35 · 50 = 1750 kN

Table 4.15: The maximum acceleration and braking length

Vertical traffic load
The vertical traffic load refers to the weight of the train, including its cargo or passengers, exerted on the system. This load is represented in the models using load models 71, SW/0, and SW/2, detailed in section 2.3 and visualised in Figure 2.12 and Figure 2.13. The specific values are provided in Table 2.4.
These vertical traffic loads are applied to the bridge deck in the models. This approach is chosen because the investigation focuses on understanding the additional stresses on the rails caused by the bridge structure. Placing the vertical load on the bridge deck accounts for the bending of the deck itself, which contributes to additional stresses on the rails. In reality, it is impractical to place the vertical load directly on the rails due to the stiffness of the ballast and sleepers under the rails, which prevents significant bending. Thus, placing the load on the bridge deck provides a more realistic representation of the stress distribution.

4.2.2.2. Locations of the loads
The train moves across the model. As a result, several locations have to be considered to handle the quasi-static behaviour of the structure. Here, the locations that are considered most unfavourable are used. The structure is symmetrical so the unfavourable location for one side is already enough to consider, as this load on exactly the other side will cause the same response of the structure. The locations of the loads in Models 1 and 2 are illustrated in Figure 4.41 and Figure 4.42, respectively.

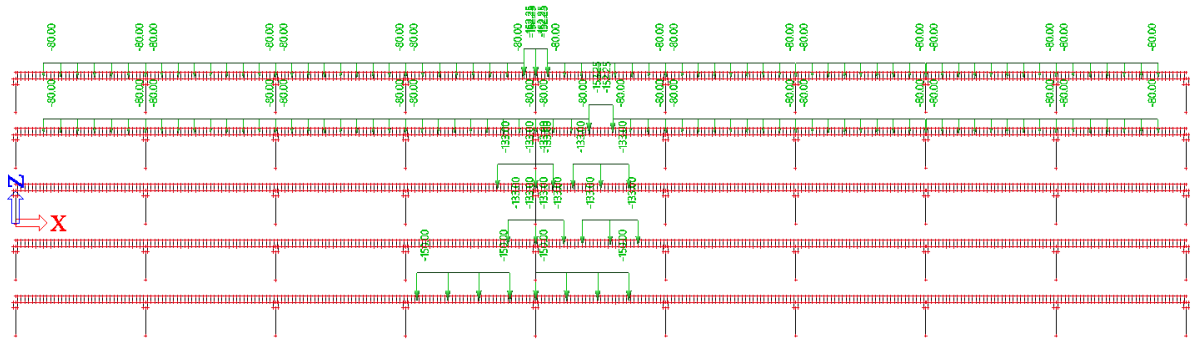

Figure 4.41: Locations of the loads for model without embankment influence (Model 1)

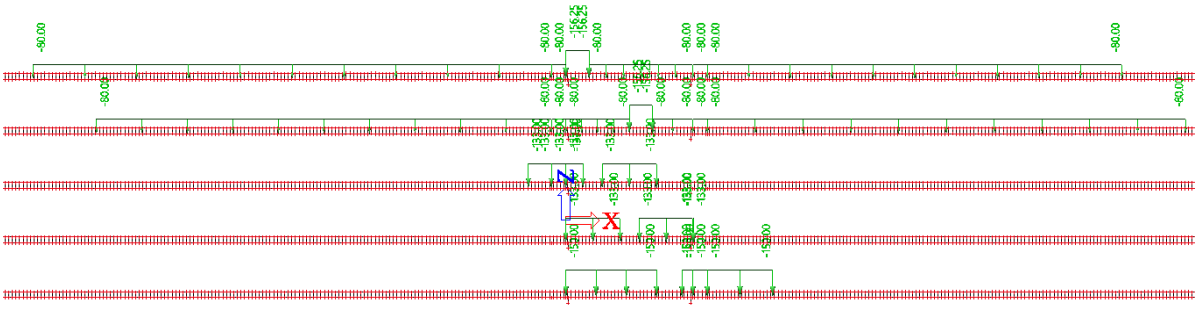

Figure 4.42: Locations of the loads for model with embankment influence (Model 2)

From top to bottom, these are the following locations:

- Rail Model 71A: Load above the support
- Rail Model 71B: Load in the middle
- Rail Model SW/0 A: Load in the middle
- Rail Model SW/0 B: Load above the support
- Rail Model SW/2

4.2.2.3. Load Combinations

To assess the longitudinal forces in the structure, the three load cases are combined. For the stresses in the rails, a combination factor of 1.00 is assumed for all three load cases, following the Eurocode (European Commitee for Standardization, 2011).

$$Q = 1.00 \cdot Q_{\text{thermal}} + 1.00 \cdot Q_{\text{longitudinal}} + 1.00 \cdot Q_{\text{vertical}} \tag{4.65}$$

The different combinations used in this investigation are as follows:

- LC1: Temperature increase + braking load (travel direction to the right) + vertical traffic load
- LC2: Temperature decrease + braking load (travel direction to the right) + vertical traffic load
- LC3: Temperature increase + acceleration load (travel direction to the right) + vertical traffic load
- LC4: Temperature decrease + acceleration load (travel direction to the right)+ vertical traffic load
- LC5: Temperature increase - braking load (travel direction to the left) + vertical traffic load
- LC6: Temperature decrease - braking load (travel direction to the left) + vertical traffic load
- LC7: Temperature increase - acceleration load (travel direction to the left) + vertical traffic load
- LC8: Temperature decrease - acceleration load (travel direction to the left)+ vertical traffic load

There are also different combinations with various locations and vertical load models (71, SW/0, and SW/2), but these combinations are included in the ones mentioned above and are divided among five different models, as explained in subsection 4.3.1.

4.2.3. Assessment Criteria

The presence of the bridge structure necessitates an evaluation of additional stresses on the rails. According to the Eurocode standards detailed in section 2.3, the maximum allowable additional rail stresses are as follows:

Maximum additional compressive stress ≤ 72 N/mm^2
Maximum additional tensile stress ≤ 92 N/mm^2
(European Commitee for Standardization, 2011)

To establish stress limits for this investigation, an initial model is created to determine the baseline stresses. This initial model represents a rail structure on an embankment and accounts solely for longitudinal forces. Thermal loads are excluded from this initial model, as explained in subsubsection 4.2.2.1, since they are applied exclusively to the bridge deck.
The stresses derived from the initial model are combined with the Eurocode's additional stress criteria to define the investigation's stress limits. Specifically, a 300-meter segment of embankment was modeled, and all longitudinal force loading models were applied with varying stiffness between the rail and embankment. The results, detailed in Table 4.16, indicate that the maximum stress due to braking and acceleration (load model 71) on the embankment reaches 22.40 N/mm^2, manifesting in both compression and tension depending on the direction of travel across the railway.

Load situation	**Stiffness rail-structure**	**Rail Stress (N/mm^2)**
71-Acceleration	High	15.06
71-Acceleration	Low	15.75
71-Braking	High	19.87
71-Braking	Low	22.40
SW/0-Acceleration	High	13.65
SW/0-Acceleration	Low	14.36
SW/0-Braking	High	8.27
SW/0-Braking	Low	8.70
SW/2-Acceleration	High	11.68
SW-2-Acceleration	Low	12.29
SW/2-Braking	High	15.09
SW/2-Braking	Low	16.55

Table 4.16: The initial stresses in the rails due to braking and acceleration

This ensures that the assessment criteria are the following additional rail stress due to presence of the structure:
Maximum compressive stress $\leq 72 + 22.40 = 94.4$ N/mm^2
Maximum tensile stress $\leq 92 + 22.40 = 114.4$ N/mm^2

4.3. Collection of Results and Method of Analysis

This section outlines the methods for collecting and analysing the results obtained. First, the process of data collection will be discussed, including how the results were stored to provide a clear overview, this will be performed in subsection 4.3.1. Subsequently, the method of analysis will be detailed, along with the expected findings, can be found in subsection 4.3.2.

4.3.1. Collection of Results

The results were collected by creating two models in the SCIA Engineer 22 software:

- Model without embankment influence - Model 1
- Model with embankment influence - Model 2

As illustrated in Figure 4.41, five different load situations were modeled, each with different models and locations. These five situations were stacked vertically to minimise changes in the locations of loaded and

unloaded springs, allowing the results of different load situations to be easily compared. Additionally, all five situations were calculated simultaneously, reducing the total number of simulations required in SCIA. Initially, the models were created with default settings and verified for accuracy. Once verified, parameters for each variable were varied within predefined investigation ranges and steps. When analysis is performed for one variable, the other variable remains at the default setting.

The results obtained for each set of parameters will be stored in an Excel file that will serve as a database. This file will be organised as follows: for every variable, an Excel sheet will be created. On each sheet, the results of the five different load situations will be listed for every iteration, with the investigation steps within the investigation bandwidth of the variable.
The results are recorded for each set of variables and load situations, both for individual load cases and for all load situations combined. This allows for analysis at the end of the process to determine whether summing the individual load cases according to the NS guideline yields the same results as the combined loads. The NS guideline suggests that linear summation of individual stresses from separate load cases is possible. However, the use of non-linear springs between the bridge deck and the rails complicates this summation according to mechanics. This analysis examines whether the NS guideline consistently errs on the side of caution and to what extent it results in more conservative estimates. The load combinations considered are listed in subsubsection 4.2.2.3.
For each iteration of the variable, the combination that yields the highest stresses is identified and stored separately as a critical value. This critical value represents the maximum stress for that iteration of the variable.

4.3.2. Method of Analysis

Once the results are obtained and stored in the dataset, they need to be analysed to identify relationships and draw conclusions. This subsection discusses the method of analysis.
As explained in subsection 4.3.1, the results for all variations of the variables for different load situations are listed for both individual loads and combinations of thermal, longitudinal traffic, and vertical traffic. Additionally, the critical values representing the maximum stress for each set of variables are identified and stored separately.
The analysis will involve creating plots with Python to explore the relationship between the critical additional rail stress and the varying parameter. This will be performed for both models with and without the embankment influence. Comparing the results of the critical additional rail stresses for the same settings between the two models will help determine the influence of the embankment.

5

Model Validation

In this chapter, both Model 1 and Model 2 are validated. This validation checks that the modeling process was accurate and that the calculations for both models with the default settings yield logical results. This ensures the reliability of the models and the conclusions drawn from them.
The validation process involves examining the normal force lines, moment lines, and, if necessary, the rotations for different individual load situations. The results from the SCIA models are compared with hand calculations from section 4.1 to verify that the answers are of the same order of magnitude and that the internal force lines have similar shapes. Although the SCIA models are more complex than the simple hand calculations, the results should still exhibit similar magnitudes and shapes. At the transition of different bridge decks, particularly at the supports, additional manual calculations of a simplified variant of the model may be carried out if needed.
This chapter is divided into three sections, each dedicated to a specific individual load situation. The first section covers the thermal load, the second section addresses the longitudinal traffic load, and the third section discusses the vertical traffic load.

5.1. Thermal Load

The first loading situation to be validated is the thermal load. For both Model 1 and Model 2, the thermal load is applied only to the bridge deck. This approach ensures that the additional rail stresses are solely due to the presence of the bridge structure. No thermal load is applied to the rail because the rail will experience this load elsewhere on the railway system, as explained in subsubsection 4.2.2.1 For Model 2, the thermal load is also not applied to the embankment or the transition structure.

The simplified model hand calculations are provided in subsection 4.1.1. For the thermal load, the normal force can be calculated using Equation 4.24, and the moment can then be derived. These internal forces depend on the cross-sectional area and inertia of the bridge deck and rails. By using the cross-sectional properties of ZIPXL2000 and the rail properties of two rails, the normal forces and moments can be calculated and compared with those from Model 1. The maximum normal force and moment occur at the center of the bridge deck, so this location will be the focus of the comparison.
The properties used are:

- EA_{deck}: 2.21×10^{11} N
- EA_{rail}: 5.86×10^{9} N
- EI_{deck}: 1.34×10^{17} Nmm^2
- EI_{rail}: 1.97×10^{13} Nmm^2

This results in the following normal forces and bending moments at the midpoint of the 35-meter bridge deck, specifically after 17 springs:

- N_{deck}: -309.57 kN
- N_{rail}: 309.57 kN
- M_{deck}: 238.35 kNm
- M_{rail}: 0.02 kNm

Model 1 produces the normal force and bending moment diagrams shown in Figure 5.2 and Figure 5.2.

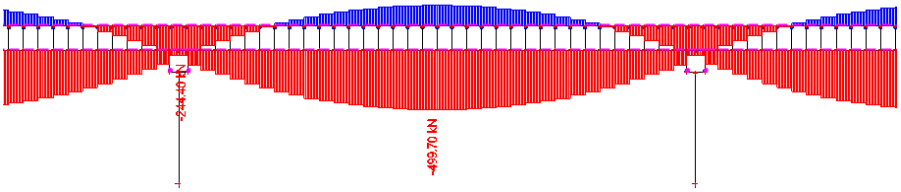

Figure 5.1: Normal force diagram for Model 1 under thermal load

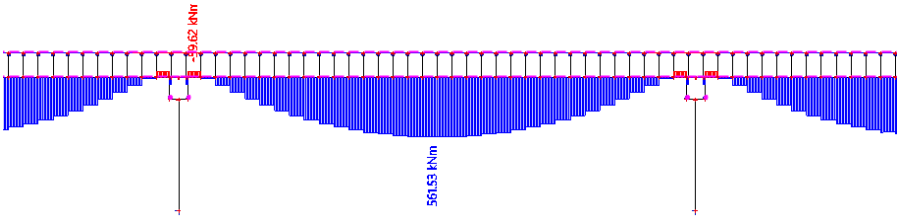

Figure 5.2: Bending moment diagram for Model 1 under thermal load

These figures show that the shapes of the diagrams are comparable to Figure 4.12. Notably, there is distortion in the normal force of the rails around the supports. This distortion occurs because the bridge decks subjected to thermal loads are allowed to expand freely, while the rails remain continuous, which was not accounted for in the hand calculations. Consequently, the rails provide additional stiffness to the bridge deck, resulting in a slightly larger normal force in the middle of the bridge deck compared to the calculated value. However, the order magnitude is similar and the increase is explainable. The same applies to the bending moments in the bridge deck.
Therefore, it can be concluded that Model 1 provides a logical response to thermal loading, validating the model. Model 2 gives similar results, thereby it is also validated.

5.2. Longitudinal Traffic Load

The second loading situation to be validated is the longitudinal traffic load, which includes both the acceleration and braking of a train. Both forces act similarly; the only difference is the magnitude and direction of the load. In the hand calculations provided in subsection 4.1.2, the braking force is used. Therefore, the braking force will also be used to validate the SCIA model to ensure consistent comparison.
The hand calculations are subdivided into two parts: the rail and the bridge deck. Consequently, the validation will also be subdivided into these parts. Firstly, the rails will be validated. In the SCIA model, the bridge deck is 35 meters long with an equally distributed load of 20 kN/m acting horizontally on top of the rail. In the hand calculations, the model is 10 meters long with the same distributed load.

Rail

The force acts along the element, so there is no bending moment in the rail. Therefore, only the normal force will be validated. The normal force diagram from the hand calculations, illustrated in Figure 4.17, clearly shows a jump of 20 kN/m at each spring location, with peaks of 10 kN in compression and 10 kN in tension. Model 1 produces the following normal force diagram for the rails, shown in Figure 5.3.

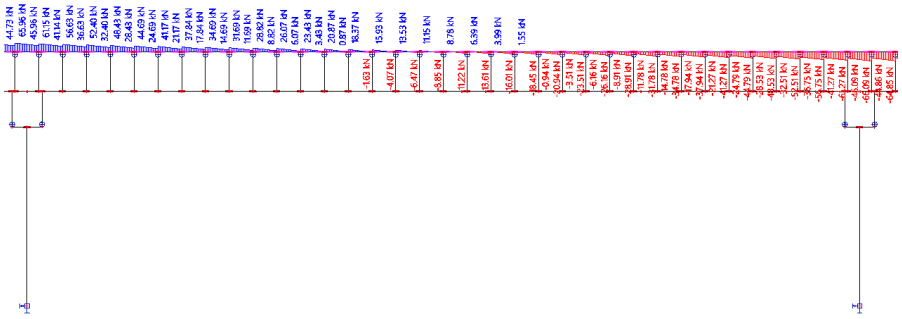

Figure 5.3: Normal force in the rail due to braking force in Model 1

The normal force diagram for Model 1 also shows an approximate 20 kN jump at each spring location. Another notable feature is that the transition between tension and compression is gradual along the length of the bridge, unlike the distinct changes at each spring location in the hand calculations. This difference arises because the rails in Model 1 are continuous, while the hand calculations assume free ends. Despite this, both diagrams exhibit a linear trend between springs and similar magnitude jumps of about 20 kN.
Thus, the normal force diagram for Model 1 is validated.

Bridge Deck
After validating the rails for the longitudinal traffic load in Model 1, the bridge deck results must also be validated. The internal force diagrams from the hand calculations are shown in Figure 4.22. This figure shows a total normal force of $20 \cdot 10 = 200$ kN for the 10-meter bridge deck. For Model 1, with a 35-meter bridge deck, the total normal force should be $20 \cdot 35 = 700$ kN. In the hand calculations, increments of 20 kN are seen at each spring location.
The normal force diagram for Model 1 is shown in Figure 5.4.

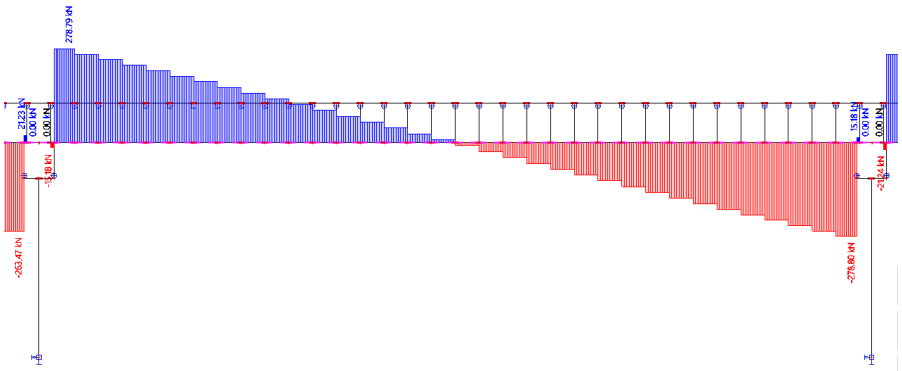

Figure 5.4: Normal force in the deck due to braking force in Model 1

This figure shows that the total normal force in the deck is as expected. However, the shape of the normal force line is slightly different. In the hand calculations, there is only tension in the deck due to a fixed support on the left. In Model 1, the supports are modeled with springs in the horizontal direction, leading to a gradual transition between compression and tension. The jumps of about 20 kN are present in both diagrams, indicating the same order of magnitude.
Therefore, the normal force in the deck is also qualified as logical for Model 1.

The last aspect to validate for the longitudinal traffic load is the bending moment in the deck. The hand calculations show a clear pattern: between the connection bars where the springs are located, the moment line is linear from -7.7 kNm to +7.7 kNm at the connection bars, with a jump of 15.4 kNm back to the negative side. The length of the connection bars in the hand calculations is 0.77 meters, while in Model 1, the length of these connection bars is 1.651 meters, resulting in higher bending moments.

The bending moment diagram for the deck due to the braking force in Model 1 is shown in Figure 5.5.

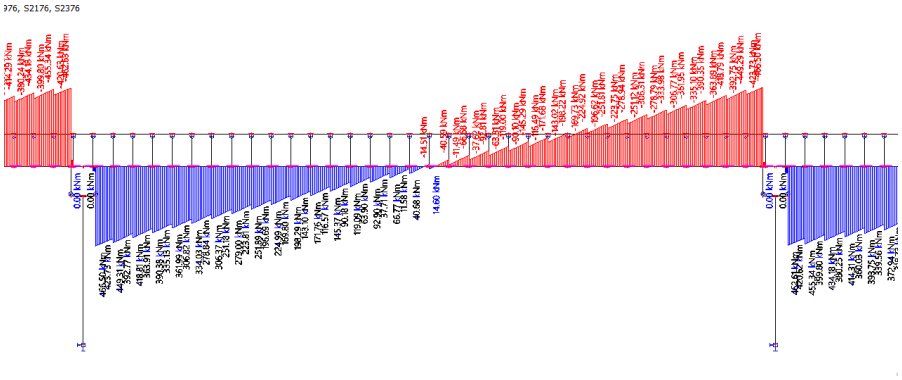

Figure 5.5: Bending moment diagram for the deck due to braking force in Model 1

Figure 5.5 shows a similar trend for Model 1. For example, at connection bar 3, the bending moment of 418.81 kNm progresses linearly to connection bar 4 with a bending moment of 363.91 kNm, then jumps back to 390.38 kNm. This trend is similar to the hand calculations, but the linear increase and jump are larger due to the longer connection bars.
The overall picture is slightly different, with a gradual transition between positive and negative moments, unlike the abrupt changes in the hand calculations. This difference is due to the continuous welded rails and the lack of fixed support in Model 1.
In summary, all magnitudes are correct, the trends are consistent, and the differences are explainable due to the simplifications in the hand calculations. Therefore, Model 1 is validated for longitudinal traffic loads. Model 2 shows similar results as Model 1 and is, therefore, also validated.

5.3. Vertical Traffic Load

The last load case to be validated is the vertical traffic load. This load is validated differently from the previous two load cases. In the previous cases, the model results were compared with the hand calculations from section 4.1. However, for the vertical load, the hand calculations placed the vertical load on the rails. As more knowledge about the rail-structure interaction was gained, it became clear that placing the load on the bridge deck better represented reality.
Placing the load on the rails produced large moments due to the fixed 1-meter spacing between springs. In reality, a thick ballast bed supports the rails, with sleepers every 60 cm, preventing such deflections and large moments. Therefore, placing the vertical rail load on the bridge deck better simulates reality, causing bridge deck deflection and resulting in rail stresses.
Consequently, the vertical load will be validated through reasoning rather than hand calculations, ensuring that logical normal forces and moments arise in the bridge deck and rails. This validation is divided into two parts: first, validating the internal forces in the bridge deck, and then validating the internal forces in the rails.

Bridge Deck

The normal forces and moments diagrams for the bridge deck in Model 1 are shown in Figure 5.6 and Figure 5.7.

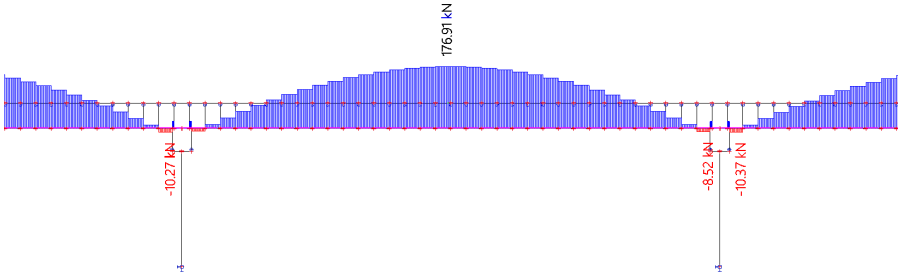

Figure 5.6: Normal force diagram for the Bridge deck in Model 1 under Vertical Traffic Load

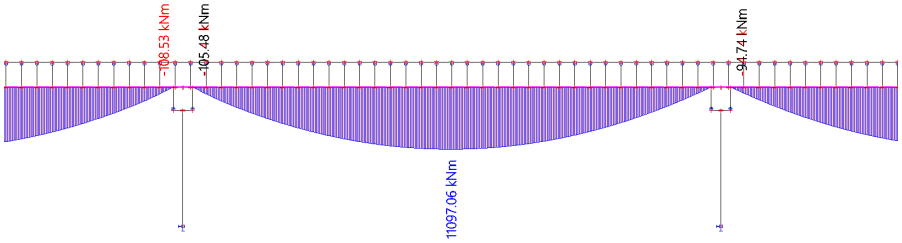

Figure 5.7: Bending moment diagram for the Bridge deck in Model 1 under Vertical Traffic Load

The vertical load is an evenly distributed load of about 80 kN/m. An evenly distributed load creates a parabolic moment line. The size of the moment in the middle can be calculated with $M = \frac{1}{8} \cdot q \cdot l^2$. Assuming 80 kN/m and 35 meters span length, the moment for the bridge deck in Model 1 should be near 12250 kNm and have a parabolic gradient. This matches the expectations, so the bridge deck is validated for moments under the vertical traffic load.
For the normal forces in the bridge deck, the springs in the connection bars are responsible. These create a shear force in the springs, producing a normal force in the deck. The magnitude of this shear force depends on the rotation of the bridge deck due to the vertical load. At the outer ends, the rotation is greatest, decreasing toward the middle and then increasing again toward the other end. Thus, the compression of the springs is greater at the ends, leading to larger transverse forces. This causes the normal force lines to have jumps proportional to the transverse forces in the springs, which is clearly seen in Figure 5.6. The larger jumps at the ends validate the bridge deck's normal forces under the vertical traffic load.

Rail
After validating the bridge deck, the rails must also be validated. The normal forces and moment diagrams for the rails in Model 1 are shown in Figure 5.8 and Figure 5.9.

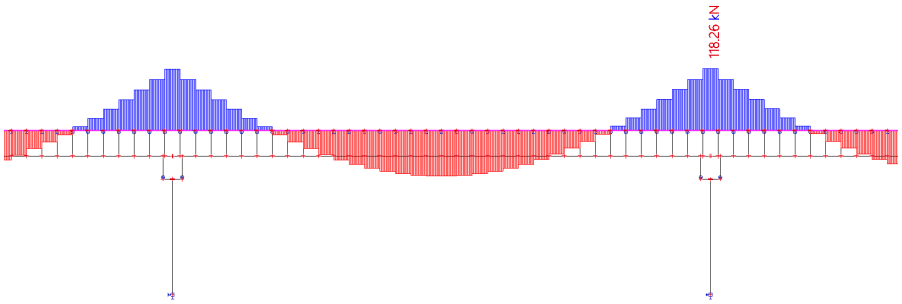

Figure 5.8: Normal force diagram for the rails in Model 1 under Vertical Traffic Load

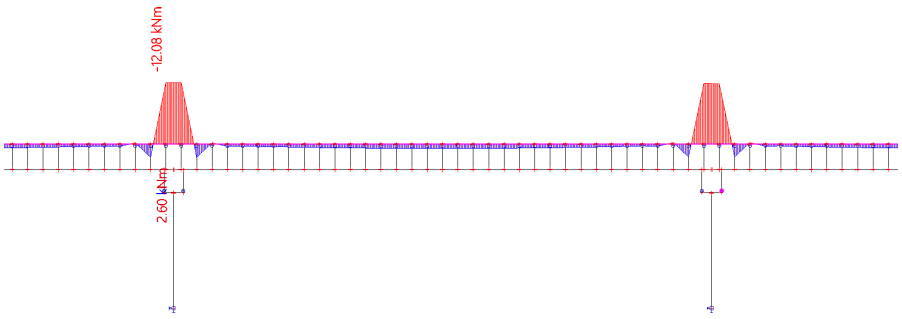

Figure 5.9: Bending moment diagram for the rails in Model 1 under Vertical Traffic Load

The normal force in the rails follows the same pattern as in the bridge deck. The magnitude of the jumps in the normal force line is of the same order, and the sum of the total normal force in the deck and the rails is the

same. The difference lies in the shape of the normal force line for the rails, which shows compression in the spans and tension at the supports because the rails are continuous. The jumps at the locations of the springs are due to the compression of the spring caused by the rotation of the bridge deck. Unlike the bridge deck, the rails run continuously, creating a transition from compression to tension, which is logical. The order of magnitude is also within expectations, validating the normal force in the rails under the vertical traffic load for Model 1.

The moments are expected to be close to zero because the vertical force is applied to the deck rather than directly on the rails, as depicted in Figure 5.9. However, noticeable peaks in moments occur at the transition points of the bridge deck near the bearings. These peaks arise because the rails pass through these points and experience moments due to angular rotations at the ends of the bridge deck. Further validation through additional hand calculations is necessary.
Hand calculations were conducted by uniformly loading two adjacent bridge decks with 80 kN/m and computing the deflection at the center (w) and the rotation at the ends (φ), as illustrated in Figure 5.10 and calculated using Equation 5.2 and Equation 5.2.

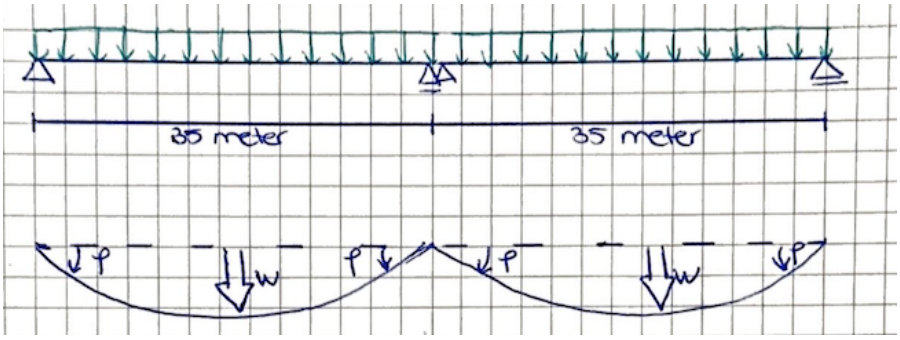

Figure 5.10: Additional hand calculations for validating the peaks

$$w = \frac{5}{384} \cdot \frac{q \cdot l^4}{EI} = 11.62 \text{ mm} \tag{5.1}$$

$$\varphi = \frac{1}{24} \cdot \frac{q \cdot l^3}{EI} = 1.06 \text{ mrad} \tag{5.2}$$

Since the rails are rigidly coupled to the bridge deck through infinitely stiff coupling bars, the rotation of the bridge deck fully transfers to the rails. However, as the rails pass through the bridge deck, moments develop in them due to angular rotations at the deck ends. This angular rotation effect in the rails is depicted in Figure 5.11.

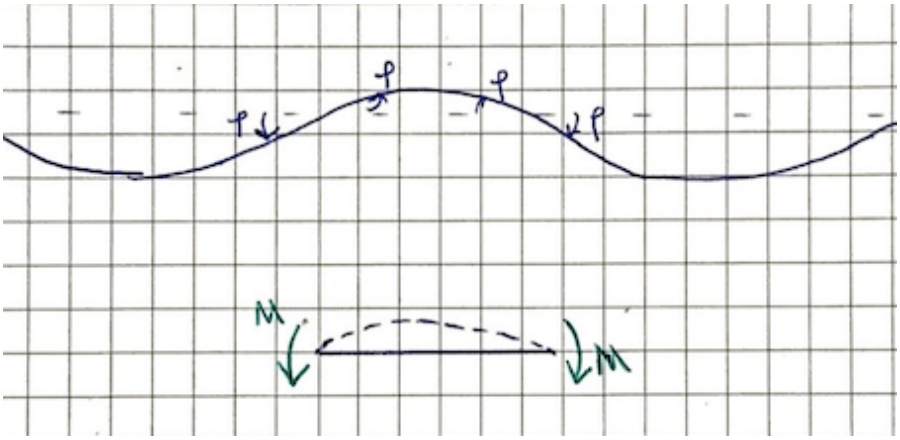

Figure 5.11: Additional hand calculations for validating the peaks 2

The rotations create moments in this intermediate piece. Assuming the transition zone where the rail stretches is 3 meters, the moment in this zone can be calculated using standard formulas. The calculations for the moments in this zone are shown in Equation 5.3 and Equation 5.4.

$$\varphi = \frac{1}{2} \cdot \frac{M \cdot l}{EI} \tag{5.3}$$

$$M = \frac{2 \cdot \varphi \cdot EI}{l} = 19.7 \text{ kNm} \tag{5.4}$$

From this, it can be concluded that the peak moments are of the same order of magnitude. Therefore, the moments in the rails under the vertical traffic load for Model 1 are validated. Similarly, Model 2 shows comparable results, thus validating Model 2 for the vertical traffic load as well.

6

Results

This chapter presents the results of the investigation into the additional rail stresses. As indicated in chapter 4, there are different variables in the two models. These variables are varied to see how different parameters affect additional rail stresses. This is done for both models, in which the influence of the variables is plotted against the additional rail stresses and the results are analysed. This analysis involves examining the differences in results within the two different models as well as the relationship between the variables and the additional rail stresses. Furthermore, the influence of the three different individual load cases—thermal, longitudinal, and vertical—is also examined. Specifically, it is investigated whether the individual stresses can be added together to arrive at the combined effect or if this approach yields too conservative results.
The chapter is divided into four sections. The first section deals with the influence of the different parameters for Model 1. The second section addresses the same analysis for Model 2. The third section compares the results of Model 1 and Model 2. The fourth and final section examines the individual contributions of the different load cases.

6.1. Model 1

This section discusses Model 1, which is the model without embankment influence. The different parameters, along with their corresponding properties and varying variables, are described in subsubsection 4.2.1.1. Each variable will have its own subsection. The first subsection will cover the variable bridge deck length. The second subsection will discuss the variable elastomeric bearings. The third subsection will address the variable bridge pier length. Finally, the fourth subsection will examine the variable foundation.

6.1.1. Variable: Bridge Deck

The first variable to be considered is the bridge deck. This variable is adjusted by its length, and when the length increases, a different bridge deck profile must be used. The bridge deck length and the bridge deck height are coupled through the slenderness ratio of 16, as described in subsubsection 4.2.1.1. The corresponding cross-section properties are presented in Table 4.5.

To analyse the influence of the variable bridge deck, a model of a single loaded span is first considered. This approach is chosen because adjustments involving various bridge lengths and profiles require substantial modeling time. By initially modeling a single loaded span instead of a multiple-loaded span, preliminary insights into the relationship between additional rail stresses and bridge deck length can be gained. This may allow a reduction in the number of bridge deck lengths considered within the investigation bandwidths. The results for the single loaded span models are presented in 6.1.1.1.
After this initial analysis, the model can be further refined by modeling the multiple-loaded spans. These results, which are more representative, are presented in subsubsection 6.1.1.2.

6.1.1.1. Single Loaded Span Model

Sub-subsection presents the results from the single loaded span model. While this model does not fully represent the real-world scenario, it provides useful insights. The model ending spring stiffness is set at 53.5

MN/m, determined based on the attenuation of load influence after 10 to 15 unloaded spans, effectively neglecting embankment effects. In this model, this spring stiffness is applied before and after a single loaded span ranging from 15 to 60 meters. However, for load model 71, the braking load can extend up to 300 meters (6000/20). Therefore, in reality, the model's ending spring stiffness of 53.5 MN/m should only be applied after at least 300 meters of loaded spans. Despite the discrepancy in the model's ending stiffness value from reality, other aspects remain consistent with the comprehensive model. This allows insights into the relationship between additional rail stress and bridge deck length, revealing that this relationship remains unchanged when extending the model.

Consequently, the single loaded span model does not accurately reflect the correct value of the model ending spring. Nevertheless, the rest of the model serves as a simplification of reality, allowing us to extract the relationship between different bridge lengths and the additional rail stresses. Therefore, this single loaded span model is considered first.
The calculations for the model with ten different lengths were carried out, and the numerical values for the compression and tension stresses in the rails can be found in Appendix A.1. The highest additional rail stresses, both in compression and tension, for all five different loading models described in chapter 4, are plotted against the bridge deck length and are presented in Figure 6.1 and Figure 6.2.

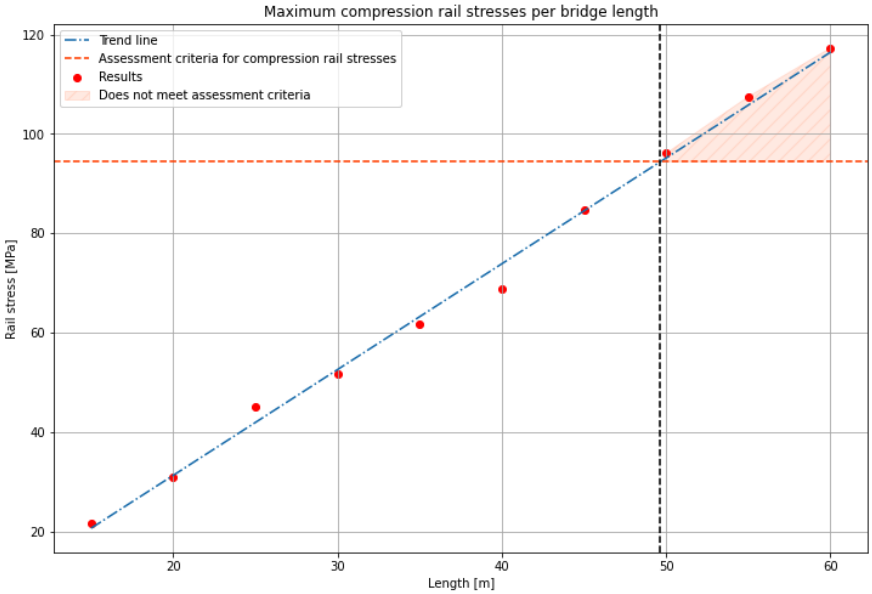

Figure 6.1: Additional compression rail stress against bridge deck length for a single loaded span model

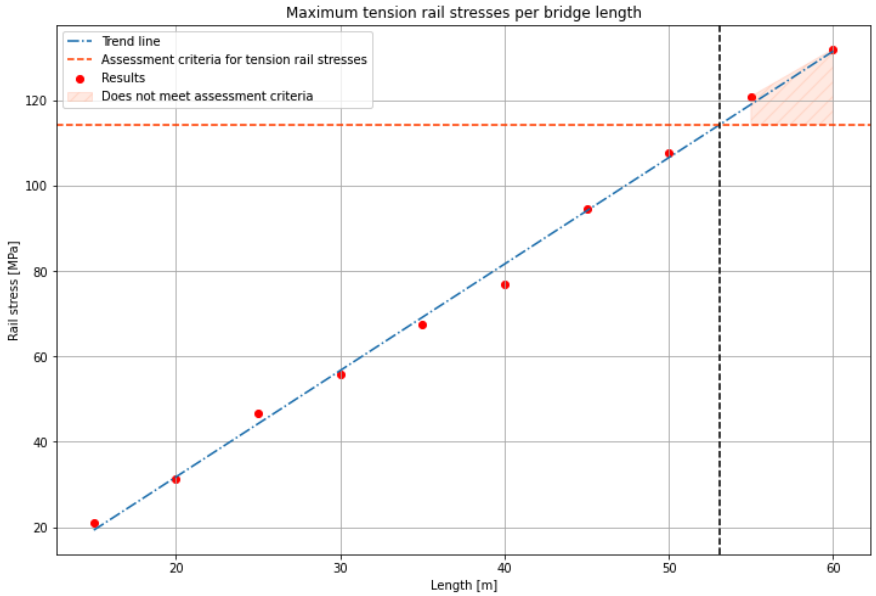

Figure 6.2: Additional rail tension stress against bridge deck length for a single loaded span model

In these figures, the results are plotted, including the assessment criteria and a trend line. It can be clearly seen that the trend between the bridge deck length and the additional rail stresses is linear. For this reason, in the multiple-loaded span model, only the lower limit, upper limit, and default lengths (15, 60, and 35 meters, respectively) are considered.

6.1.1.2. Multiple-loaded Span Model

As indicated in the previous sub-subsection, the analysis of the single loaded span model showed a linear relationship between bridge deck length and additional rail stresses. Therefore, only three different lengths (upper limit, lower limit, and default setting) are considered for the multiple-loaded span model. This approach reduces computing time while still providing sufficient data to draw conclusions about this variable. From this point, only the multiple-loaded span model will be used, as it best represents the unloaded spans with the model ending spring, closely approximating reality. Hence, the multiple-loaded span model is referred to as Model 1 in this investigation.

Calculations for the multiple-loaded span model are carried out for these three different span lengths with default settings for all other variables. The numerical values for compression and tension can be found in Appendix A.2.
In this Appendix, it can be clearly seen that for compression, load combination 5 (temperature increase - braking + vertical) is the most critical for all bridge span lengths. For lengths of 15 and 60 meters, load model SW/2 is the most critical, whereas for a length of 35 meters, load model 71A at the location above the support is the most critical. Therefore, the resulting additional rail stresses for load combination 5 for both load model SW/2 and 71A are plotted against bridge span length in Figure 6.3. The red dots and trend line represent 71A, while the blue dots and trend line depict SW/2. The black trend line shows the maximum additional rail stresses across various bridge span lengths. The orange line represents the compression assessment criteria from the Eurocode, supplemented by stresses from the initial model simulating rail traffic on the embankment. The continuous black line indicates the intersection of the maximum additional rail stress with the assessment criteria.

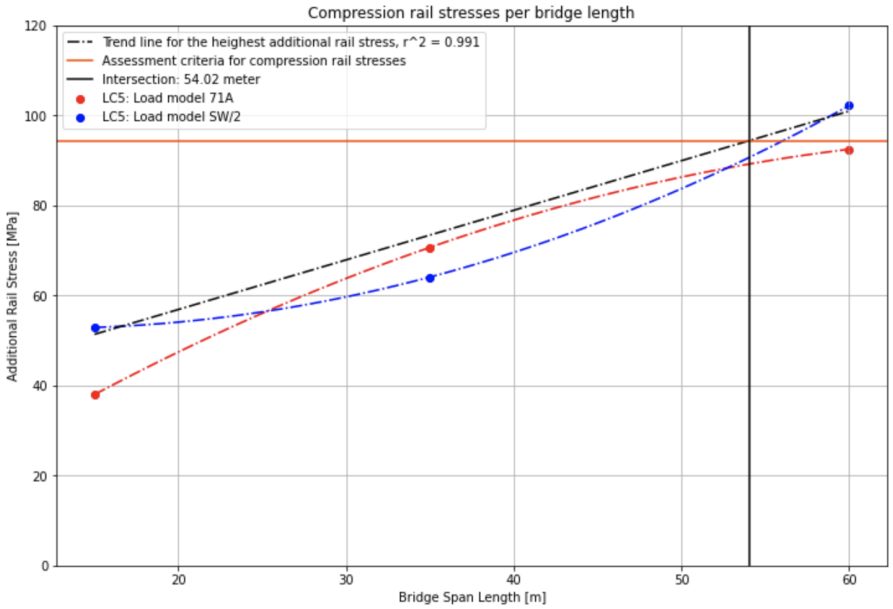

Figure 6.3: Additional compression rail stress against bridge deck length for Model 1

Figure 6.3 shows that for SW/2, the additional rail stresses increase as the bridge length increases. For 71A, the slope is larger at smaller bridge lengths and decreases as the bridge lengths increase. This could be because the SW/2 has a greater vertical force than load model 71A. As the bridge deck lengths get longer, this causes more deflection of the bridge deck and therefore more rotation at the end of the bridge deck, leading to increased rail stresses. As a result, for SW/2, the moment will increase more than the stiffness due to the larger profile of the bridge deck as the bridge span length increases. As the bridge span length increases, for 71A, the bending moment in the bridge deck, and consequently in the rails, increases less due to the larger profile of the bridge deck. Consequently, the vertical force has a greater influence on the combined additional rail stress. The analysis of the individual contribution of the individual loads is performed in section 6.4.
When the maximum of each bridge length is combined into a trend line (black line), thus combining the maximum of 71A and SW/2, it gives a linear relationship with an r^2 of 0.991.

The same analysis can be done for the additional tension rail stresses for the three different bridge lengths. Again, reference is made to Appendix A.2. Here, it can be seen that for tension, the highest additional rail stresses occur for load combination 2 (temperature decrease + braking + vertical) and for all three bridge lengths, this occurs for load model SW/2. In Figure 6.4, the results of load combination 2 - load model SW/2 are shown with blue points and a blue trend line. The assessment criteria from the Eurocode are given in orange, and the intersection of the trend line with the assessment criteria is shown with a black line, indicating the length at which the tensile additional rail stress exceeds the assessment criteria.

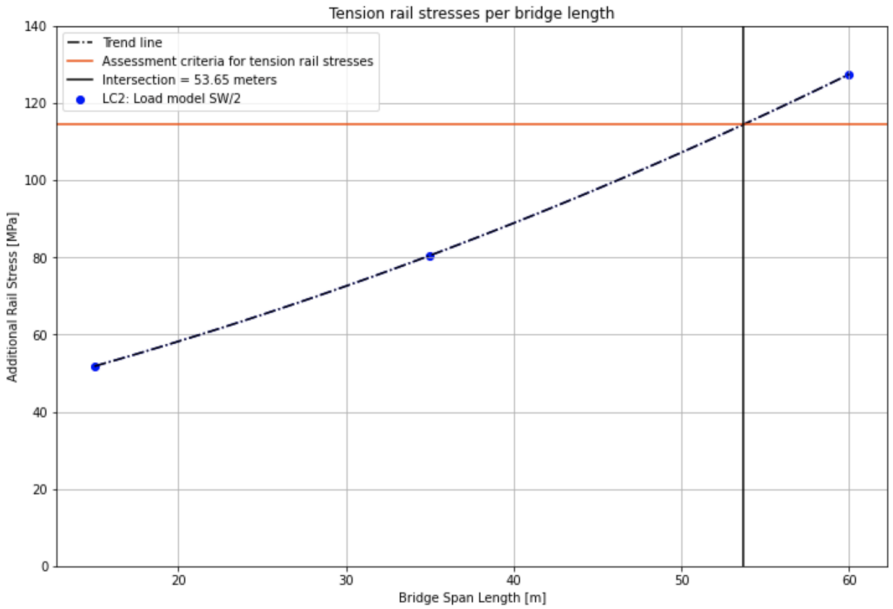

Figure 6.4: Additional rail tension stress against bridge deck length for Model 1

Comparing these results with the single loaded span model, it is noticeable that the initial stresses are higher at smaller bridge lengths. However, the stresses increase less as the bridge spans become longer compared to the single loaded span model.
This outcome aligns with expectations. In the single loaded span model, the total load magnitude increased with the loaded length and larger spans. In Model 1, where 300 meters of loaded span are consistently modeled, the total load remains constant while only the span lengths change. For example, at 15 meters, 20 spans of 15 meters are needed, while at 60 meters, only 5 spans are required. However, the total force on the model does not change. As a result, the stress increase for both tension and compression is less steep than in the single loaded span model.
Additionally, it can be observed that with default settings for other variables, the trend indicates that additional rail stresses are expected to exceed the compression assessment criteria at lengths of 54.02 meters and the tension criteria at lengths of 53.65 meters. Therefore, bridge spans up to approximately 50 meters can be utilized with default settings for other variables and ZIPXL bridges, focusing on longitudinal forces without exceeding prescribed limits. Utilising fixed points could potentially allow longer bridge lengths to meet the assessment criteria.

6.1.2. Variable: Elastomeric Bearings

The second variable considered is the elastomeric bearing. The elastomeric bearing investigation points are listed in Table 4.14.
Calculations for various elastomeric bearing stiffnesses were performed for Model 1. The numerical values for compression and tension can be found in Appendix A.3.
In the Appendix, it can be clearly seen that for compression, load combination 5 is the most critical for all the various elastomeric bearings. For elastomeric bearings with horizontal stiffnesses of 1.5, 3.0, 6.0, and 8.0 MN/m, the most critical additional rail stress occurs due to load model SW/2. However, for horizontal stiffness of 4.0 MN/m, the critical stress occurs due to load model 71A at the location above the support. Therefore, the results for both load models 71A and SW/2 are visualised in Figure 6.3, where the additional rail stresses are plotted against the various horizontal stiffnesses of the elastomeric bearings.
In this plot, the red dots and trend line represent load model 71A, while the blue dots and trend line represent load model SW/2. A black dashed-dotted line indicates the trend line for the highest additional rail stress for the various elastomeric bearings. The assessment criteria for compression are shown with an orange line. The intersection of the assessment criteria with the trend line for the highest additional rail stress is indicated by the black line, with the value of the intersection given in the legend.

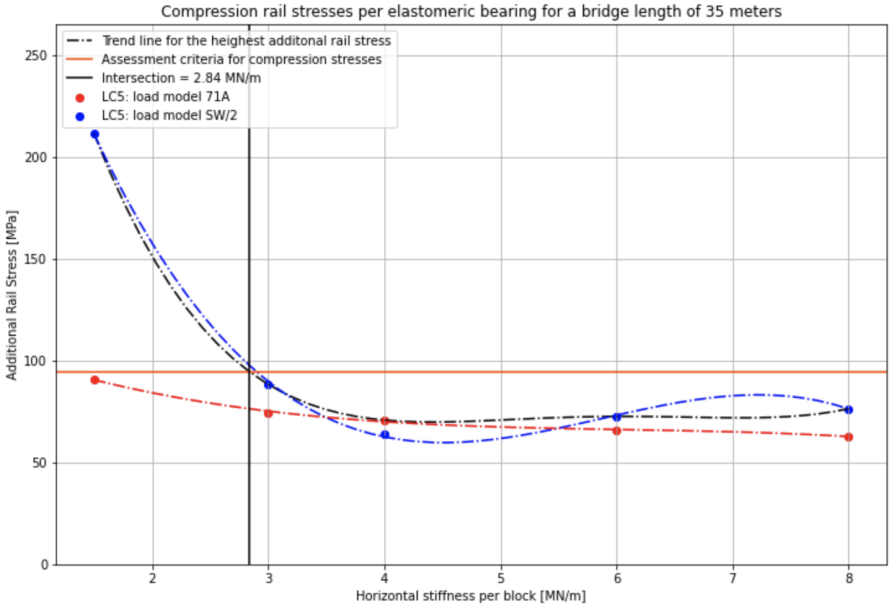

Figure 6.5: Additional compression rail stress against elastomeric bearing stiffnesses for Model 1

Figure 6.5 shows that the additional rail stresses are very sensitive to the stiffness of the elastomeric bearings. This aligns with the expectations given in subsubsection 4.2.1.3, which indicated that the elastomeric bearings were the lowest stiffness part of the railway bridge substructure, resulting in the combined stiffness of the substructure being closest to the stiffness of the elastomeric bearings.
Examining the differences between the red and blue points in the plot (i.e., the differences between load models 71A and SW/2), it can be seen that SW/2 produces much higher additional rail stress at the smallest elastomeric bearings with 1.5 MN/m horizontal stiffness. This difference can be attributed to the fact that the vertical load of SW/2 is much higher than that of 71A. The elastomeric bearings also have a vertical stiffness linked to the horizontal stiffness of the bearings, as given in Table 4.14. Therefore, the smallest bearings are even more sensitive to vertical loads than the larger bearings. This explains the difference between the results for 71A and SW/2 at the smallest elastomeric bearing, where the vertical force for SW/2 is 150 kN/m and for 71A it is 80 kN/m.

The same analysis can be done for the additional tensile rail stress for the various elastomeric bearings. In Appendix A.3, it is shown that for tension, the most critical load combination for all the various elastomeric bearings is load combination 2 (temperature decrease + braking + vertical). There is no single critical load model that gives the most critical additional rail stresses. For elastomeric bearing stiffnesses of 1.5, 3.0, 4.0, and 8.0 MN/m, SW/2 is the most critical load model, whereas for elastomeric bearing stiffness of 6.0 MN/m, load model 71B (location in the middle of the span) is the most critical. Therefore, for load combination 2, the additional rail stresses for load models 71B and SW/2 are plotted against the horizontal stiffness of the various elastomeric bearings in Figure 6.6. The same legend is used as in the compression plot for the various elastomeric bearings.

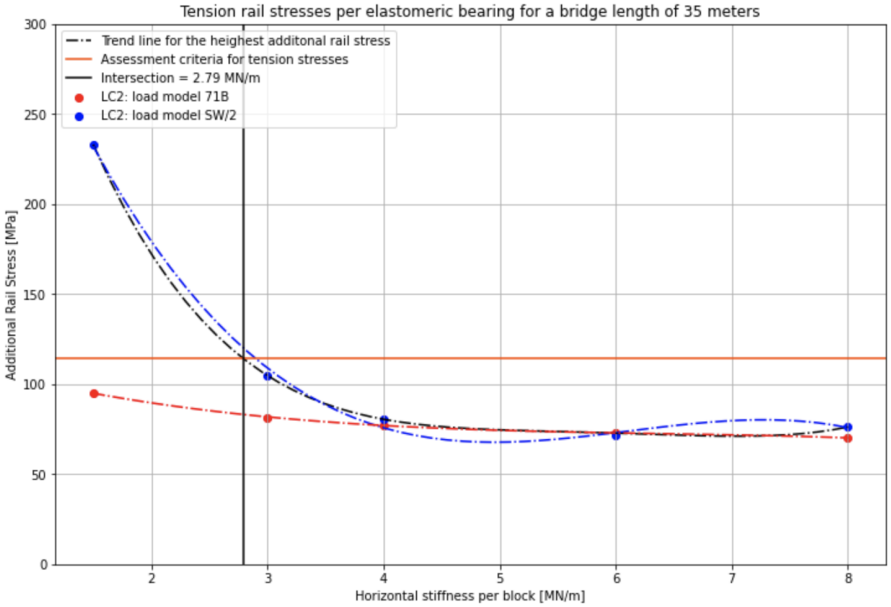

Figure 6.6: Additional rail tension stress against elastomeric bearing stiffnesses for Model 1

The same conclusions about the influence of the different elastomeric bearings on compression rail stresses apply to the tension rail stresses. The magnitude of the additional rail stresses is very sensitive to the elastomeric bearings used. The differences between the red and blue lines can be attributed to the same factors. Both figures show that for the smallest bearings, the additional rail stress is very sensitive to the stiffness of the bearings. However, this sensitivity decreases as the bearings become stiffer and larger, indicating that the influence of the stiffness of the elastomeric bearing diminishes when larger bearings are used. For instance, it can be seen that for both compression and tension, once the bearing stiffness exceeds 4 MN/m, further increases in stiffness have little impact on the rail stresses. This is evident as the trend line for the highest additional rail stress (black dashed-dotted line) runs almost flat beyond this point. At the intersection of this line with the assessment criteria, it can be seen that for compression, the additional rail stresses fall below the assessment criteria when using bearings with a horizontal stiffness greater than 2.84 MN/m, assuming all other variables are set to default. For tension, this threshold is 2.79 MN/m. This leads to the conclusion that if the default settings for the other variables are used, bearings with a stiffness greater than 3 MN/m will not cause problems, and the rail stresses will remain below the limit.
For longer bridges, other design criteria may already require the use of larger elastomeric bearings, which is why the additional stress in the rails may not guide the choice of bearings.

Because the analysis detailed in subsubsection 4.2.1.3 highlighted that elastomeric bearings significantly influence the combined stiffness of the substructure, they were further analysed across three different bridge span lengths. The results are presented in plots for both compression and tension against the bridge span length in Figure 6.7 and Figure 6.8.
In these figures, different elastomeric bearings are distinguished by color: the 1.5 MN/m elastomeric bearing is shown in red, the 3.0 MN/m in blue, the 4.0 MN/m in black, the 6.0 MN/m in orange, and the 8.0 MN/m in green. Each plot represents the highest additional rail stresses observed for each bridge length with each type of elastomeric bearing. Specifically, load model SW/2 is predominant for compression with load combination 5 and for tension with load combination 2.

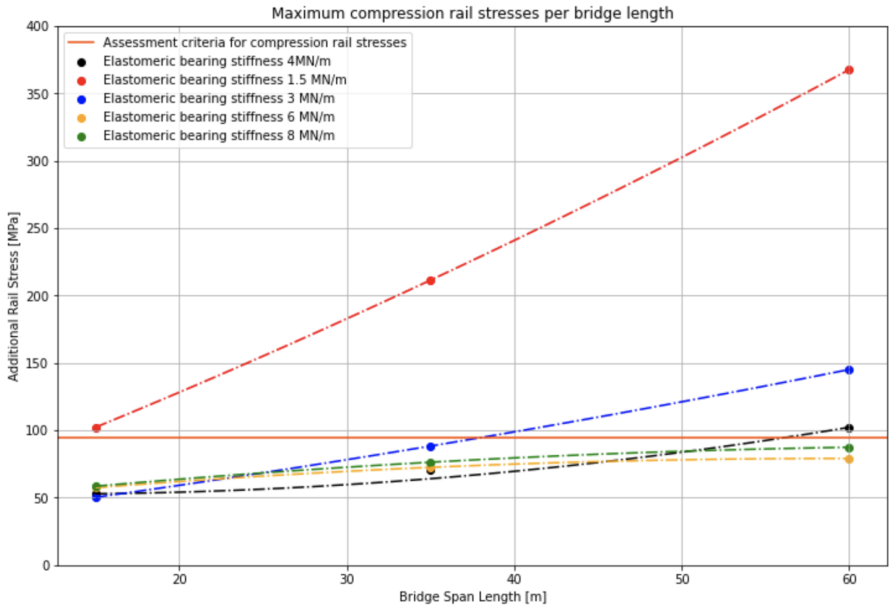

Figure 6.7: Additional compression rail stress against bridge length with different elastomeric bearing stiffnesses for Model 1

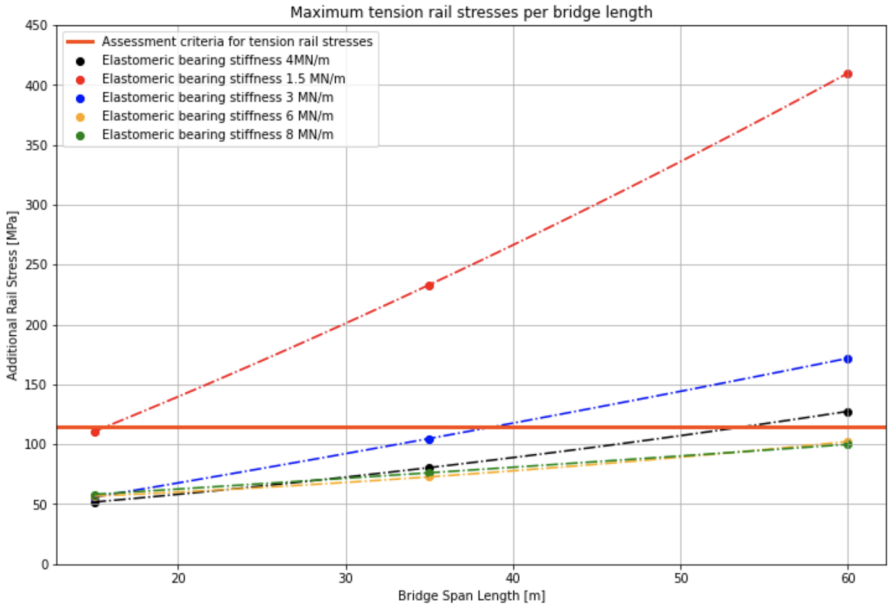

Figure 6.8: Additional rail tension stress against bridge length with different elastomeric bearing stiffnesses for Model 1

These figures demonstrate that the relationship between additional rail stress and elastomeric bearing stiffness for the other two bridge deck span lengths aligns with the patterns shown in Figure 6.5 and Figure 6.6. The smallest bearings, with a stiffness of 1.5 MN/m, result in significantly higher additional rail stresses compared to other bearings. When these elastomeric bearings are used, the additional rail stress exceeds the assessment criteria at a bridge length of 15 meters.
For elastomeric bearings with horizontal stiffness of 3 and 4 MN/m, the additional rail stress remains below the assessment criteria for bridge lengths of 15 and 35 meters but exceeds the criteria at a bridge length of 60 meters. Elastomeric bearings with a horizontal stiffness of 6 and 8 MN/m consistently remain below the assessment criteria for all three bridge lengths, assuming default settings for bridge pier length and foundation stiffness. This analysis suggests that elastomeric bearings with a stiffness of at least 6 MN/m are necessary to ensure that additional rail stresses remain within acceptable limits across various bridge lengths, under default settings for other variables.

6.1.3. Variable: Bridge Pier Length

The third variable considered for Model 1 is the bridge pier length. The length of the pier influences the horizontal stiffness of the combined substructure system. The pier lengths investigated are 5, 7.5, and 10 meters, as described in subsubsection 4.2.1.3. Longer bridge piers are less rigid in the horizontal direction due to their fixed cross-section of 2500 x 1250 mm, with stiffness determined by the following equation:

$$w = \frac{F \cdot l^3}{3EI} \tag{6.1}$$

The spring stiffness is calculated as follows:

$$k = \frac{3EI}{l^3} \tag{6.2}$$

Where the inertia (I) for the pillar is $\frac{1}{12} \cdot b \cdot h^3$, with b = 1250 mm and h = 2500 mm, resulting in an inertia of $1.63 \cdot 10^{12}$ mm^4. Given E = 32800 N/mm^2, the corresponding stiffnesses for different pier lengths are:

Bridge pier length [m]	Corresponding stiffness [MN/m]
5	1281
7.5	380
10	160

Table 6.1: Stiffness corresponding to the pier length

The numerical values of the additional rail stresses for different pier lengths for both compression and tension are given in Appendix A.4.
The appendix shows that for compression, load combination 5 (Temperature increase - braking + vertical) is the most critical, with load model 71A (location above the support) resulting in the highest additional rail stresses. These stresses are plotted against bridge pier length in Figure 6.9.

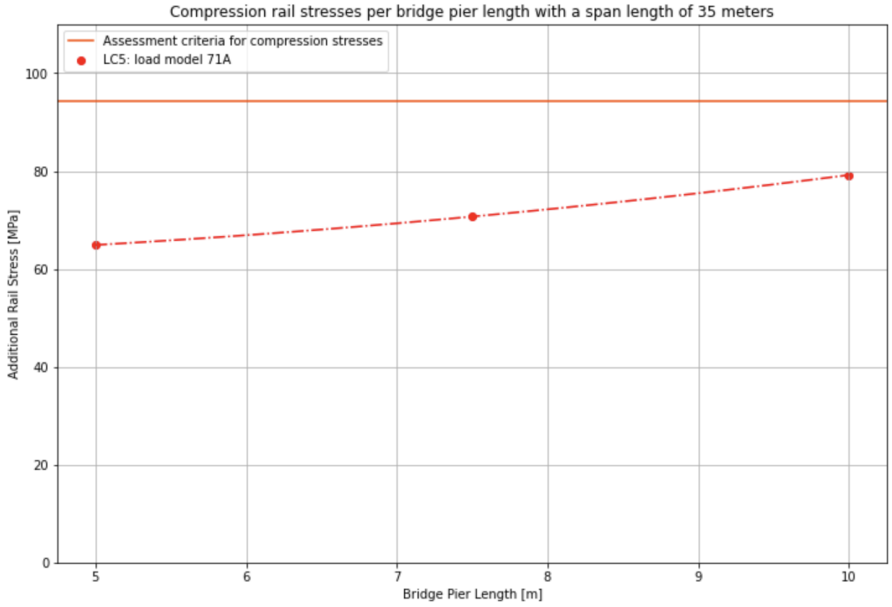

Figure 6.9: Additional compression rail stress against pier lengths for Model 1

In Figure 6.9, the additional compression in the rails shows minimal variation with increasing pier length. Despite longer piers having lower stiffness, the additional compression in the rails remains relatively stable. This consistency aligns with expectations, as shown in Table 4.11, where the combined stiffness of the substructure system is primarily influenced by elastomeric bearings rather than pier length.
A similar analysis for additional tension in the rails is presented in Appendix A.4. For tension, the most critical stresses occur under load combination 2 (Temperature decrease + braking + vertical) and load model SW/2. These stresses are depicted against pier length in Figure 6.10.

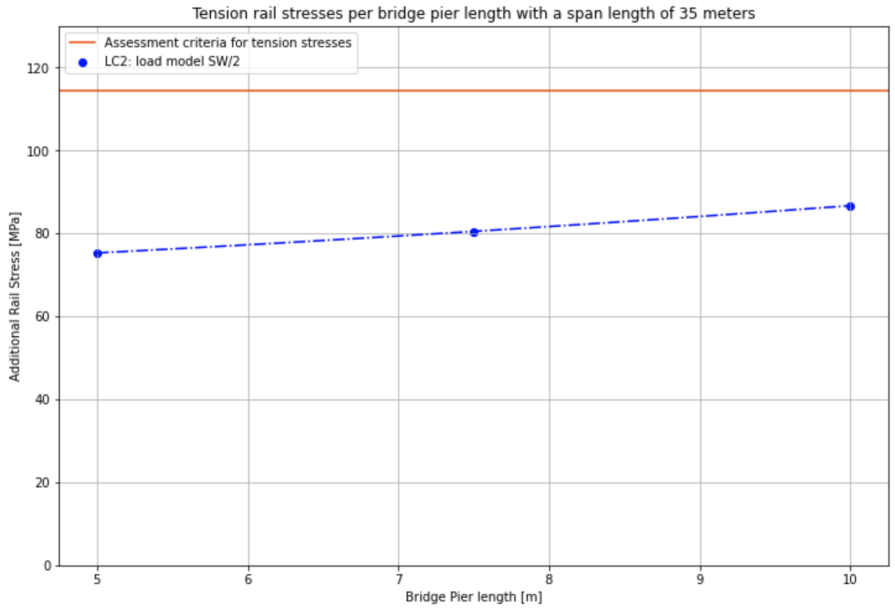

Figure 6.10: Additional tension rail stress against pier lengths for Model 1

As observed with compression, the additional tension in the rails shows minimal variation with varying bridge pier lengths, as depicted in Figure 6.10.
In conclusion, the length of the piers has little influence on the longitudinal forces in the rails. Adjusting pier lengths is unlikely to significantly affect whether a bridge system meets the additional rail stress assessment criteria.

6.1.4. Variable: Foundation Stiffness

The fourth and final variable for Model 1 is the foundation. For this analysis, the horizontal stiffness of the foundation of Theemswegtracé serves as the reference point, set as the default. The lower and upper limits are determined by subtracting and adding 50% of the default value, resulting in investigation points of 35, 68, and 105 MN/m.
Calculations were conducted for these three foundation stiffness values using Model 1. The numerical values for the additional compression and tension rail stresses are detailed in Appendix A.5.
In the appendix, it can be observed that additional compression rail stresses occur primarily with load combination 5 (Temperature increase - braking + vertical), in conjunction with load model 71A at the location above the support. Similar results are found for load combination 1 (Temperature increase + braking + vertical) also paired with load model 71A. The additional compression rail stresses for load combination 5 and load model 71A are plotted against the different foundation stiffnesses to establish the relationship between this variable and the resulting additional rail stress. This relationship is illustrated in Figure 6.11, using the same legend as in other plots depicting additional rail stress against varying variables.

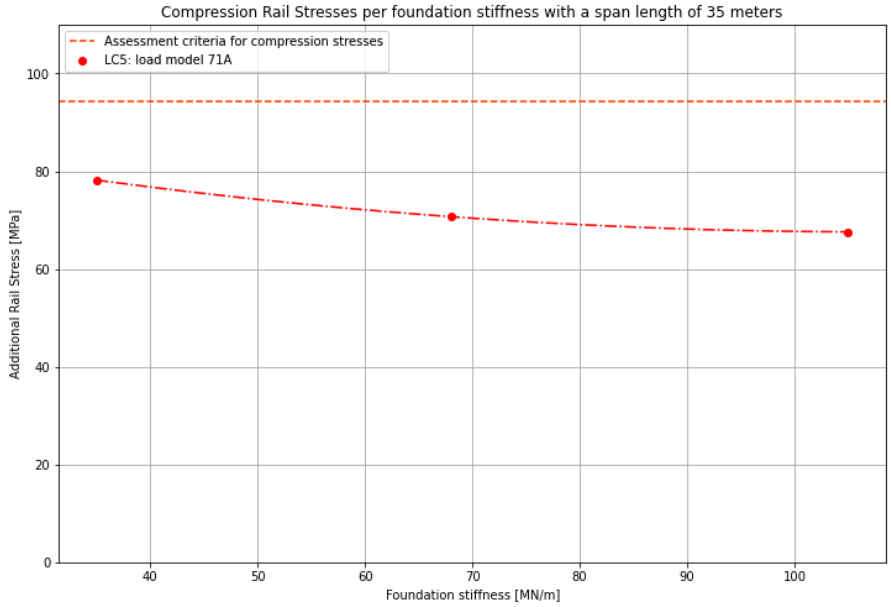

Figure 6.11: Additional compression rail stress against foundation stiffness for Model 1

Figure 6.11 illustrates that varying the foundation stiffness has minimal impact on the additional compression stresses in the rails. This observation aligns with expectations, as detailed in Table 4.12, where variations in foundation stiffness showed little effect on the combined stiffness of the substructure. Therefore, it is anticipated that the foundation will exert little influence on additional rail stresses.

The tension-related additional rail stresses are also detailed in the appendix. It shows that critical tensile stresses occur under two different combinations of load models and load combinations. For foundation stiffnesses of 68 and 105 MN/m, the critical tensile stress is observed with load combination 2 (Temperature decrease + braking + vertical) and load model SW/2. Conversely, for a foundation stiffness of 35 MN/m, the critical tensile stress occurs with load combination 6 (Temperature decrease - braking + vertical) and load model 71B at the location in the middle of the span. Given these differences, both critical scenarios are plotted against the foundation stiffness for a span length of 35 meters. The results for load combination 6 and load model 71B are depicted as red dots with their trend lines, while load combination 2 and load model SW/2 are shown in blue. The assessment criteria are represented by an orange line.

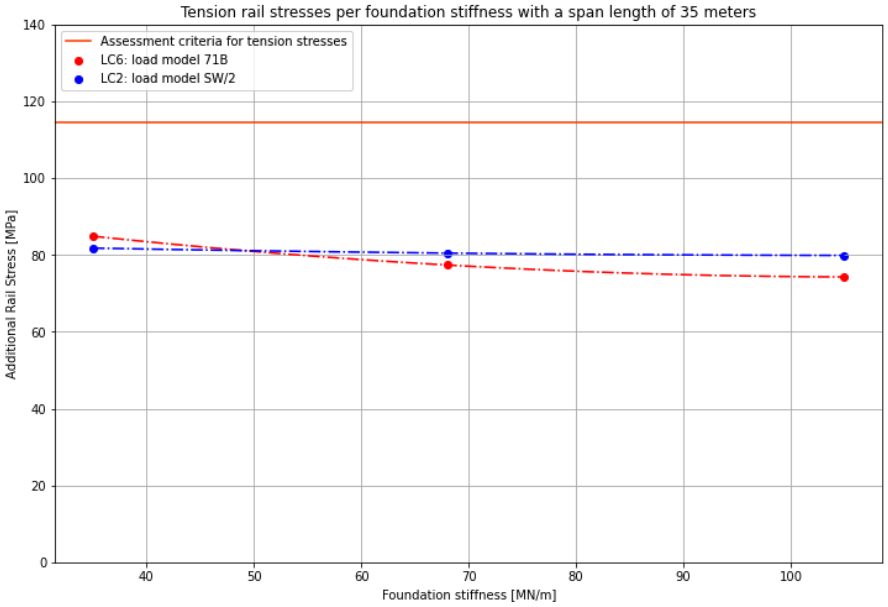

Figure 6.12: Additional tension rail stress against foundation stiffness for Model 1

Figure 6.12 demonstrates a pattern similar to the additional compression rail stresses, indicating that variations in foundation stiffness have minimal impact on the additional rail stress.
In conclusion, the horizontal stiffness of the foundation exerts little to no influence on the additional rail stresses. Therefore, in the context of longitudinal force analysis, as addressed in this thesis, foundation stiffness is not a critical factor.

6.2. Model 2

This section discusses the results of Model 2, which includes the influence of the embankment. The additional rail stresses will be analysed with respect to all variable parameters. Each variable parameter will be addressed in its own subsection. The first subsection covers the variable bridge deck length, the second subsection addresses the variable elastomeric bearings, and the final subsection discusses the variable foundation stiffness at the abutment.

6.2.1. Variable: Bridge Deck

The first variable considered for Model 2 is the bridge deck, specifically its span length. Similar to Model 1, the bridge deck height and the eccentricity of the rails relative to the centerline of the deck are determined by the span length, maintaining a slenderness ratio of $\lambda = 16$, as detailed in subsubsection 4.2.1.1. The corresponding cross-sectional properties of the bridge deck for each span length are presented in Table 4.5.

Calculations for the variable bridge deck were performed using Model 2 to assess the influence of bridge deck span length on additional rail stresses. Numerical values for both compression and tension are listed in Appendix B.1.
The appendix shows that for additional compression rail stresses, two critical combinations of load combinations and load models exist. At a bridge length of 15 meters, load combination 6 (Temperature decrease - braking + vertical) with load model SW/2 yields the most critical compression stress in the rails. For bridge lengths of 35 and 60 meters, load combination 8 (Temperature decrease - acceleration + vertical) with load model 71A at the location above the support provides the most critical compression stresses. Both combinations are plotted against the variable bridge span length and presented in Figure 6.13, using the same legends as in Model 1.

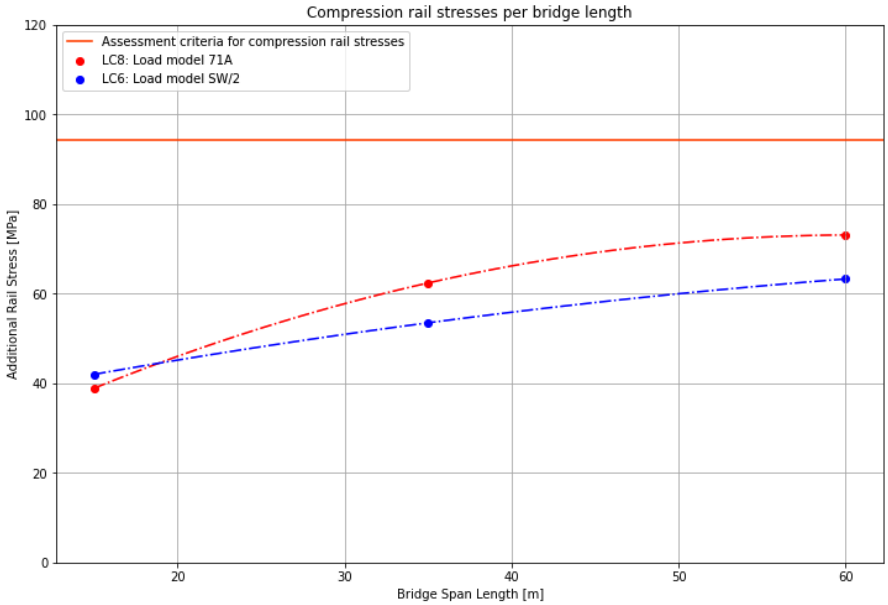

Figure 6.13: Additional compression rail stress against bridge deck length for Model 2

Figure 6.13 demonstrates that within the range of possible span lengths for precast concrete bridges, all bridge lengths meet the design criteria for additional rail stresses considering the railway bridge structure with embankment influence. Furthermore, it is evident that as the span length increases, the rate of increase in additional compression rail stress becomes slightly less steep.

A similar analysis was conducted for tension stresses. Appendix B.1 shows that for tension, two combinations of load combinations and load models yield critical tensile stresses for different bridge span lengths. Specifically, for spans of 15 and 60 meters, the critical combination is load combination 1 (Temperature increase + braking + vertical) with load model SW/2. For a span of 35 meters, the critical stress occurs with load combination 3 (Temperature increase + acceleration + vertical) and load model 71B at the location in the middle of the span. These critical combinations are plotted against the variable span length in Figure 6.14.

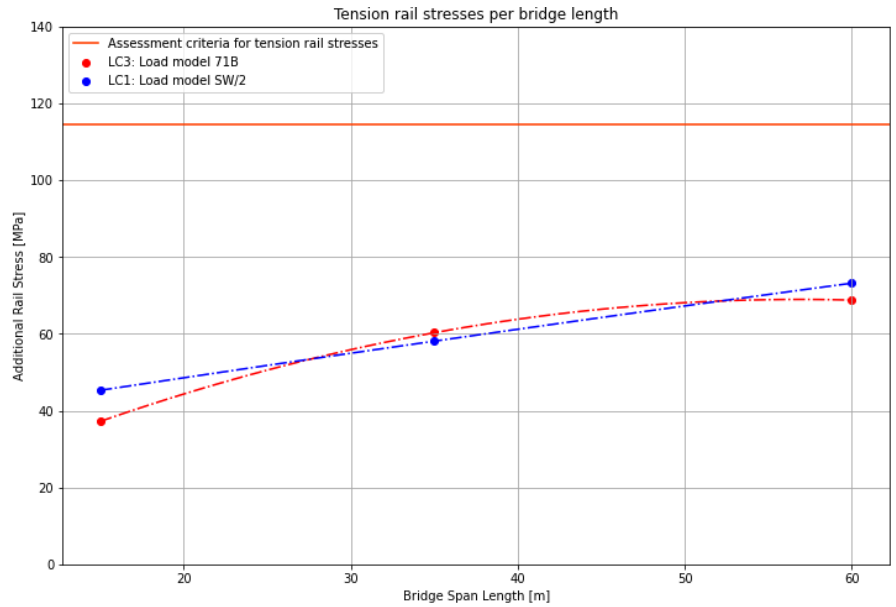

Figure 6.14: Additional rail tension stress against bridge deck length for Model 2

Figure 6.14 shows that the additional rail stresses for tensile forces follow a similar pattern as observed for compression forces, indicating compliance across all investigated bridge lengths.

It can be concluded that constructing a bridge deck with embankments on both sides poses no issues regarding longitudinal forces when default settings for foundation stiffness at the abutments and elastomeric bearings are maintained, and bridge spans ranging from 15 to 60 meters are used. The trend lines for both compression and tension suggest that even longer bridge spans than 60 meters could be feasible in terms of longitudinal forces, although practical structural considerations may limit their implementation. For instance, at a span length of 60 meters, a bridge deck height of 3.5 meters is already substantial. Using larger spans would require further increases in deck height, potentially leading to structural challenges due to the increased weight of concrete bridge decks and other factors such as production and transport to the project site.

6.2.2. Variable: Elastomeric Bearings

The second variable for Model 2 is the elastomeric bearings. Five support bearings are positioned at each of the two supports, evenly distributed across the bridge deck width. The investigation points for these elastomeric bearings are detailed in Table 4.14.
Calculations for the variable elastomeric bearings were conducted using Model 2 to assess their influence within the embankment model. Numerical values for the five different elastomeric bearings, considering both compression and tension, are outlined in Appendix B.2. These calculations assume default settings for bridge deck length and the foundation stiffness at the abutment.
Appendix results indicate that for compression stresses in the rails, a critical combination of load combination and model emerges: load combination 8 (Temperature decrease - acceleration + vertical) with load model 71A above the support. These additional compression rail stresses are plotted for each elastomeric bearing in the investigation and visualised in Figure 6.15.

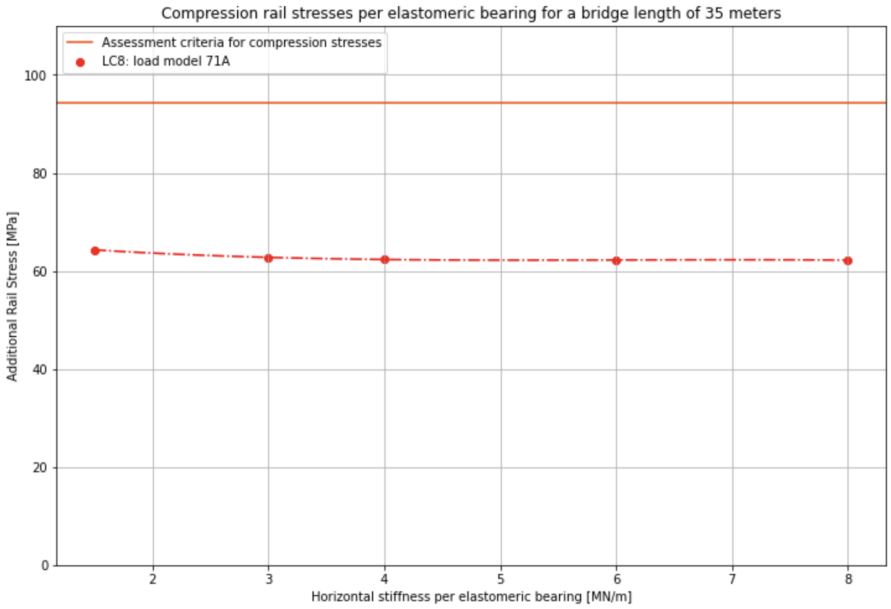

Figure 6.15: Additional compression rail stress against elastomeric bearing stiffness for Model 2

Figure 6.15 illustrates that elastomeric bearings have minimal impact on additional compression rail stresses. The plot shows a nearly flat line across varying elastomeric bearing stiffnesses.

A similar analysis was conducted for tension in the rails. According to Appendix B.2, critical rail stresses for additional tension are driven by load combination 3 (Temperature increase + acceleration + vertical) and load model 71B at the span's midpoint. These findings are plotted against elastomeric bearing stiffness in Figure 6.16.

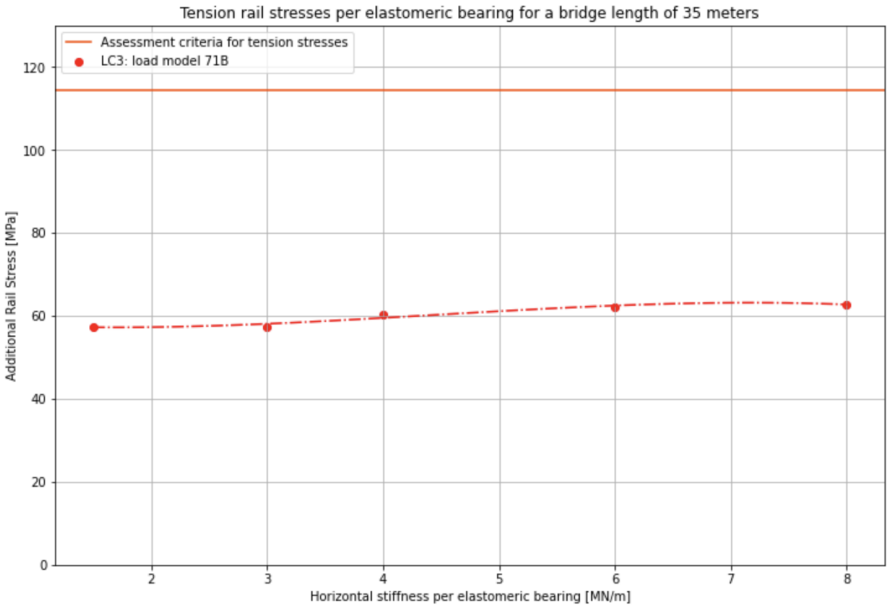

Figure 6.16: Additional rail tension stress against elastomeric bearing stiffness for Model 2

Figure 6.16 shows a similar pattern to compression. The nearly flat line of additional tension rail stresses indicates that the elastomeric bearings have little to no influence on their magnitude.

This lack of influence can be attributed to the design of the bridge, where a short transition structure follows the elastomeric bearings, leading into 150 meters of embankment supported every meter. This configuration effectively absorbs longitudinal forces through the embankment, minimizing the impact of elastomeric bearing stiffness on rail stress gradients. This phenomenon is evident in both compression and tension scenarios.

6.2.3. Variable: Foundation Stiffness at the Abutment

The final variable considered for Model 2 is the foundation stiffness at the abutment. The foundation stiffness at the abutment has three stiffness values under investigation: 70, 136, and 205 MN/m, as detailed in subsubsection 4.2.1.2.

Similar to the analysis in subsubsection 4.2.1.3, the foundation at the abutment has higher stiffness compared to the elastomeric bearings. Consequently, the combined stiffness of the foundation at the abutment and elastomeric bearings is expected to change minimally with varying abutment foundation stiffness. This is because the combined stiffness tends towards the parameter with the lowest stiffness. Therefore, the stiffness of the abutment foundation is anticipated to have little influence on the additional rail stresses.
To validate this expectation, calculations were performed for the three foundation stiffness values using Model 2. The numerical results for both compression and tension are detailed in Appendix B.3.
Appendix B.3 illustrates that for additional compression rail stresses with varying abutment foundation stiffness, the critical combination occurs with load combination 8 (Temperature decrease - acceleration + vertical) and load model 71A above the support. These stresses are plotted against the variable foundation stiffness at the abutment in Figure 6.17.

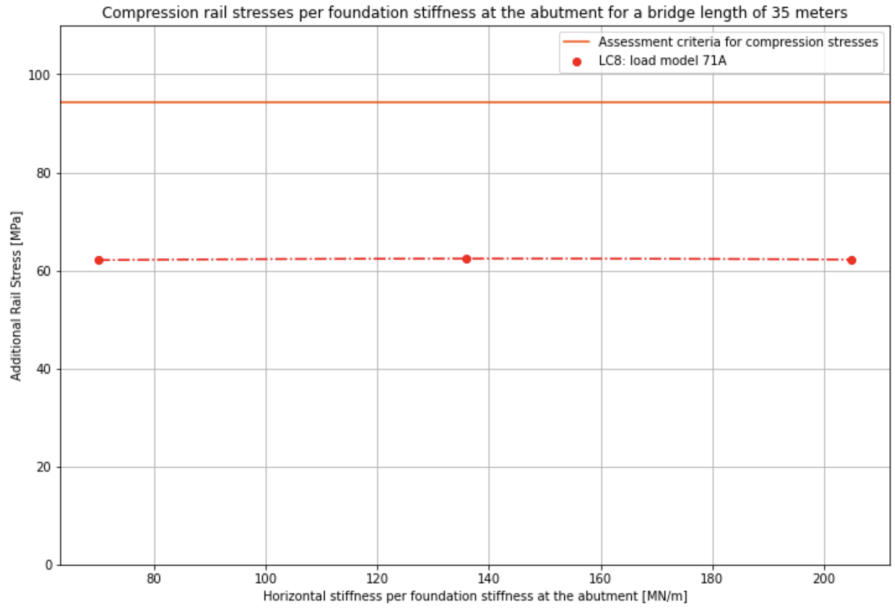

Figure 6.17: Additional compression rail stress against foundation stiffness at the abutment for Model 2

Figure 6.17 shows that the stiffness of foundation at the abutment does not affect the magnitude of the longitudinal forces in the rails, as indicated by the flat line of the additional rail stress against the stiffness of the foundation at the abutment.

Appendix B.3 also provides rail stresses for tension in the rails. In this appendix, it can be seen that the most critical stresses occur when load combination 3 (Temperature increase + acceleration + vertical) and load model 71B at the location in the middle of the span are applied to Model 2. To understand the influence of the parameter on the stresses in the rails, the rail stresses were plotted against the foundation stiffness at the abutment, as visualised in Figure 6.18.

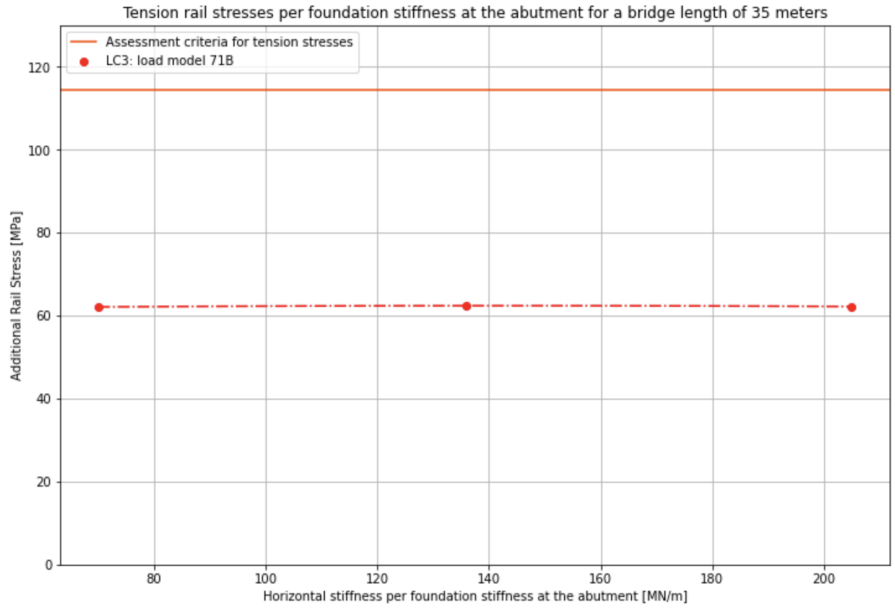

Figure 6.18: Additional tension rail stress against foundation stiffness at the abutment for Model 2

Figure 6.18 also shows that the foundation stiffness at the abutment has no influence on the longitudinal forces in the rails.

Since it is observed that both compression and tension show no sensitivity to the foundation stiffness at the abutments, it can be concluded that the type of foundation at the abutment is insignificant for longitudinal force analysis. It is important to note that while the abutment foundation type may not impact longitudinal forces, it could be significant for other structural considerations. The lack of influence aligns with expectations, given the minimal impact observed with the previous variable, elastomeric bearings. The combined stiffness primarily determined by the elastomeric bearings implies that the foundation stiffness at the abutment has no effect on the longitudinal forces in the rails.

6.3. Differences between Model 1 and Model 2

This section compares the results of Model 1 (without embankment influence) and Model 2 (with embankment influence). It examines the influence of variable parameters on the magnitude of the additional rail stresses and considers the potential causes of these differences. Additionally, it explores whether different combinations of load combination and load model yield the critical values for both compression and tension in the rails.

In the previous sections, the results of Model 1 and Model 2 were discussed in detail, with a specific focus on the influence of each parameter on the additional rail stresses. These results and the influence of the variable parameters can now be properly compared.

One noticeable difference is that Model 1 is much more sensitive to the variable parameters than Model 2, particularly regarding the substructure-related parameters. In Model 1, these parameters include the elastomeric bearings, bridge piers, and foundation, whereas in Model 2, they include the elastomeric bearings and the foundation stiffness at the abutment. For Model 1, the choice of elastomeric bearings significantly impacts the magnitude of the additional rail stresses. Thus, for Model 1, the choice of elastomeric bearings can ensure that the additional rail stresses meet the design assessment criteria, whereas they might not for other bearings. Consequently, for Model 1, span lengths of 60 meters can be achieved with larger bearings. In contrast, the variable substructure parameters have little to no influence on the additional rail stresses in Model 2. The plots for these parameters mainly show flat lines, indicating that varying these parameters makes little to no difference in the results. The minimal influence of the substructure parameters in Model 2 can be explained, as discussed in subsection 6.2.2. The stiffness of the substructure is of less importance in the longitudinal force analysis because the rails already experience significant stiffness from the transition structure before and after the railway bridge, and the 150-meter embankment on both sides of the transition structures, which is supported every meter, provides considerable stiffness to the overall system.

Another noticeable difference between Model 1 and Model 2 is observed when considering the variable bridge deck length. In Model 1, bridge lengths of 15 and 35 meters meet the design criteria for both compression and tension. However, at 60 meters, the additional rail tensions no longer meet the design criteria when the default settings are used for the other variable parameters. For compression, the stresses increase from 50.9 MPa at 15 meters to 102.2 MPa at 60 meters, and for tension, the stresses increase from 51.8 MPa at 15 meters to 127.5 MPa at 60 meters. In Model 2, all three bridge lengths meet the design criteria for both compression and tension when the default settings are used for the other parameters. For compression, the stresses increase from 42 MPa at 15 meters to 73.1 MPa at 60 meters, and for tension, the stresses increase from 45.3 MPa at 15 meters to 73.2 MPa at 60 meters.
Additionally, the additional rail stresses for Model 2 are significantly lower than those for Model 1, and Model 1's additional rail stresses are more sensitive to span length increases than those of Model 2. This difference can also be attributed to the increased stiffness the rails experience due to the presence of the embankment in Model 2. The embankment absorbs many forces and stresses that would otherwise remain in the rails. Furthermore, Model 1 features multiple spans in sequence, meaning the vertical load is distributed across different fields, causing increased moments in the rails above the supports, leading to higher stresses due to vertical contributions. This moment above the supports due to rails passing over different bridge decks was also considered in section 5.3.

Finally, an analysis was conducted to determine if the critical values for the additional rail stresses occur with different load combinations and load models for the two models. For Model 1, the most critical values for additional rail stresses occurred under compression with load combination 5 (Temperature increase - braking + vertical) with both load model 71 and SW/2. For tension, the most critical values occurred under load combination 2 (Temperature decrease + braking + vertical) with both load model 71 and SW/2. For Model 2, the most critical values for additional rail stresses occurred under compression with load combination 8 (Temperature decrease - acceleration + vertical) with load model 71, and occasionally with SW/2. For tension, the most critical values occurred under load combination 3 (Temperature increase + acceleration + vertical) with load model 71.

6.4. Individual contributions of different loads

The final section of the results chapter examines the individual contributions of different load cases using the default settings of both Model 1 and Model 2. This analysis focuses on the individual non-linear additional rail stresses and evaluates whether their combined sum matches the overall effect when considered together. If the sum of individual stresses does not align with the combined non-linear effect, the investigation will determine whether their aggregation provides a conservative estimate and quantify the extent of deviation from the combined effect.
This analysis employs load model SW/2 and emphasises the location where the non-linear combination produces maximum stress. This approach maximises the likelihood of observing spring straightening in the non-linear branch, which occurs when displacements cause the springs to exhibit non-linear behaviour.
It is important to note that the location of maximum rail stresses varies with the non-linear combined effect, potentially differing between above the supports or in the middle of the span for different load combinations. Consequently, the values for individual load contributions across the eight different load combinations vary significantly. Therefore, while comparing values within each load combination is appropriate, comparisons between different load combinations should not be made in this investigation.

This analysis was conducted for both Model 1 and Model 2. First, Model 1 was analysed.
Table 6.2 displays the contribution of each individual load to the total compression stress. The table indicates that summing these non-linear stresses from individual loads generally results in higher, and thus more conservative, values compared to the non-linear combination calculated by SCIA Engineer. Only for LC2 and LC8 is this not the case, with values being very close.
At the location of maximum rail stresses, an examination was also conducted to determine whether spring elongations exceed 2.8 mm, as shown in Figure 2.16. When spring elongations exceed 2.8 mm, the springs between the bridge deck and rails enter the non-linear branch, indicating slip between the bridge deck and the rails. Conversely, when spring elongations are 2.8 mm or less, the springs remain in the linear branch of the non-linear springs. Results of these spring elongation analyses are presented in Table 6.3.
Comparing both Table 6.2 and Table 6.3, it is evident that when the springs remain in the linear branch, the summed stresses closely align with the non-linear combined stress. On average, the difference is 1.5 MPa in the linear branch compared to 4.1 MPa in the non-linear branch.

Load combinations	Stress due to thermal load [MPa]	Stress due to longitudinal load [MPa]	Stress due to vertical load [MPa]	Individual stresses added together [MPa]	Non-linear combined responds [MPa]
LC1 (Temperature increase + braking +vertical)	-10.7	-41.6	-13.8	-66.1	-63.5
LC2 (Temperature decrease + braking +vertical)	9.3	-41.6	-13.8	-46.1	-49.1
LC3 (Temperature increase + acceleration +vertical)	-12.0	-3.7	-42.0	-57.7	-50.8
LC4 (Temperature decrease + acceleration +vertical)	-12.9	-8.6	-16.2	-37.7	-34.0
LC5 (Temperature increase - braking +vertical)	-10.8	44.8	-19.0	-74.6	-64.1
LC6 (Temperature decrease - braking +vertical)	10.8	44.8	-19.0	-53.0	-49.2
LC7 (Temperature increase - acceleration +vertical)	-12.0	1.9	-42.0	-55.9	-53.5
LC8 (Temperature decrease - acceleration +vertical)	9.1	1.9	-42.0	-34.8	-36.9

Table 6.2: Load contributions for compression for Model 1 SW/2

Load combination	Spring elongation [mm]	Linear/ Non-linear Branch
LC1	6.0	Non Linear
LC2	2.7	Linear
LC3	5.1	Non Linear
LC4	0.9	Linear
LC5	8.5	Non Linear
LC6	1.0	Linear
LC7	3.7	Non Linear
LC8	5.6	Non Linear

Table 6.3: Spring between bridge deck and rail in linear or non linear branch for Model 1 Compression

Besides compression, tension was also examined. The individual contributions of Model 1 to load model SW/2 for all load combinations were analysed, with the results shown in Table 6.4. It is evident that all summed non-linear individual stresses from the individual loads are higher than the summed non-linear combination from SCIA Engineer.
The investigation also examined whether the springs between the bridge deck and the rails are in the linear or non-linear branch at the locations of maximum stress, as presented in Table 6.5. Similar to the compression analysis, it was observed that when the springs are in the linear branch, the summed individual stresses are closer to the non-linear combination stress than when the springs are in the non-linear branch. This is reflected in the average differences: in the linear branch, the difference is 0.9 MPa, while in the non-linear branch, it is 4.7 MPa.

Load combinations	Stress due to thermal load [MPa]	Stress due to longitudinal load [MPa]	Stress due to vertical load [MPa]	Individual stresses added together [MPa]	Non-linear combined responds [MPa]
LC1 (Temperature increase + braking +vertical)	-9.3	44.8	30.0	65.5	64.6
LC2 (Temperature decrease + braking +vertical)	10.8	44.8	30.0	85.6	80.5
LC3 (Temperature increase + acceleration +vertical)	-12.0	1.9	55.3	45.2	43.2
LC4 (Temperature decrease + acceleration +vertical)	12.0	1.9	55.3	69.2	58.4
LC5 (Temperature increase - braking +vertical)	-8.6	-41.4	16.0	48.8	47.9
LC6 (Temperature decrease - braking +vertical)	10.1	-41.4	16.0	67.5	62.3
LC7 (Temperature increase - acceleration +vertical)	-9.1	-3.7	55.3	49.9	49.4
LC8 (Temperature decrease - acceleration +vertical)	12.0	-3.7	55.3	71	66.6

Table 6.4: Load contributions for tension for Model 1 SW/2

Load combination	Spring elongation [mm]	Linear/ Non-linear Branch
LC1	0.7	Linear
LC2	9.3	Non Linear
LC3	5.1	Non Linear
LC4	2.9	Non Linear
LC5	0.9	Linear
LC6	8.5	Non Linear
LC7	3.7	Non Linear
LC8	5.6	Non Linear

Table 6.5: Spring between bridge deck and rail in linear or non linear branch for Model 1 Tension

Based on the results of both compression and tension for SW/2 in Model 2 for the different load cases, when the loads are added together, the average contribution of each load is as follows: the thermal load contributes 3.78% (1.17 MPa), the longitudinal traffic load contributes 40.11% (36.52 MPa), and the vertical traffic load contributes 56.11% (62.30 MPa).

The analysis of load contributions performed for Model 2, using load model SW/2, followed a similar methodology as that used for Model 1. This analysis considered all load combinations and focused on the non-linear individual stress contributions of each load to identify the greatest tensile and compressive stresses in the rails under combined loading conditions.
Table 6.6 presents the contribution of each individual load to the total additional compression in the rails. This table indicates that the summed individual stresses are almost always higher than the combined non-linear stresses calculated using SCIA. In cases where the values are not greater, they are equal or nearly equal.

Furthermore, displacements in the springs between the rails and the bridge deck were analysed to determine whether these springs operate within the non-linear or linear branch of their characteristic curve. The results of this analysis are shown in Table 6.7.
From the data in Table 6.6 and Table 6.7, it is evident that when the springs are in the non-linear branch, the summed individual stresses tend to be more conservative, showing a greater deviation from the non-linear combined effect. This is highlighted by the average difference between the summed individual contributions and the non-linear combined effect, which is 3.05 MPa when the springs are in the non-linear branch, compared to 1.3 MPa when the springs are in the linear branch.

Load combinations	**Stress due to thermal load [MPa]**	**Stress due to longitudinal load [MPa]**	**Stress due to vertical load [MPa]**	**Individual stresses added together [MPa]**	**Non-linear combined responds [MPa]**
LC1 (Temperature increase + braking +vertical)	4.3	-13.9	1.0	-8.6	-8.6
LC2 (Temperature decrease + braking +vertical)	-25.6	2.4	-16.0	-39.2	-42.2
LC3 (Temperature increase + acceleration +vertical)	20.2	-8.7	-11.6	-0.1	0.0
LC4 (Temperature decrease + acceleration +vertical)	-34.6	-1.8	-15.0	-51.4	-48.7
LC5 (Temperature increase - braking +vertical)	20.2	15.3	-11.6	-6.7	-4.1
LC6 (Temperature decrease - braking +vertical)	-23.5	15.3	-11.6	-50.4	-53.5
LC7 (Temperature increase - acceleration +vertical)	4.1	7.9	1.0	-2.8	-2.6
LC8 (Temperature decrease - acceleration +vertical)	-34.7	0.0	-15.0	-49.7	-47.5

Table 6.6: Load contributions for compression for Model 2 SW/2

Load combination	**Spring elongation [mm]**	**Linear/ Non-linear Branch**
LC1	0.8	Linear
LC2	4.0	Non Linear
LC3	1.6	Linear
LC4	1.3	Linear
LC5	1.0	Linear
LC6	3.4	Non Linear
LC7	0.2	Linear
LC8	1.3	Linear

Table 6.7: Spring between bridge deck and rail in linear or non linear branch for Model 2 Compression

For Model 2, the additional tension in the rails and the individual contributions of these loads were also considered. The results are presented in Table 6.8. This table shows that the summed individual contributions usually result in higher tensile stress than the non-linear combined response from SCIA, indicating more con-

servative results. The displacement of the springs between the rails and the bridge deck is shown in Table 6.9, which determines whether the springs are in the linear or non-linear branch. As seen in both Table 6.8 and Table 6.9, the summed stresses become more conservative when the springs are in the non-linear branch. The average difference between the summed stresses and the non-linear combined response is 2.3 MPa for situations where the springs are in the non-linear branch and 0.2 MPa for situations where the springs are in the linear branch.

Load combinations	**Stress due to thermal load [MPa]**	**Stress due to longitudinal load [MPa]**	**Stress due to vertical load [MPa]**	**Individual stresses added together [MPa]**	**Non-linear combined responds [MPa]**
LC1 (Temperature increase + braking +vertical)	22	15.3	23.9	61.2	58.1
LC2 (Temperature decrease + braking +vertical)	-20.2	15.3	23.9	19	20.3
LC3 (Temperature increase + acceleration +vertical)	25.6	-1.4	27.1	51.3	50.1
LC4 (Temperature decrease + acceleration +vertical)	-4.1	7.9	1.0	4.8	4.8
LC5 (Temperature increase - braking +vertical)	25.6	2.4	27.1	50.3	47.6
LC6 (Temperature decrease - braking +vertical)	-4.1	-14.1	1.0	11.0	11.0
LC7 (Temperature increase - acceleration +vertical)	25.6	-2.4	27.1	55.1	52.6
LC8 (Temperature decrease - acceleration +vertical)	-19.7	-8.7	23.9	12.9	12.9

Table 6.8: Load contributions for tension for Model 2 SW/2

Load combination	**Spring elongation [mm]**	**Linear/ Non-linear Branch**
LC1	3.9	Non Linear
LC2	0.5	Linear
LC3	3.2	Non Linear
LC4	0.4	Linear
LC5	4.1	Non Linear
LC6	1.0	Linear
LC7	1.0	Linear
LC8	0.3	Linear

Table 6.9: Spring between bridge deck and rail in linear or non linear branch for Model 2 Tension

When considering the contributions of individual loads to the combined additional tension and compression rail stresses, the average contribution of each load case can be calculated assuming they can be summed. For Model 2, the contributions are as follows: the thermal load contributes 25.35% (19.09 MPa), the longitudinal traffic load contributes 25.37% (22.55 MPa), and the vertical traffic load contributes 49.27% (58.36 MPa).

7

Conclusion and Recommendations

After conducting a comprehensive literature review, analysing reference projects, performing hand calculations, and obtaining results using two different SCIA Engineer models designed to depict distinct scenarios, the findings have been derived and analysed in the previous chapter. With these tasks completed, it is now time to present the conclusions and recommendations of this master's thesis.
The primary aim of this investigation was to enhance the understanding of the interaction between railway bridge structures and the rails. To achieve this, several aspects were explored. Therefore, this chapter is structured as follows:
The first section presents the conclusions of this investigation, focusing on the goal of gaining more knowledge about the interaction between the rails and the railway bridge structure without the use of fixed points. This includes answering the main question with the help of several sub-questions.
The second section provides recommendations for future structures seeking to mitigate issues related to additional rail stresses. This section also includes recommendations for simplifying modeling for engineering purposes and suggestions for follow-up research.

7.1. Conclusion

The railway system in the Netherlands is widely used, with trains running on continuous welded rails. These rails are exposed to various forces, including temperature changes, which cause the rails to expand and contract, as well as forces exerted by trains, such as braking and acceleration, which create longitudinal forces in the rails. These forces occur throughout the entire railway system. However, additional rail stresses may arise due to the presence of a rail bridge structure. These additional stresses can cause the rails to buckle or fracture, which is the problem investigated in this thesis. Continuous welded rails extend over the joints of railway bridges, which are not continuous, leading to additional rail stresses due to the relative displacement of the bridge deck with respect to the rails.
This relative displacement, and therefore the stresses in the rails, occur due to the expansion and contraction of the bridge deck caused by temperature changes, the displacement of the bridge deck due to the braking and acceleration of trains on the bridge structure, and the vertical self-weight of the train on the bridge structure. This self-weight causes the bridge deck to deflect, leading to rotations at the ends of the bridge deck. The rails want to expand, but this is not possible, causing additional stresses.

The main question of this investigation is:

- How can the understanding of the longitudinal force transfer in railway bridges in the Netherlands be enhanced, so that the rail stresses do not exceed the safety limits if no fixed points are applied?

To answer this research question, a literature review was conducted and projects were analysed. It quickly became evident that there are two types of structures: those with embankment influence and those without embankment influence. Consequently, two longitudinal force models were created: one with embankment influence and one without. The investigation then focused on identifying parameters that could potentially influence the magnitude of the additional rail stresses. These parameters were chosen as variables in the two models to see how varying them affects the magnitude of the additional rail stresses. For the model without embankment influence (Model 1), the variables are the bridge deck span length, elastomeric bearings, the

length of the bridge piers, and the stiffness of the foundation. For the model with embankment influence (Model 2), the variables are the bridge deck span length, elastomeric bearings, and the stiffness of the foundation at the abutment. Using these two longitudinal force models and the variable parameters, different results for the magnitude of the additional rail stresses were obtained for eight different load combinations and three different load models.

By obtaining these results, the sub-questions can be answered, which in turn help address the main question. The four sub-questions encompass three main aspects extracted from the results, for which conclusions can be drawn. These components include the influence of variable parameters, differences between structures with and without embankment influence, and the linear summation of individual load contributions. The conclusions for each component are provided in this section. Ultimately, the main research question is conclusively addressed.

Influence of the Variable Parameters
The following conclusions can be drawn about the influence of the variable parameters:

- For the structure without embankment influence (Model 1), the stiffness of the substructure, particularly the elastomeric bearings, significantly influences the magnitude of the additional rail stresses. It was observed that the element with the lowest stiffness in the substructure exerts the most influence on the magnitude of additional rail stresses. Therefore, reinforcing the foundation or bridge piers to reduce stresses in the rails may be ineffective if the elastomeric bearings remain unchanged.
- For the structure with embankment influence (Model 2), the stiffness of the substructure has little influence on the magnitude of the additional rail stresses. This is because the presence of the embankment on both ends of the bridge structure provides substantial stiffness, resulting in lower stresses in the rails. Consequently, adjustments to the stiffness of the elastomeric bearings or the foundation at the abutment have minimal to no influence on the magnitude of the additional rail stresses.
- In both Model 1 and Model 2, the span length (i.e., bridge deck length) significantly influences additional rail stresses. Longer bridge decks deflect more under vertical traffic loads. Despite the increased structural height due to a slenderness ratio of 16, this increased deflection of the bridge deck leads to increased rail stresses. Additionally, increased span length can elevate stresses along the span due to the greater distance from the supports.

Differences between a Structure with and without Embankment Influence
When comparing the structure without embankment influence (Model 1) to the structure with embankment influence (Model 2), the following conclusions can be drawn:

- The magnitude of the additional rail stresses in the structure without embankment influence (Model 1) is significantly affected by the stiffness of the bridge substructure. This stiffness impacts the transmission of longitudinal forces and, consequently, the additional stress levels in the rails. Conversely, the structure with embankment influence (Model 2) is almost unaffected by substructure stiffness when focusing on longitudinal force analysis, thanks to the substantial longitudinal stiffness provided by the embankment.
- In addition to being less influenced by substructure parameters, Model 2 exhibits lower stresses for both compression and tension due to the increased stiffness from the embankment. It also demonstrates lower sensitivity to span length extensions compared to Model 1. Consequently, while Model 1 restricts bridge deck lengths to 15 and 35 meters at default settings, the additional rail stresses in Model 2 for all bridge lengths (15, 35, and 60 meters) remain beneath the design requirement stresses for longitudinal forces and therefore do not cause issues.
- Furthermore, the additional stresses in Model 1 are primarily determined by vertical and longitudinal traffic loads, whereas the additional rail stresses in Model 2 are more influenced by thermal loads.

Load Contributions
Based on the results of the individual load contributions and the spring elongations of the non-linear springs between the bridge deck and the rails, the following conclusions can be drawn:

- Superposition of the individual load contributions generally produces additional rail stresses that are higher or equal to the non-linear combined effect in SCIA. This indicates that summing the individual load cases provides a safer estimate, ensuring conservative results.

- When the spring elongations between the bridge deck and the rails are in the linear branch, the linear summation of the stresses from the individual load cases is, on average, 0.75 MPa higher, thus providing a conservative estimate. When the spring elongations are in the non-linear branch, the summation results are, on average, 2.68 MPa higher. Therefore, the deviation between the summation and the non-linear combination increases as the springs enter the non-linear branch.
- The difference between the linear summation of individual stresses and the combined non-linear stresses is relatively small, only a few megapascals. Thus, linear summation yields results that are nearly equivalent to those obtained from non-linear combinations, allowing for faster calculations since non-linear combinations increase computational time.
- Due to the 50 mm joint between the different bridge decks in the structure without embankment influence, the thermal load has less impact on the combined additional rail stress. In contrast, the model with embankment influence, where the bridge deck is more constrained by the embankment, results in higher additional rail stresses due to the thermal load. In the model without embankment influence, the thermal load contributes an average of 3.78% to the combined effect, averaging 2.19 MPa. In the model with embankment influence, the thermal load contributes an average of 25.35
- For both structures, with and without embankment influence, the vertical load has the most significant impact on the combined additional rail stress. In the structure without embankment influence (Model 1), the vertical load contributes an average of 32.56 MPa, accounting for 56.11% of the combined effect. In the structure with embankment influence (Model 2), it contributes an average of 14.61 MPa, accounting for 49.27% of the combined effect. Reducing the additional stress due to vertical force can significantly influence whether the combined stress remains below the assessment criteria. Therefore, one might consider using less slender bridge decks to increase inertia, thereby reducing deflection in the middle and rotation at the ends of the bridge decks.

Answering the Main Research Question
Based on these conclusions, the main research question can be addressed as follows:

- For structures with embankment influence, the system benefits significantly from the added stiffness provided by the embankment. This ensures that additional rail stresses remain below the assessment criteria across all investigated scenarios. Hence, it can be concluded that in models with embankment influence, there are no safety concerns when fixation points are not utilised. Moreover, longer bridge decks are impractical due to concerns over excessive height and self-weight.
- Conversely, structures without embankment influence exhibit higher additional rail stresses, sometimes exceeding the assessment criteria. In such instances, practical application of fixation points can mitigate these stresses. However, the focus of this research is on ensuring that additional rail stresses remain within safe limits without reliance on fixation points. The findings suggest that employing larger and stiffer elastomeric bearings can achieve this goal. Another viable approach involves using less slender bridge decks to minimize deflection and consequently reduce additional stresses induced by vertical traffic loads. Given that vertical loads contribute 56% to the combined additional rail stress, reducing deflection has a substantial impact on overall stress levels.

7.2. Recommendations

Based on the findings and conclusions drawn in the previous section, several recommendations can be provided. These recommendations are divided into different categories: recommendations for future structures, recommendations for simplifying modelling and reducing computational time, and recommendations for follow-up research.

7.2.1. Recommendations for Future Structures

The conclusions indicate that the challenges in meeting the assessment criteria for additional rail stresses occur primarily with long bridge structures, those without embankment influence. Two key recommendations are proposed to mitigate these rail stresses for railway bridges, ensuring compliance with assessment criteria:

- Use Larger Elastomeric Bearings: Enhancing the size of elastomeric bearings increases stiffness in both horizontal and vertical directions, thus making the substructure stiffer. As shown in Figure 6.7 and Figure 6.8, using bearings with a horizontal stiffness per bearing of 6 and 8 MN/m, corresponding to bearings of 400 x 600 mm and 400 x 800 mm, ensures that additional rail stresses for all bridge deck lengths remain below the assessment criteria for both compression and tension.

- Implement Stiffer Bridge Decks: Adjusting the bridge deck design to use a lower slenderness ratio will increase the deck height, making the bridge deck stiffer with a higher moment of inertia. This change will result in less deflection at the middle of the span and reduced rotation at the ends of the bridge decks, thereby decreasing rail stresses due to vertical traffic load, which is the load case that contributes most to the combined effect.

7.2.2. Recommendations for simplifying modelling and reducing computational time

Based on the results of this investigation, several recommendations can be made for engineers involved in longitudinal force analysis for railway bridge projects. These recommendations focus on reducing computational time and avoiding unnecessary model complexity in the initial phases:

- Use of Linear Summation for Initial Analysis: The analysis indicates that summing the individual additional non-linear rail stresses linearly typically results in rail stresses equal to or higher than those from the non-linear combination. The difference in stress magnitude is generally minimal, often just a few megapascals. It has also been verified that summing the individual linear rail stresses together yields results higher than the non-linear combination, with a similar slight difference. Despite these small differences, the linear approach significantly reduces computation time, particularly for large projects where processing times can range from hours to days. Therefore, it is recommended to use linear summation for the individual cases in the initial phase of analysis and reserve the non-linear combination check for final calculations. This practice can lead to substantial time savings during the design phase, especially for longitudinal force analysis.
- Exclude Load Model SW/0 in Initial Analysis: Analysis of the numerical results presented in the Appendix reveals that load model SW/0 does not contribute to the critical rail stress in both Model 1 and Model 2. Thus, it is advisable to exclude load model SW/0 from the longitudinal force analyses in the initial phase. This will reduce model size and computation times, saving time in the design phase. While Eurocode requires compliance with load models 71, SW/0, and SW/2, the absence of critical stresses from SW/0 in this study suggests that the final model's check on SW/0 is unlikely to pose issues.

7.2.3. Recommendations for follow-up research

The following recommendations for follow-up research aim to further enhance the understanding of railway bridge interaction. These areas of investigation can provide deeper insights and more robust data:

- Expand Scope to Longer Bridge Decks: Future research should consider extending the scope to include longer bridge deck lengths. For the prefabricated bridge decks used in this investigation, lengths beyond 60 meters become impractically thick and heavy. Exploring other precast girder types that can be extended to longer lengths without becoming too heavy, or using steel bridge decks for longer spans, could be beneficial. Additionally, in-situ concrete bridge decks present an interesting opportunity to study the impacts of shrinkage and creep on additional rail stresses.
- Field Measurements of Existing Bridges: Conducting field measurements of actual rail stresses on existing railway bridges in the Netherlands would provide valuable data. Modeling these bridges using the same material and cross-sectional properties as those used in the field can allow researchers to compare calculated stresses to observed values. This comparison would offer insights into the accuracy of current models and their alignment with real-world conditions. Furthermore, measuring the forces exerted by trains crossing these bridges could verify their correspondence to load models 71, SW/0, and SW/2, further enhancing the understanding of the interaction between the rail and the railway bridge. Knowing that these load models also consider future parameters and the possible use of other types of trains in the future, it would be possible to see how closely the calculated loads match the actual loads.

Bibliography

Besix. (n.d.). Buitenring parkstad limburg [https://www.besix.nl/nl/projects/buitenring-parkstad-limburg].

Enshaeian, A., & Rizzo, P. (2020). Stability of continuous welded rails: A state-of-the-art review of structural modeling and nondestructive evaluation. *Institution of Mechanical Engineers*.

Esveld, P. C. (2005). Geometrisch en constructief ontwerp van wegen en spoorwegen. *TU Delft*.

European Commitee for Standardization. (2011). Eurocode 1: Actions on structures - part 2: Traffic loads on bridges (nen-en 1991-2). *NEN*.

European Commitee for Standardization. (2018). Nen-en 1337-3: Structural bearings - part 3: Elastomeric bearings. *NEN*.

European Commitee for Standardization. (2019). National annex to nen-en 1991-2+c1: Eurocode 1: Actions on structures – part 2: Traffic loads on bridges. *NEN*.

Globe Gazette. (n.d.). https://bloximages.chicago2.vip.townnews.com/globegazette.com/content/tncms/assets/v3/editorial/6/70/670360c3-8133-51dc-b0d7-c32a06dd60c7/670360c3-8133-51dc-b0d7-c32a06dd60c7.image.jpg

Lim, N.-H., Park, N.-H., & Kang, Y.-J. (2003). Stability of continuous welded rail track. *Elsevier*.

Meteoor. (n.d.-a). Monoliggers type merk 2 [https://www.meteoor.nl/producten/railcon/monoliggers-type-merk2].

Meteoor. (n.d.-b). Monoliggers type ns90 [https://www.meteoor.nl/producten/railcon/monoliggers-type-ns90].

Midas. (n.d.). Bridge - rail structure interaction. *Research Gate*.

Mobilis. (n.d.). Theemswegtracé [https://www.mobilis.nl/projecten/theemswegtrace].

ProRail. (n.d.). Blik op het spoor: Dwarsliggers [https://www.prorail.nl/series/blik-op-het-spoor/dwarsliggers].

ProRail. (2016a). Spoorstaafbevestiging ns90 dwarsligger voor spoorstaaf 46e3, 54e1/e5 en 60e1/e2(spc00282).

ProRail. (2016b). Spoorstaafbevestiging op rug(helling)plaat voor spoorstaaf 46e3, 54e1/54e5 en 60e1/60e2(spc00281).

ProRail. (2018). Ontwerpvoorschriften-kunstwerken-deel 6 - aanvullingen en wijzigingen op nen-en normen (ovs00030-6).

ProRail. (2019). Zware spoorstaafbevestiging voor ns90 dwarsligger voor spoorstaaf 54e1/e5 en 60e1/e2(spc00282-1).

ProRail. (2023a). Spoorstaafbevestiging op rughellingplaat voor spoorstaaf 54e1/54e5 en 60e1/60e2 met skl 3-veerklem(spc00281-1).

ProRail. (2023b). Ontwerpvoorschriften-baan en bovenbouw-spoor in ballast(ovs00056-5.1).

ProRail. (2024, January). Update dienstregeling hogesnelheidslijn [https://www.prorail.nl/nieuws/minder-treinen-tussen-amsterdam-en-rotterdam].

Spanbeton. (2017). Zipxl railbalkoplossingen.

Verheijen, E. (n.d.). Railprofiel [https://www.infrasite.nl/glossary/railprofiel/].

Voestalpine. (n.d.). Elastic rail fastening system skl [https://www.voestalpine.com/railway-systems/en/products/elastic-rail-fastening-system-skl/].

Wagemaker. (2015). Vo/do/uo limburg - realisatie onderdoorgang en viaduct bpl.

Wagemaker. (2018). Langskrachtenanalyse dt2 en dt3-theemswegtrace.

A

Model 1

A.1. Single loaded span model

Compression										
Length	**Stress (MPa) LC1-71A**	**Stress (MPa) LC1-71B**	**Stress (MPa) LC1-SW/0 A**	**Stress (MPa) LC1-SW/0 B**	**Stress (MPa) LC1-SW/2**	**Stress (MPa) LC2-71A**	**Stress (MPa) LC2-71B**	**Stress (MPa) LC2-SW/0 A**	**Stress (MPa) LC2-SW/0 B**	**Stress (MPa) LC2-SW/2**
15	-13.9	-14.2	-10.2	-10.2	-16.3	-14.2	-15.7	-16	-16	-19.1
20	-14.4	-15.5	-17.5	-22.1	-20	-19.1	-20.9	-19.4	-19.9	-24.6
25	-19.8	-19.4	-12.3	-19.3	-20.3	-23.2	-24.7	-20	-24.1	-23.7
30	-24.9	-24.4	-15.5	-30.8	-28.2	-28.1	-29.6	-24.4	-33.1	-35
35	-34.1	-34.2	-15.1	-44.1	-35.6	-34.9	-35.1	-28	-45	-39.1
40	-41.6	-41.8	-18.1	-30.8	-45.5	-40.5	-41	-32.2	-34.6	-45.3
45	-49.2	-49.6	-25.6	-26	-75.6	-46.2	-46.9	-35.5	-37.7	-73.8
50	-57	-57.6	-32.8	-32.9	-91.4	-52	-52.9	-39.4	-40.6	-88
55	-64.9	-65.6	-39.9	-39.9	-106.3	-57.7	-58.9	-42.6	-43.2	-101.1
60	-72.9	-73.8	-36.1	-46.6	-101	-63.5	-64.9	-45.3	-45.5	-93.6
Tension										
Length	**Stress (MPa) LC1-71A**	**Stress (MPa) LC1-71B**	**Stress (MPa) LC1-SW/0 A**	**Stress (MPa) LC1-SW/0 B**	**Stress (MPa) LC1-SW/2**	**Stress (MPa) LC2-71A**	**Stress (MPa) LC2-71B**	**Stress (MPa) LC2-SW/0 A**	**Stress (MPa) LC2-SW/0 B**	**Stress (MPa) LC2-SW/2**
15	12.4	15.7	10.7	10.7	16.7	15.1	12.9	9.5	9.5	16
20	19.7	15.8	18.2	12.7	20.8	24.1	12.9	16.4	16.5	25.2
25	32	19.5	12.1	27.2	18.6	37.8	12.9	10.4	32.9	24.4
30	37	23.8	15.5	32.1	44.2	45	12.9	21.1	40	51.5
35	45.5	32.3	27.9	40.7	57.8	55.9	12.9	36.2	51	67.6
40	51.9	38.5	37.1	46	54.9	64.8	12.9	47.8	57.9	67.2
45	58.3	44.9	45.7	51.7	79.4	74	12.9	58.9	65.5	94.5
50	64.7	51.4	54	57.3	90	83.3	12.9	69.7	73.3	107.7
55	71.2	58	62.1	62.5	100.8	92.7	12.9	80.5	80.9	121
60	77.9	64.6	57.9	67.2	110.1	102.3	12.9	79.6	88.3	132.1

Compression										
Length	**Stress (MPa) LC3-71A**	**Stress (MPa) LC3-71B**	**Stress (MPa) LC3-SW/0 A**	**Stress (MPa) LC3-SW/0 B**	**Stress (MPa) LC3-SW/2**	**Stress (MPa) LC4-71A**	**Stress (MPa) LC4-71B**	**Stress (MPa) LC4-SW/0 A**	**Stress (MPa) LC4-SW/0 B**	**Stress (MPa) LC4-SW/2**
15	-16.9	-19.9	-15.4	-15.4	-15.5	-21.7	-19.1	-18	-18	-18.8
20	-26.4	-22.6	-23.3	-17.5	-18.9	-30.9	-22.9	-21.8	-21.5	-24.3
25	-41.9	-27.8	-18	-35.4	-37.3	-45.2	-31.1	-23.1	-38.5	-40.8
30	-49.5	-34.3	-21.5	-42.8	-43.5	-51.7	-36.6	-25.8	-44.9	-46
35	-57.1	-41.8	-37.2	-50.7	-58.8	-57.9	-42.8	-38.6	-51.9	-60.1
40	-62.5	-46.9	-49.6	-61	-68.8	-61.4	-46.1	-49.4	-60.7	-68.5
45	-68	-52.2	-61.2	-68.5	-76.1	-65	-49.5	-59.6	-66.9	-74.1
50	-73.5	-57.6	-72.4	-76.2	-83.2	-68.5	-52.9	-69.4	-73.2	-79.4
55	-79.1	-63.1	-83.5	-83.9	-90.3	-72	-56.3	-78.8	-79.2	-84.8
60	-84.9	-68.8	-81.4	-91.3	-98	-75.5	-59.8	-73.9	-84.9	-91.3
Tension										
Length	**Stress (MPa) LC3-71A**	**Stress (MPa) LC3-71B**	**Stress (MPa) LC3-SW/0 A**	**Stress (MPa) LC3-SW/0 B**	**Stress (MPa) LC3-SW/2**	**Stress (MPa) LC4-71A**	**Stress (MPa) LC4-71B**	**Stress (MPa) LC4-SW/0 A**	**Stress (MPa) LC4-SW/0 B**	**Stress (MPa) LC4-SW/2**
15	19.9	20.3	15.8	15.8	15.9	16.8	17.4	15	15	15.1
20	21.1	22.5	23.4	28	19.7	20.3	20.5	21.5	25.8	24.1
25	28.6	28.6	17.5	25.8	37.4	34.3	34.4	15.8	31.1	43.2
30	34.7	34.6	21.1	37.8	25	42.7	42.5	19	45.5	26.8
35	40	40.6	23.3	46.6	34.3	50.5	51	22.4	56.8	42.8
40	43.1	44.1	26.8	38.6	51.1	56.1	56.9	25.8	50.2	62.8
45	46.4	47.7	28.5	30.5	62.3	62.1	63.2	29.3	42.9	76.9
50	49.8	51.4	31	31.5	71.9	68.4	69.6	33.1	39.2	89.2
55	53.3	55.2	32.1	32.6	80.9	74.8	76.2	36.9	37.5	100.8
60	57	59.1	33.3	33.9	74.4	81.4	83.1	39.5	37.5	95.9

Compression										
Length	**Stress (MPa) LC5-71A**	**Stress (MPa) LC5-71B**	**Stress (MPa) LC5-SW/0 A**	**Stress (MPa) LC5-SW/0 B**	**Stress (MPa) LC5-SW/2**	**Stress (MPa) LC6-71A**	**Stress (MPa) LC6-71B**	**Stress (MPa) LC6-SW/0 A**	**Stress (MPa) LC6-SW/0 B**	**Stress (MPa) LC6-SW/2**
15	-11.9	-14.7	-10.2	-10.2	-16.3	-16.5	-15.7	-16	-16	-19.1
20	-19.7	-15.5	-17.7	-12.3	-20	-24.2	-20.9	-19.4	-16.6	-24.6
25	-33.5	-19.4	-12.4	-28.7	-19.8	-36.8	-24.7	-20	-31.8	-29.7
30	-39.5	-24.3	-15.8	-34.5	-44.8	-41.6	-29.6	-23.1	-36.6	-47.3
35	-49.4	-34.1	-30.5	-44.3	-60.3	-50.2	-35.1	-31.9	-45.2	-61.6
40	-57.4	-41.8	-41.8	-50.8	-60	-56.3	-41	-41.6	-50.4	-59.5
45	-65.4	-49.6	-52.4	-58	-84.6	-62.4	-46.9	-50.7	-56.2	-82.8
50	-73.5	-57.6	-62.7	-65.6	-96.1	-68.5	-52.9	-59.4	-62.3	-92.6
55	-81.7	-65.6	-72.8	-73.1	-107.5	-74.5	-58.9	-67.7	-68	-102.4
60	-89.9	-73.8	-70.4	-80.4	-117.3	-80.5	-64.9	-62.4	-73.5	-111
Tension										
Length	**Stress (MPa) LC5-71A**	**Stress (MPa) LC5-71B**	**Stress (MPa) LC5-SW/0 A**	**Stress (MPa) LC5-SW/0 B**	**Stress (MPa) LC5-SW/2**	**Stress (MPa) LC6-71A**	**Stress (MPa) LC6-71B**	**Stress (MPa) LC6-SW/0 A**	**Stress (MPa) LC6-SW/0 B**	**Stress (MPa) LC6-SW/2**
15	14.8	15.2	10.7	10.7	16.7	11.8	12.3	9.5	9.5	16
20	14.3	15.8	18	23	20.8	13.1	13.1	16.2	20.7	25.2
25	19.6	19.5	12.1	18.9	18.9	25.4	25.4	10.3	24.2	24.8
30	23.9	23.8	14.9	28.9	26.4	31.8	31.7	13.2	36.7	28.2
35	31.6	32.3	16.9	40.5	35.8	42.1	42.6	15.4	50.8	44.3
40	37.6	38.5	19.7	27.7	41.9	50.5	51.3	21.6	39.4	53.5
45	43.6	44.9	21.4	21	71.4	59.3	60.4	29	32.5	86
50	49.8	51.4	23.5	23	85.9	68.4	69.6	36.2	36.7	103.3
55	56.1	58	26.6	26.6	99.7	77.6	79	43.5	43.5	119.8
60	62.5	64.7	25.9	30.9	95.4	87	88.7	41	50.1	116.8

Compression											
Length	**Stress (MPa) LC7-71A**	**Stress (MPa) LC7-71B**	**Stress (MPa) LC7-SW/0 A**	**Stress (MPa) LC7-SW/0 B**	**Stress (MPa) LC7-SW/2**	**Stress (MPa) LC8-71A**	**Stress (MPa) LC8-71B**	**Stress (MPa) LC8-SW/0 A**	**Stress (MPa) LC8-SW/0 B**	**Stress (MPa) LC8-SW/2**	**Heighest stress per length**
15	-19.1	-19.4	-15.4	-15.4	-15.5	-18.1	-18.6	-18	-18	-18.8	-21.7
20	-21.5	-22.6	-23.2	-27.6	-18.9	-21.8	-22.9	-21.8	-25.2	-24.3	-30.9
25	-28.1	-27.8	-17.9	-25.6	-37.3	-31.4	-31.2	-23.1	-29.2	-40.8	-45.2
30	-34.9	-34.4	-21.8	-39	-26.8	-37.1	-36.6	-28	-41.3	-34.5	-51.7
35	-41.8	-41.8	-22.2	-49.5	-34.3	-42.5	-42.8	-31.9	-50.3	-38.4	-61.6
40	-46.7	-46.9	-24.4	-40.7	-53.9	-45.6	-46.1	-36.6	-39.4	-53.7	-68.8
45	-51.8	-52.2	-26.5	-32.5	-67.3	-48.8	-49.5	-40.1	-40.5	-65.5	-84.6
50	-57	-57.6	-28.4	-28.3	-78.7	-52	-52.9	-44.5	-44.6	-75	-96.1
55	-62.4	-63.1	-30.3	-30.3	-89.1	-55.2	-56.3	-47.9	-48.5	-83.6	-107.5
60	-67.9	-68.8	-30.2	-35.6	-82.1	-58.5	-59.8	-50.8	-52.3	-74.3	-117.3
Tension											
Length	**Stress (MPa) LC7-71A**	**Stress (MPa) LC7-71B**	**Stress (MPa) LC7-SW/0 A**	**Stress (MPa) LC7-SW/0 B**	**Stress (MPa) LC7-SW/2**	**Stress (MPa) LC8-71A**	**Stress (MPa) LC8-71B**	**Stress (MPa) LC8-SW/0 A**	**Stress (MPa) LC8-SW/0 B**	**Stress (MPa) LC8-SW/2**	**Heighest stress per length**
15	17.7	20.9	15.8	15.8	15.9	20.3	17.9	15	15	15.1	20.9
20	26.9	22.6	23.6	18.2	19.7	31.2	20.5	21.7	21.9	24.1	31.2
25	41	28.5	17.5	34.3	37.4	46.8	34.4	15.7	39.9	43.2	46.8
30	47.9	34.6	21.7	41.1	42.8	55.9	42.5	27.3	49	50.1	55.9
35	53.8	40.6	35.2	47.5	56.2	64.3	51	43.5	58	66	67.6
40	57.4	44.1	45.5	57.1	64.5	70.5	56.9	56.3	69.1	76.9	76.9
45	61.1	47.7	55.2	63	70.2	76.8	63.1	68.5	77	85.2	94.5
50	64.7	51.4	64.6	68.8	76	83.3	69.6	80.5	85	93.5	107.7
55	68.5	55.2	73.7	74.2	82	89.9	76.2	92.4	93	101.9	121
60	72.3	59.1	70.1	79.2	89.1	96.7	83	92	100.5	110.8	132.1

A.2. Model 1: Variable Bridge Length

Compression										
Length	**Stress (MPa) LC1-71A**	**Stress (MPa) LC1-71B**	**Stress (MPa) LC1-SW/0 A**	**Stress (MPa) LC1-SW/0 B**	**Stress (MPa) LC1-SW/2**	**Stress (MPa) LC2-71A**	**Stress (MPa) LC2-71B**	**Stress (MPa) LC2-SW/0 A**	**Stress (MPa) LC2-SW/0 B**	**Stress (MPa) LC2-SW/2**
15	-38	-38	-28.6	-28.6	-51.3	-34.7	-34.7	-24.8	-24.8	-47.7
35	-70.7	-70.6	-36.2	-36.2	-63.5	-53.9	-53.9	-26.2	-25.6	-49.1
60	-92.3	-92	-42.6	-42.4	-93.7	-71.2	-71.2	-38.6	-39	-66
Tension										
Length	**Stress (MPa) LC1-71A**	**Stress (MPa) LC1-71B**	**Stress (MPa) LC1-SW/0 A**	**Stress (MPa) LC1-SW/0 B**	**Stress (MPa) LC1-SW/2**	**Stress (MPa) LC2-71A**	**Stress (MPa) LC2-71B**	**Stress (MPa) LC2-SW/0 A**	**Stress (MPa) LC2-SW/0 B**	**Stress (MPa) LC2-SW/2**
15	37.9	37.9	25.5	25.5	47.3	42.1	42.1	29.9	29.9	51.8
35	58.6	58.6	20.5	20.4	64.6	77.4	42.1	36.8	35.3	80.5
60	71.5	71.8	43.9	48.8	98.2	106	42.1	77.5	82.3	127.5

Compression										
Length	**Stress (MPa) LC3-71A**	**Stress (MPa) LC3-71B**	**Stress (MPa) LC3-SW/0 A**	**Stress (MPa) LC3-SW/0 B**	**Stress (MPa) LC3-SW/2**	**Stress (MPa) LC4-71A**	**Stress (MPa) LC4-71B**	**Stress (MPa) LC4-SW/0 A**	**Stress (MPa) LC4-SW/0 B**	**Stress (MPa) LC4-SW/2**
15	-42	-38.6	-32.2	-32.2	-38.8	-35.1	-31.4	-28	-28	-34.1
35	-55.4	-63.1	-38.7	-39.6	-50.8	-42.2	-35.8	-32.2	-29.4	-34
60	-77.9	-75.9	-73.4	-78.3	-87.3	-52.1	-54.7	-41.9	-46.9	-55.7
Tension										
Length	**Stress (MPa) LC3-71A**	**Stress (MPa) LC3-71B**	**Stress (MPa) LC3-SW/0 A**	**Stress (MPa) LC3-SW/0 B**	**Stress (MPa) LC3-SW/2**	**Stress (MPa) LC4-71A**	**Stress (MPa) LC4-71B**	**Stress (MPa) LC4-SW/0 A**	**Stress (MPa) LC4-SW/0 B**	**Stress (MPa) LC4-SW/2**
15	39	35.3	33.7	33.7	34.1	46.6	42.8	39	39	38.2
35	37.6	45.7	29.2	33.3	43.2	64.3	73.1	46.1	50.4	58.4
60	43.1	49.2	29.5	29.6	65.9	89.8	97.6	55.8	53.3	98.4

Compression											
Length	**Stress (MPa) LC5-71A**	**Stress (MPa) LC5-71B**	**Stress (MPa) LC5-SW/0 A**	**Stress (MPa) LC5-SW/0 B**	**Stress (MPa) LC5-SW/2**	**Stress (MPa) LC6-71A**	**Stress (MPa) LC6-71B**	**Stress (MPa) LC6-SW/0 A**	**Stress (MPa) LC6-SW/0 B**	**Stress (MPa) LC6-SW/2**	
15	-38	-38	-26.1	-26.1	-52.9	-34.7	-34.7	-21.7	-21.7	-48.7	
35	-70.7	-70.6	-35.7	-34.7	-64.1	-53.9	-53.9	-24.1	-21.7	-49.2	
60	-92.5	-92	-64.8	-69.5	-102.2	-71.2	-71.2	-31.5	-36.2	-74.7	
Tension											
Length	**Stress (MPa) LC5-71A**	**Stress (MPa) LC5-71B**	**Stress (MPa) LC5-SW/0 A**	**Stress (MPa) LC5-SW/0 B**	**Stress (MPa) LC5-SW/2**	**Stress (MPa) LC6-71A**	**Stress (MPa) LC6-71B**	**Stress (MPa) LC6-SW/0 A**	**Stress (MPa) LC6-SW/0 B**	**Stress (MPa) LC6-SW/2**	
15	37.9	37.9	24.7	24.7	45.5	42.1	42.1	29	29	49.4	
35	58.6	58.7	18.9	22.5	47.9	77.4	77.4	36.5	40.5	62.3	
60	71.4	71.8	24.6	24.2	88.8	106	106.1	46.3	44.1	117.7	

Compression											
Length	**Stress (MPa) LC7-71A**	**Stress (MPa) LC7-71B**	**Stress (MPa) LC7-SW/0 A**	**Stress (MPa) LC7-SW/0 B**	**Stress (MPa) LC7-SW/2**	**Stress (MPa) LC8-71A**	**Stress (MPa) LC8-71B**	**Stress (MPa) LC8-SW/0 A**	**Stress (MPa) LC8-SW/0 B**	**Stress (MPa) LC8-SW/2**	**Highest stress per length**
15	-42.1	-38.6	-38.2	-38.2	-36.9	-35.2	-31.5	-34.6	-34.6	-32.7	-52.9
35	-55.7	-63.1	-45.8	-46.2	-53.5	-41.9	-35.8	-32.7	-30.3	-36.9	-70.7
60	-74.7	-78.1	-52	-51.7	-79.4	-56.6	-51.6	-43.3	-44.9	-48	-102.2
Tension											
Length	**Stress (MPa) LC7-71A**	**Stress (MPa) LC7-71B**	**Stress (MPa) LC7-SW/0 A**	**Stress (MPa) LC7-SW/0 B**	**Stress (MPa) LC7-SW/2**	**Stress (MPa) LC8-71A**	**Stress (MPa) LC8-71B**	**Stress (MPa) LC8-SW/0 A**	**Stress (MPa) LC8-SW/0 B**	**Stress (MPa) LC8-SW/2**	**Highest stress per length**
15	39	35.3	28.1	28.1	34.9	46.6	42.8	32.1	32.1	39.6	51.8
35	38	45.7	28.3	27.9	49.4	64	73	37.7	41.3	66.6	80.5
60	46.6	47	56.5	61.7	75.5	95.8	93.2	89	94.2	107.5	127.5

A.3. Model 1: Variable Elastomeric Bearings

Compression										
Horizontal stiffness	**Stress (MPa) LC1-71A**	**Stress (MPa) LC1-71B**	**Stress (MPa) LC1-SW/0 A**	**Stress (MPa) LC1-SW/0 B**	**Stress (MPa) LC1-SW/2**	**Stress (MPa) LC2-71A**	**Stress (MPa) LC2-71B**	**Stress (MPa) LC2-SW/0 A**	**Stress (MPa) LC2-SW/0 B**	**Stress (MPa) LC2-SW/2**
1.5	-90.5	-90.4	-101.7	-118.5	-146.9	-72.4	-72.4	-83.7	-100.3	-132.2
3.0	-74.5	-74.4	-42.1	-47.6	-66.3	-57.7	-57.8	-26.7	-29.2	-51.8
4.0	-70.7	-70.6	-36.2	-36.2	-63.5	-53.9	-53.9	-26.2	-25.6	-49.1
6.0	-65.8	-65.8	-42.9	-44.4	-70.8	-49.6	-49.6	-25.4	-25.1	-57.1
8.0	-62.7	-62.6	-44.8	-46.9	-72.6	-47.2	-47.2	-26.2	-28.1	-59.6
Tension										
Horizontal stiffness	**Stress (MPa) LC1-71A**	**Stress (MPa) LC1-71B**	**Stress (MPa) LC1-SW/0 A**	**Stress (MPa) LC1-SW/0 B**	**Stress (MPa) LC1-SW/2**	**Stress (MPa) LC2-71A**	**Stress (MPa) LC2-71B**	**Stress (MPa) LC2-SW/0 A**	**Stress (MPa) LC2-SW/0 B**	**Stress (MPa) LC2-SW/2**
1.5	78.9	79	63.3	80.9	218.9	94.9	95	79.4	97.2	233.1
3.0	63.3	63.4	20.8	25.8	89.4	81.5	81.5	33.2	44.2	104.8
4.0	58.6	58.6	20.5	20.4	64.6	77.4	77.4	36.8	35.3	80.5
6.0	53.4	53.4	21.6	23.1	55.6	72.7	72.8	40.7	42.2	71.3
8.0	50.6	50.7	22.5	25.3	60.1	70.2	70.2	42.5	45.2	76.2

Compression										
Horizontal stiffness	**Stress (MPa) LC3-71A**	**Stress (MPa) LC3-71B**	**Stress (MPa) LC3-SW/0 A**	**Stress (MPa) LC3-SW/0 B**	**Stress (MPa) LC3-SW/2**	**Stress (MPa) LC4-71A**	**Stress (MPa) LC4-71B**	**Stress (MPa) LC4-SW/0 A**	**Stress (MPa) LC4-SW/0 B**	**Stress (MPa) LC4-SW/2**
1.5	-56.8	-77.8	-58.3	-92	-192.5	-44.3	-50.2	-41.8	-74.2	-175.7
3.0	-56	-61.6	-34	-42.6	-73	-42.7	-36.7	-32.9	-30.1	-55.9
4.0	-55.4	-63.1	-38.7	-39.6	-50.8	-42.2	-35.8	-32.2	-29.4	-34
6.0	-54.2	-64.1	-41.9	-45.7	-55.7	-41.5	-35.6	-31.3	-28.5	-37.9
8.0	-53.1	-63.8	-42.7	-47.6	-60.1	-41.1	-35.6	-30.7	-29.2	-42.8
Tension										
Horizontal stiffness	**Stress (MPa) LC3-71A**	**Stress (MPa) LC3-71B**	**Stress (MPa) LC3-SW/0 A**	**Stress (MPa) LC3-SW/0 B**	**Stress (MPa) LC3-SW/2**	**Stress (MPa) LC4-71A**	**Stress (MPa) LC4-71B**	**Stress (MPa) LC4-SW/0 A**	**Stress (MPa) LC4-SW/0 B**	**Stress (MPa) LC4-SW/2**
1.5	39.9	63	105.7	124.6	146.3	64.3	88.1	121	140.1	161.1
3.0	38.4	48.6	41.5	47.9	52.4	64.5	75.5	58	64.6	67.1
4.0	37.6	45.7	29.2	33.3	43.2	64.3	73.1	46.1	50.4	58.4
6.0	36.4	43	33.2	35.2	39.4	63.8	71	49.7	51.7	55.3
8.0	35.4	42.7	35.2	37.9	42.3	63.2	70	51.9	54.7	58.3

Compression										
Horizontal stiffness	**Stress (MPa) LC5-71A**	**Stress (MPa) LC5-71B**	**Stress (MPa) LC5-SW/0 A**	**Stress (MPa) LC5-SW/0 B**	**Stress (MPa) LC5-SW/2**	**Stress (MPa) LC6-71A**	**Stress (MPa) LC6-71B**	**Stress (MPa) LC6-SW/0 A**	**Stress (MPa) LC6-SW/0 B**	**Stress (MPa) LC6-SW/2**
1.5	-90.6	-90.4	-69.4	-86.2	-211.4	-72.3	-72.3	-51.7	-67.7	-196.4
3.0	-74.4	-74.4	-31.1	-38.2	-88.3	-57.7	-57.7	-24.6	-22.2	-73.2
4.0	-70.7	-70.6	-35.7	-34.7	-64.1	-53.9	-53.9	-24.1	-21.7	-49.2
6.0	-65.8	-65.8	-38.9	-41	-72.5	-49.6	-49.6	-23.4	-21.1	-57.6
8.0	-62.7	-62.6	-39.8	-43	-76.3	-47.2	-47.2	-23	-22.5	-62
Tension										
Horizontal stiffness	**Stress (MPa) LC5-71A**	**Stress (MPa) LC5-71B**	**Stress (MPa) LC5-SW/0 A**	**Stress (MPa) LC5-SW/0 B**	**Stress (MPa) LC5-SW/2**	**Stress (MPa) LC6-71A**	**Stress (MPa) LC6-71B**	**Stress (MPa) LC6-SW/0 A**	**Stress (MPa) LC6-SW/0 B**	**Stress (MPa) LC6-SW/2**
1.5	78.9	79	95.2	113.8	147.1	94.9	94.9	111.1	129.9	160.4
3.0	63.3	63.4	31	37	64.1	81.5	81.5	48.2	54.5	78.2
4.0	58.6	58.7	18.9	22.5	47.9	77.4	77.4	36.5	40.5	62.3
6.0	53.4	53.5	25.6	27	52.2	72.8	72.8	42.8	44.6	66.8
8.0	50.7	50.7	28.1	30.2	54.2	70.2	70.2	45.5	47.9	69.1

Compression											
Horizontal stiffness	**Stress (MPa) LC7-71A**	**Stress (MPa) LC7-71B**	**Stress (MPa) LC7-SW/0 A**	**Stress (MPa) LC7-SW/0 B**	**Stress (MPa) LC7-SW/2**	**Stress (MPa) LC8-71A**	**Stress (MPa) LC8-71B**	**Stress (MPa) LC8-SW/0 A**	**Stress (MPa) LC8-SW/0 B**	**Stress (MPa) LC8-SW/2**	**Highest stress per length**
1.5	-56.6	-77.9	-111.6	-128.7	-138.9	-43.7	-50.3	-94.4	-111.4	-122.4	-211.4
3.0	-56.2	-61.7	-50.4	-56.2	-60.9	-42.4	-36.7	-33.7	-38.7	-44.5	-88.3
4.0	-55.7	-63.1	-45.8	-46.2	-53.5	-41.9	-35.8	-32.7	-30.3	-36.9	-70.7
6.0	-54.5	-64.1	-52.1	-54	-55.3	-41.2	-35.6	-34.2	-36.1	-39.2	-72.5
8.0	-53.5	-63.8	-53.7	-56.2	-57.7	-40.9	-35.6	-36.3	-38.8	-42.3	-76.3
Tension											
Horizontal stiffness	**Stress (MPa) LC7-71A**	**Stress (MPa) LC7-71B**	**Stress (MPa) LC7-SW/0 A**	**Stress (MPa) LC7-SW/0 B**	**Stress (MPa) LC7-SW/2**	**Stress (MPa) LC8-71A**	**Stress (MPa) LC8-71B**	**Stress (MPa) LC8-SW/0 A**	**Stress (MPa) LC8-SW/0 B**	**Stress (MPa) LC8-SW/2**	**Highest stress per stiffness**
1.5	40.6	62.9	53.3	83.2	198.9	64.4	88.1	68.6	99.4	214.2	233.1
3.0	38.8	48.6	28.8	32.1	69.9	64.3	75.5	37.3	50.2	86.6	104.8
4.0	38	45.7	28.3	27.9	49.4	64	73	37.7	41.3	66.6	80.5
6.0	36.7	43	27.7	27.1	44.1	63.4	71	41.1	44.5	61.9	72.8
8.0	35.8	42.7	27.3	28.8	46.6	62.8	70	42.5	47.1	64.2	76.2

A.4. Model 1: Variable Bridge Pier Length

Compression										
Length [m]	**Stress (MPa) LC1-71A**	**Stress (MPa) LC1-71B**	**Stress (MPa) LC1-SW/0 A**	**Stress (MPa) LC1-SW/0 B**	**Stress (MPa) LC1-SW/2**	**Stress (MPa) LC2-71A**	**Stress (MPa) LC2-71B**	**Stress (MPa) LC2-SW/0 A**	**Stress (MPa) LC2-SW/0 B**	**Stress (MPa) LC2-SW/2**
5	-64.9	-64.8	-35.8	-35.9	-61.3	-53.1	-53.1	-26	-25.5	-46.9
7.5	-70.7	-70.6	-36.2	-36.2	-63.5	-53.9	-53.9	-26.2	-25.6	-49.1
10	-79.2	-79.1	-37.2	-37.1	-67	-57.6	-57.7	-26.4	-25.9	-52.7
Tension										
Length [m]	**Stress (MPa) LC1-71A**	**Stress (MPa) LC1-71B**	**Stress (MPa) LC1-SW/0 A**	**Stress (MPa) LC1-SW/0 B**	**Stress (MPa) LC1-SW/2**	**Stress (MPa) LC2-71A**	**Stress (MPa) LC2-71B**	**Stress (MPa) LC2-SW/0 A**	**Stress (MPa) LC2-SW/0 B**	**Stress (MPa) LC2-SW/2**
5	52.7	52.8	20.4	20.4	59.2	71	71	38.6	37.1	75.3
7.5	58.6	58.6	20.5	20.4	64.6	77.4	77.4	36.8	35.3	80.5
10	67.2	67.3	20.6	20.6	70.9	86.5	86.6	34.6	37.4	86.7

Compression										
Length [m]	**Stress (MPa) LC3-71A**	**Stress (MPa) LC3-71B**	**Stress (MPa) LC3-SW/0 A**	**Stress (MPa) LC3-SW/0 B**	**Stress (MPa) LC3-SW/2**	**Stress (MPa) LC4-71A**	**Stress (MPa) LC4-71B**	**Stress (MPa) LC4-SW/0 A**	**Stress (MPa) LC4-SW/0 B**	**Stress (MPa) LC4-SW/2**
5	-53.7	-61.5	-37	-38.2	-51.7	-42	-35.6	-32	-29.3	-34.5
7.5	-55.4	-63.1	-38.7	-39.6	-50.8	-42.2	-35.8	-32.2	-29.4	-34
10	-57.7	-65.4	-41.2	-41.8	-49.3	-42.4	-37.3	-32.5	-29.7	-34.4
Tension										
Length [m]	**Stress (MPa) LC3-71A**	**Stress (MPa) LC3-71B**	**Stress (MPa) LC3-SW/0 A**	**Stress (MPa) LC3-SW/0 B**	**Stress (MPa) LC3-SW/2**	**Stress (MPa) LC4-71A**	**Stress (MPa) LC4-71B**	**Stress (MPa) LC4-SW/0 A**	**Stress (MPa) LC4-SW/0 B**	**Stress (MPa) LC4-SW/2**
5	35.8	44.9	29.1	30.3	44.7	62.5	70.8	45.6	47.4	60
7.5	37.6	45.7	29.2	33.3	43.2	64.3	73.1	46.1	50.4	58.4
10	40.2	48.6	32.6	36.9	40.9	66.8	76	49.5	54	55.8

Compression											
Length [m]	**Stress (MPa) LC5-71A**	**Stress (MPa) LC5-71B**	**Stress (MPa) LC5-SW/0 A**	**Stress (MPa) LC5-SW/0 B**	**Stress (MPa) LC5-SW/2**	**Stress (MPa) LC6-71A**	**Stress (MPa) LC6-71B**	**Stress (MPa) LC6-SW/0 A**	**Stress (MPa) LC6-SW/0 B**	**Stress (MPa) LC6-SW/2**
5	-64.9	-64.8	-34.7	-34.1	-64.9	-53.1	-53.1	-23.9	-21.6	-49.8
7.5	-70.7	-70.6	-35.7	-34.7	-64.1	-53.9	-53.9	-24.1	-21.7	-49.2
10	-79.2	-79.1	-37.2	-35.9	-62.3	-57.6	-57.7	-24.3	-22	-47.6
Tension										
Length [m]	**Stress (MPa) LC5-71A**	**Stress (MPa) LC5-71B**	**Stress (MPa) LC5-SW/0 A**	**Stress (MPa) LC5-SW/0 B**	**Stress (MPa) LC5-SW/2**	**Stress (MPa) LC6-71A**	**Stress (MPa) LC6-71B**	**Stress (MPa) LC6-SW/0 A**	**Stress (MPa) LC6-SW/0 B**	**Stress (MPa) LC6-SW/2**
5	52.7	52.8	20	20.3	48.6	71	71.1	37.4	38.2	63
7.5	58.6	58.7	18.9	22.5	47.9	77.4	77.4	36.5	40.5	62.3
10	67.2	67.3	21.2	25	53.2	86.5	86.6	38.8	42.9	67.4

Compression												
Length [m]	**Stress (MPa) LC7-71A**	**Stress (MPa) LC7-71B**	**Stress (MPa) LC7-SW/0 A**	**Stress (MPa) LC7-SW/0 B**	**Stress (MPa) LC7-SW/2**	**Stress (MPa) LC8-71A**	**Stress (MPa) LC8-71B**	**Stress (MPa) LC8-SW/0 A**	**Stress (MPa) LC8-SW/0 B**	**Stress (MPa) LC8-SW/2**	**Highest stress per length**
5	-54	-61.5	-44.7	-45.2	-50.6	-41.7	-35.6	-32.5	-30.1	-35.6	-64.9
7.5	-55.7	-63.1	-45.8	-46.2	-53.5	-41.9	-35.8	-32.7	-30.3	-36.9	-70.7
10	-57.9	-65.4	-47.7	-48	-56.8	-42.1	-37.3	-33	-30.7	-40.4	-79.2
Tension											
Length [m]	**Stress (MPa) LC7-71A**	**Stress (MPa) LC7-71B**	**Stress (MPa) LC7-SW/0 A**	**Stress (MPa) LC7-SW/0 B**	**Stress (MPa) LC7-SW/2**	**Stress (MPa) LC8-71A**	**Stress (MPa) LC8-71B**	**Stress (MPa) LC8-SW/0 A**	**Stress (MPa) LC8-SW/0 B**	**Stress (MPa) LC8-SW/2**	**Highest stress per length**
5	36.2	44.9	28.2	27.8	46.6	62.1	70.8	40.3	40.8	64.1	75.3
7.5	38	45.7	28.3	27.9	49.4	64	73	37.7	41.3	66.6	80.5
10	40.5	48.6	28.5	28.1	52.7	66.7	76	36.5	44.6	69.7	86.7

A.5. Model 1: Variable Foundation

Compression										
Horizontal stiffness	**Stress (MPa) LC1-71A**	**Stress (MPa) LC1-71B**	**Stress (MPa) LC1-SW/0 A**	**Stress (MPa) LC1-SW/0 B**	**Stress (MPa) LC1-SW/2**	**Stress (MPa) LC2-71A**	**Stress (MPa) LC2-71B**	**Stress (MPa) LC2-SW/0 A**	**Stress (MPa) LC2-SW/0 B**	**Stress (MPa) LC2-SW/2**
35	-78.2	-78.1	-36	-35.9	-64.4	-59.7	-59.7	-26.8	-26.2	-50.6
68	-70.7	-70.6	-36.2	-36.2	-63.5	-53.9	-53.9	-26.2	-25.6	-49.1
105	-67.6	-67.5	-36.3	-36.3	-63	-51.6	-51.6	-25.9	-25.4	-48.4
Tension										
Horizontal stiffness	**Stress (MPa) LC1-71A**	**Stress (MPa) LC1-71B**	**Stress (MPa) LC1-SW/0 A**	**Stress (MPa) LC1-SW/0 B**	**Stress (MPa) LC1-SW/2**	**Stress (MPa) LC2-71A**	**Stress (MPa) LC2-71B**	**Stress (MPa) LC2-SW/0 A**	**Stress (MPa) LC2-SW/0 B**	**Stress (MPa) LC2-SW/2**
35	67.4	67.5	21.1	21.2	66.8	84.8	84.8	36.7	35	81.8
68	58.6	58.6	20.5	20.4	64.6	77.4	77.4	36.8	35.3	80.5
105	54.8	54.9	20.1	20.1	63.6	74.3	74.3	36.8	35.4	79.9

Compression										
Horizontal stiffness	**Stress (MPa) LC3-71A**	**Stress (MPa) LC3-71B**	**Stress (MPa) LC3-SW/0 A**	**Stress (MPa) LC3-SW/0 B**	**Stress (MPa) LC3-SW/2**	**Stress (MPa) LC4-71A**	**Stress (MPa) LC4-71B**	**Stress (MPa) LC4-SW/0 A**	**Stress (MPa) LC4-SW/0 B**	**Stress (MPa) LC4-SW/2**
35	-55.8	-62.8	-38.1	-39.1	-51	-43	-36.9	-33	-30.3	-35
68	-55.4	-63.1	-38.7	-39.6	-50.8	-42.2	-35.8	-32.2	-29.4	-34
105	-55.2	-63.2	-39.1	-39.9	-51	-41.8	-35.3	-31.9	-29.1	-33.5
Tension										
Horizontal stiffness	**Stress (MPa) LC3-71A**	**Stress (MPa) LC3-71B**	**Stress (MPa) LC3-SW/0 A**	**Stress (MPa) LC3-SW/0 B**	**Stress (MPa) LC3-SW/2**	**Stress (MPa) LC4-71A**	**Stress (MPa) LC4-71B**	**Stress (MPa) LC4-SW/0 A**	**Stress (MPa) LC4-SW/0 B**	**Stress (MPa) LC4-SW/2**
35	39	46.5	30.4	34.5	44.2	64.6	72.8	46.4	50.7	58.6
68	37.6	45.7	29.2	33.3	43.2	64.3	73.1	46.1	50.4	58.4
105	37	45.3	28.6	32.8	42.7	64.2	73.1	45.9	50.2	58.2

Compression											
Horizontal stiffness	**Stress (MPa) LC5-71A**	**Stress (MPa) LC5-71B**	**Stress (MPa) LC5-SW/0 A**	**Stress (MPa) LC5-SW/0 B**	**Stress (MPa) LC5-SW/2**	**Stress (MPa) LC6-71A**	**Stress (MPa) LC6-71B**	**Stress (MPa) LC6-SW/0 A**	**Stress (MPa) LC6-SW/0 B**	**Stress (MPa) LC6-SW/2**
35	-78.2	-78.1	-35	-34	-66.2	-59.7	-59.7	-24.7	-22.4	-52
68	-70.7	-70.6	-35.7	-34.7	-64.1	-53.9	-53.9	-24.1	-21.7	-49.2
105	-67.6	-67.5	-36.1	-35	-63.1	-51.5	-51.6	-23.8	-21.4	-47.9
Tension										
Horizontal stiffness	**Stress (MPa) LC5-71A**	**Stress (MPa) LC5-71B**	**Stress (MPa) LC5-SW/0 A**	**Stress (MPa) LC5-SW/0 B**	**Stress (MPa) LC5-SW/2**	**Stress (MPa) LC6-71A**	**Stress (MPa) LC6-71B**	**Stress (MPa) LC6-SW/0 A**	**Stress (MPa) LC6-SW/0 B**	**Stress (MPa) LC6-SW/2**
35	67.4	67.5	19.9	23.5	50	84.8	84.9	36.6	40.5	63.6
68	58.6	58.7	18.9	22.5	47.9	77.4	77.4	36.5	40.5	62.3
105	54.9	54.9	18.4	22.1	46.9	74.3	74.3	36.4	40.4	61.6

Compression											
Horizontal stiffness	**Stress (MPa) LC7-71A**	**Stress (MPa) LC7-71B**	**Stress (MPa) LC7-SW/0 A**	**Stress (MPa) LC7-SW/0 B**	**Stress (MPa) LC7-SW/2**	**Stress (MPa) LC8-71A**	**Stress (MPa) LC8-71B**	**Stress (MPa) LC8-SW/0 A**	**Stress (MPa) LC8-SW/0 B**	**Stress (MPa) LC8-SW/2**	**Highest stress per stiffness**
35	-55.9	-62.8	-45.9	-46.1	-52.4	-42.6	-36.9	-33.7	-31.2	-36.8	-78.2
68	-55.7	-63.1	-45.8	-46.2	-53.5	-41.9	-35.8	-32.7	-30.3	-36.9	-70.7
105	-55.5	-63.2	-45.8	-46.2	-54	-41.5	-35.3	-32.3	-29.9	-37	-67.6
Tension											
Horizontal stiffness	**Stress (MPa) LC7-71A**	**Stress (MPa) LC7-71B**	**Stress (MPa) LC7-SW/0 A**	**Stress (MPa) LC7-SW/0 B**	**Stress (MPa) LC7-SW/2**	**Stress (MPa) LC8-71A**	**Stress (MPa) LC8-71B**	**Stress (MPa) LC8-SW/0 A**	**Stress (MPa) LC8-SW/0 B**	**Stress (MPa) LC8-SW/2**	**Highest stress per stiffness**
35	39.4	46.5	29.2	28.8	49.7	64.4	72.8	37.9	41.1	66.2	84.9
68	38	45.7	28.3	27.9	49.4	64	73	37.7	41.3	66.6	80.5
105	37.3	45.3	27.9	27.4	49.3	63.8	73.1	37.6	41.4	66.8	79.9

B

Model 2

B.1. Model 2: Variable Bridge Length

Compression										
Length [m]	**Stress (MPa) LC1-71A**	**Stress (MPa) LC1-71B**	**Stress (MPa) LC1-SW/0 A**	**Stress (MPa) LC1-SW/0 B**	**Stress (MPa) LC1-SW/2**	**Stress (MPa) LC2-71A**	**Stress (MPa) LC2-71B**	**Stress (MPa) LC2-SW/0 A**	**Stress (MPa) LC2-SW/0 B**	**Stress (MPa) LC2-SW/2**
15	-6.6	-5.1	-3.2	-3.6	-13.1	-33.9	-35.1	-32.7	-27.5	-30
35	-8.3	-7.1	0	0	-8.6	-46.3	-47.1	-45.6	-47	-44.2
60	-8.6	-8.3	0	0	0	-62.6	-64	-60.1	-59.9	-63.7
Tension										
Length [m]	**Stress (MPa) LC1-71A**	**Stress (MPa) LC1-71B**	**Stress (MPa) LC1-SW/0 A**	**Stress (MPa) LC1-SW/0 B**	**Stress (MPa) LC1-SW/2**	**Stress (MPa) LC2-71A**	**Stress (MPa) LC2-71B**	**Stress (MPa) LC2-SW/0 A**	**Stress (MPa) LC2-SW/0 B**	**Stress (MPa) LC2-SW/2**
15	35.3	37.5	30.3	35.3	45.3	4.6	6.8	4.2	6.8	17.1
35	44.7	47.9	45.2	46.2	58.1	4.6	8.1	0	6.3	20.3
60	56.9	60.9	54.5	52.9	73.2	7.5	12.7	10.9	10.2	35.3

Compression										
Length [m]	**Stress (MPa) LC3-71A**	**Stress (MPa) LC3-71B**	**Stress (MPa) LC3-SW/0 A**	**Stress (MPa) LC3-SW/0 B**	**Stress (MPa) LC3-SW/2**	**Stress (MPa) LC4-71A**	**Stress (MPa) LC4-71B**	**Stress (MPa) LC4-SW/0 A**	**Stress (MPa) LC4-SW/0 B**	**Stress (MPa) LC4-SW/2**
15	-7.1	-4.2	-8.7	-7.7	-4.7	-31.2	-39.8	-29.2	-38.1	-35.6
35	-2.3	0	-0.4	0	0	-39.9	-52.9	-40	-46.7	-48.7
60	0	0	0	0	0	-55.6	-72.9	-53.6	-51	-63.5
Tension										
Length [m]	**Stress (MPa) LC3-71A**	**Stress (MPa) LC3-71B**	**Stress (MPa) LC3-SW/0 A**	**Stress (MPa) LC3-SW/0 B**	**Stress (MPa) LC3-SW/2**	**Stress (MPa) LC4-71A**	**Stress (MPa) LC4-71B**	**Stress (MPa) LC4-SW/0 A**	**Stress (MPa) LC4-SW/0 B**	**Stress (MPa) LC4-SW/2**
15	42.1	37.2	40.1	31.2	34.7	7.3	7.5	12	9	7.2
35	48.6	60.3	45.3	49.7	50.1	1.6	12.5	2	10.3	4.8
60	58.7	68.8	50.5	48.5	72.1	7.4	17.5	0.8	0	31.5

Compression										
Length [m]	**Stress (MPa) LC5-71A**	**Stress (MPa) LC5-71B**	**Stress (MPa) LC5-SW/0 A**	**Stress (MPa) LC5-SW/0 B**	**Stress (MPa) LC5-SW/2**	**Stress (MPa) LC6-71A**	**Stress (MPa) LC6-71B**	**Stress (MPa) LC6-SW/0 A**	**Stress (MPa) LC6-SW/0 B**	**Stress (MPa) LC6-SW/2**
15	-4.6	-6.8	-3.8	-3.1	-10.8	-33.1	-35.3	-28.2	-33.4	-42
35	-4.6	-8.1	0	0	-4.1	-45.6	-47.6	-41.1	-46.8	-53.5
60	-4.6	-8.6	0	0	0	-61.7	-64.1	-56.2	-54.2	-63.3
Tension										
Length [m]	**Stress (MPa) LC5-71A**	**Stress (MPa) LC5-71B**	**Stress (MPa) LC5-SW/0 A**	**Stress (MPa) LC5-SW/0 B**	**Stress (MPa) LC5-SW/2**	**Stress (MPa) LC6-71A**	**Stress (MPa) LC6-71B**	**Stress (MPa) LC6-SW/0 A**	**Stress (MPa) LC6-SW/0 B**	**Stress (MPa) LC6-SW/2**
15	35.3	37.4	35.1	30.1	34.1	6.6	5.1	6.7	4.1	13.3
35	45.5	48.1	42.9	46	47.6	8.3	7.1	0	6.1	11
60	58	60.8	48.9	47	72.7	9	12.6	0	0	32.6

Compression											
Length [m]	**Stress (MPa) LC7-71A**	**Stress (MPa) LC7-71B**	**Stress (MPa) LC7-SW/0 A**	**Stress (MPa) LC7-SW/0 B**	**Stress (MPa) LC7-SW/2**	**Stress (MPa) LC8-71A**	**Stress (MPa) LC8-71B**	**Stress (MPa) LC8-SW/0 A**	**Stress (MPa) LC8-SW/0 B**	**Stress (MPa) LC8-SW/2**	**Highest stress per length**
15	-4.1	-6.4	-7.6	-8.5	-7.1	-38.9	-33.9	-37.2	-28.2	-31	-42
35	0	0	0	0	-2.6	-62.4	-52.9	-47.6	-45.8	-47.5	-62.4
60	0	0	0	0	0	-73.1	-65	-62.3	-63	-64.9	-73.1
Tension											
Length [m]	**Stress (MPa) LC7-71A**	**Stress (MPa) LC7-71B**	**Stress (MPa) LC7-SW/0 A**	**Stress (MPa) LC7-SW/0 B**	**Stress (MPa) LC7-SW/2**	**Stress (MPa) LC8-71A**	**Stress (MPa) LC8-71B**	**Stress (MPa) LC8-SW/0 A**	**Stress (MPa) LC8-SW/0 B**	**Stress (MPa) LC8-SW/2**	**Highest stress per length**
15	34.2	43.2	31.6	40.4	38.4	7.9	8.7	9.3	12.3	9.4	45.3
35	46	57.2	45.9	51	52.6	6.8	10.1	4.9	11.5	12.9	60.3
60	58.7	66.3	58.4	57.1	72.5	10.4	14.8	15.7	14.9	34.2	73.2

B.2. Model 2: Variable Elastomeric Bearings

Compression										
Horizontal stiffness	**Stress (MPa) LC1-71A**	**Stress (MPa) LC1-71B**	**Stress (MPa) LC1-SW/0 A**	**Stress (MPa) LC1-SW/0 B**	**Stress (MPa) LC1-SW/2**	**Stress (MPa) LC2-71A**	**Stress (MPa) LC2-71B**	**Stress (MPa) LC2-SW/0 A**	**Stress (MPa) LC2-SW/0 B**	**Stress (MPa) LC2-SW/2**
1.5	-8.3	-7.1	0	-0.5	-7.6	-47.4	-48	-46.7	-48.1	-44.9
3.0	-8.3	-7.1	0	0	-8.4	-46.5	-47.3	-45.8	-47.3	-42.4
4.0	-8.3	-7.1	0	0	-8.6	-46.3	-47.1	-45.6	-47	-44.2
6.0	-8.3	-7.1	0	0	-8.7	-46.2	-47	-45.4	-46.8	-46.1
8.0	-8.3	-7.1	0	0	-8.7	-46.1	-46.9	-45.4	-46.7	-46.7
Tension										
Horizontal stiffness	**Stress (MPa) LC1-71A**	**Stress (MPa) LC1-71B**	**Stress (MPa) LC1-SW/0 A**	**Stress (MPa) LC1-SW/0 B**	**Stress (MPa) LC1-SW/2**	**Stress (MPa) LC2-71A**	**Stress (MPa) LC2-71B**	**Stress (MPa) LC2-SW/0 A**	**Stress (MPa) LC2-SW/0 B**	**Stress (MPa) LC2-SW/2**
1.5	46.4	49.7	47.9	44.9	55.1	4.7	8.1	12.9	12.7	24.7
3.0	42.1	45.9	42.1	43.1	54.6	4.6	8.1	0.1	3.2	16.5
4.0	44.7	47.9	45.2	46.2	58.1	4.6	8.1	0	6.3	20.3
6.0	46.4	49.3	47.3	48.2	60.5	4.6	8.1	1.8	8.6	23.1
8.0	47	49.7	48	48.9	61.2	4.6	8.1	2.7	9.4	24.1

Compression										
Horizontal stiffness	**Stress (MPa) LC3-71A**	**Stress (MPa) LC3-71B**	**Stress (MPa) LC3-SW/0 A**	**Stress (MPa) LC3-SW/0 B**	**Stress (MPa) LC3-SW/2**	**Stress (MPa) LC4-71A**	**Stress (MPa) LC4-71B**	**Stress (MPa) LC4-SW/0 A**	**Stress (MPa) LC4-SW/0 B**	**Stress (MPa) LC4-SW/2**
1.5	-0.4	0	-1.4	-4.1	-3	-44.4	-54.5	-42.8	-47.6	-50.1
3.0	-2	0	-0.1	0	0	-37.3	-53.2	-39.5	-46.8	-49.1
4.0	-2.3	0	-0.4	0	0	-39.9	-52.9	-40	-46.7	-48.7
6.0	-2.5	0	-0.5	-1.1	0	-41.6	-52.6	-41.5	-48.4	-48.4
8.0	-2.6	0	-0.6	-1.7	-0.2	-42.2	-52.5	-42	-48.9	-48.3
Tension										
Horizontal stiffness	**Stress (MPa) LC3-71A**	**Stress (MPa) LC3-71B**	**Stress (MPa) LC3-SW/0 A**	**Stress (MPa) LC3-SW/0 B**	**Stress (MPa) LC3-SW/2**	**Stress (MPa) LC4-71A**	**Stress (MPa) LC4-71B**	**Stress (MPa) LC4-SW/0 A**	**Stress (MPa) LC4-SW/0 B**	**Stress (MPa) LC4-SW/2**
1.5	45.5	57.4	40.5	49.5	49.7	8.8	19.7	0.4	18.2	12
3.0	46.2	57.4	43.9	46.9	47.1	0	9.5	0.6	7.1	4.9
4.0	48.6	60.3	45.3	49.7	50.1	1.6	12.5	2	10.3	4.8
6.0	50.2	62.2	46.1	51.6	52.1	3.3	14.6	3	12.5	4.7
8.0	50.7	62.8	46.3	52.3	52.7	4	15.4	3.4	13.4	5.6

Compression										
Horizontal stiffness	**Stress (MPa) LC5-71A**	**Stress (MPa) LC5-71B**	**Stress (MPa) LC5-SW/0 A**	**Stress (MPa) LC5-SW/0 B**	**Stress (MPa) LC5-SW/2**	**Stress (MPa) LC6-71A**	**Stress (MPa) LC6-71B**	**Stress (MPa) LC6-SW/0 A**	**Stress (MPa) LC6-SW/0 B**	**Stress (MPa) LC6-SW/2**
1.5	-4.6	-8.1	0	0	-8.5	-46.4	-48.5	-42.2	-48	-50.7
3.0	-4.6	-8.1	0	0	-1.5	-45.7	-47.7	-41.4	-47.1	-50.2
4.0	-4.6	-8.1	0	0	-4.1	-45.6	-47.6	-41.1	-46.8	-53.5
6.0	-4.6	-8.1	0	0	-6	-45.5	-47.5	-40.9	-46.6	-55.8
8.0	-4.6	-8.1	0	0	-6.6	-45.4	-47.4	-40.8	-46.5	-56.6
Tension										
Horizontal stiffness	**Stress (MPa) LC5-71A**	**Stress (MPa) LC5-71B**	**Stress (MPa) LC5-SW/0 A**	**Stress (MPa) LC5-SW/0 B**	**Stress (MPa) LC5-SW/2**	**Stress (MPa) LC6-71A**	**Stress (MPa) LC6-71B**	**Stress (MPa) LC6-SW/0 A**	**Stress (MPa) LC6-SW/0 B**	**Stress (MPa) LC6-SW/2**
1.5	51.4	48.6	41.9	45.4	47.8	8.3	7.1	4.9	13.3	12.5
3.0	43.7	45.8	40.7	42.8	44.9	8.3	7.1	0	2.9	11.1
4.0	45.5	48.1	42.9	46	47.6	8.3	7.1	0	6.1	11
6.0	46.6	49.6	45.1	48	49.4	8.3	7.1	0	8.4	10.9
8.0	47	50	45.8	48.7	50	8.3	7.1	0	9.3	10.9

Compression											
Horizontal stiffness	**Stress (MPa) LC7-71A**	**Stress (MPa) LC7-71B**	**Stress (MPa) LC7-SW/0 A**	**Stress (MPa) LC7-SW/0 B**	**Stress (MPa) LC7-SW/2**	**Stress (MPa) LC8-71A**	**Stress (MPa) LC8-71B**	**Stress (MPa) LC8-SW/0 A**	**Stress (MPa) LC8-SW/0 B**	**Stress (MPa) LC8-SW/2**	**Highest stress per stiffness**
1.5	0	-3.9	0	-5.1	-1.7	-64.3	-47.7	-48.3	-46.8	-48.5	-64.3
3.0	0	0	0	0	-2.5	-62.7	-51	-47.8	-46	-47.8	-62.7
4.0	0	0	0	0	-2.6	-62.4	-52.9	-47.6	-45.8	-47.5	-62.4
6.0	0	-0.6	0	0	-2.7	-62.2	-54.3	-47.5	-47.3	-47.2	-62.2
8.0	0	-1	0	-0.5	-2.7	-62.2	-54.8	-47.4	-47.9	-47.1	-62.2
Tension											
Horizontal stiffness	**Stress (MPa) LC7-71A**	**Stress (MPa) LC7-71B**	**Stress (MPa) LC7-SW/0 A**	**Stress (MPa) LC7-SW/0 B**	**Stress (MPa) LC7-SW/2**	**Stress (MPa) LC8-71A**	**Stress (MPa) LC8-71B**	**Stress (MPa) LC8-SW/0 A**	**Stress (MPa) LC8-SW/0 B**	**Stress (MPa) LC8-SW/2**	**Highest stress per stiffness**
1.5	52.2	51.8	49.7	48.5	50.8	13.9	14.8	14.6	17.2	18.5	57.4
3.0	42.9	54.4	42.9	48.1	49.3	7	7.3	5.1	8.4	8.9	57.4
4.0	46	57.2	45.9	51	52.6	6.8	10.1	4.9	11.5	12.9	60.3
6.0	48	59	47.8	52.8	54.8	6.6	12.1	4.7	13.7	15.7	62.2
8.0	48.7	59.6	48.4	53.4	55.6	6.6	12.8	4.7	14.5	16.8	62.8

B.3. Model 2: Variable Abutment

Compression										
Horizontal stiffness	**Stress (MPa) LC1-71A**	**Stress (MPa) LC1-71B**	**Stress (MPa) LC1-SW/0 A**	**Stress (MPa) LC1-SW/0 B**	**Stress (MPa) LC1-SW/2**	**Stress (MPa) LC2-71A**	**Stress (MPa) LC2-71B**	**Stress (MPa) LC2-SW/0 A**	**Stress (MPa) LC2-SW/0 B**	**Stress (MPa) LC2-SW/2**
70	-8.3	-7.1	0	0	-8.7	-46.1	-46.9	-45.4	-46.7	-46.7
136	-8.3	-7.1	0	0	-8.6	-46.3	-47.1	-45.6	-47	-44.2
205	-8.3	-7.1	0	0	-8.7	-46.1	-46.9	-45.4	-46.7	-46.7
Tension										
Horizontal stiffness	**Stress (MPa) LC1-71A**	**Stress (MPa) LC1-71B**	**Stress (MPa) LC1-SW/0 A**	**Stress (MPa) LC1-SW/0 B**	**Stress (MPa) LC1-SW/2**	**Stress (MPa) LC2-71A**	**Stress (MPa) LC2-71B**	**Stress (MPa) LC2-SW/0 A**	**Stress (MPa) LC2-SW/0 B**	**Stress (MPa) LC2-SW/2**
70	47.1	49.8	48.1	49	61.3	4.6	8.1	2.7	9.4	24
136	44.7	47.9	45.2	46.2	58.1	4.6	8.1	0	6.3	20.3
205	46.9	49.6	47.9	48.9	61.2	4.6	8.1	2.7	9.4	24.1

Compression										
Horizontal stiffness	**Stress (MPa) LC3-71A**	**Stress (MPa) LC3-71B**	**Stress (MPa) LC3-SW/0 A**	**Stress (MPa) LC3-SW/0 B**	**Stress (MPa) LC3-SW/2**	**Stress (MPa) LC4-71A**	**Stress (MPa) LC4-71B**	**Stress (MPa) LC4-SW/0 A**	**Stress (MPa) LC4-SW/0 B**	**Stress (MPa) LC4-SW/2**
70	-2.6	0	-0.6	-1.7	-0.3	-42.1	-52.5	-42	-48.9	-48.3
136	-2.3	0	-0.4	0	0	-39.9	-52.9	-40	-46.7	-48.7
205	-2.6	0	-0.6	-1.6	-0.2	-42.2	-52.5	-42	-49	-48.3
Tension										
Horizontal stiffness	**Stress (MPa) LC3-71A**	**Stress (MPa) LC3-71B**	**Stress (MPa) LC3-SW/0 A**	**Stress (MPa) LC3-SW/0 B**	**Stress (MPa) LC3-SW/2**	**Stress (MPa) LC4-71A**	**Stress (MPa) LC4-71B**	**Stress (MPa) LC4-SW/0 A**	**Stress (MPa) LC4-SW/0 B**	**Stress (MPa) LC4-SW/2**
70	50.8	62.9	46.4	52.4	52.8	3.9	15.4	3.3	13.3	5.5
136	48.6	60.3	45.3	49.7	50.1	1.6	12.5	2	10.3	4.8
205	50.7	62.8	46.3	52.2	52.7	4	15.5	3.4	13.4	5.6

Compression										
Horizontal stiffness	**Stress (MPa) LC5-71A**	**Stress (MPa) LC5-71B**	**Stress (MPa) LC5-SW/0 A**	**Stress (MPa) LC5-SW/0 B**	**Stress (MPa) LC5-SW/2**	**Stress (MPa) LC6-71A**	**Stress (MPa) LC6-71B**	**Stress (MPa) LC6-SW/0 A**	**Stress (MPa) LC6-SW/0 B**	**Stress (MPa) LC6-SW/2**
70	-4.6	-8.1	0	0	-6.7	-45.4	-47.4	-40.8	-46.5	-56.6
136	-4.6	-8.1	0	0	-4.1	-45.6	-47.6	-41.1	-46.8	-53.5
205	-4.6	-8.1	0	0	-6.6	-45.4	-47.4	-40.8	-46.5	-56.6
Tension										
Horizontal stiffness	**Stress (MPa) LC5-71A**	**Stress (MPa) LC5-71B**	**Stress (MPa) LC5-SW/0 A**	**Stress (MPa) LC5-SW/0 B**	**Stress (MPa) LC5-SW/2**	**Stress (MPa) LC6-71A**	**Stress (MPa) LC6-71B**	**Stress (MPa) LC6-SW/0 A**	**Stress (MPa) LC6-SW/0 B**	**Stress (MPa) LC6-SW/2**
70	47.1	50.1	45.9	48.8	50.1	8.3	7.1	0	9.2	10.9
136	45.5	48.1	42.9	46	47.6	8.3	7.1	0	6.1	11
205	46.9	50	45.8	48.7	49.9	8.3	7.1	0	9.3	10.9

Compression											
Horizontal stiffness	**Stress (MPa) LC7-71A**	**Stress (MPa) LC7-71B**	**Stress (MPa) LC7-SW/0 A**	**Stress (MPa) LC7-SW/0 B**	**Stress (MPa) LC7-SW/2**	**Stress (MPa) LC8-71A**	**Stress (MPa) LC8-71B**	**Stress (MPa) LC8-SW/0 A**	**Stress (MPa) LC8-SW/0 B**	**Stress (MPa) LC8-SW/2**	**Highest stress per stiffness**
70	0	-1	0	-0.6	-2.7	-62.1	-54.8	-47.4	-47.8	-47.1	-62.1
136	0	0	0	0	-2.6	-62.4	-52.9	-47.6	-45.8	-47.5	-62.4
205	0	-1	0	-0.5	-2.7	-62.2	-54.8	-47.4	-47.9	-47.1	-62.2
Tension											
Horizontal stiffness	**Stress (MPa) LC7-71A**	**Stress (MPa) LC7-71B**	**Stress (MPa) LC7-SW/0 A**	**Stress (MPa) LC7-SW/0 B**	**Stress (MPa) LC7-SW/2**	**Stress (MPa) LC8-71A**	**Stress (MPa) LC8-71B**	**Stress (MPa) LC8-SW/0 A**	**Stress (MPa) LC8-SW/0 B**	**Stress (MPa) LC8-SW/2**	**Highest stress per stiffness**
70	48.8	59.7	48.5	53.5	55.7	6.6	12.8	4.6	14.5	16.7	62.9
136	46	57.2	45.9	51	52.6	6.8	10.1	4.9	11.5	12.9	60.3
205	48.6	59.5	48.4	53.4	55.5	6.6	12.9	4.7	14.6	16.8	62.8